Novel Carbon Based Nano-Architectures As Efficient Oxygen Reduction Reaction Catalysts for Fuel Cells and Li-Air Battery

Badam Rajashekar

Japan Advanced Institute of Science and Technology

September 2016

DEDICATED TO MY DEAREST GRAND PARENTS

(THATHA & BAMMA)

Preface

The present dissertation is submitted for the degree of Doctor of Philosophy at Japan Advanced Institute of Science and Technology (JAIST), Japan. The research work embodied in this dissertation entitled "Novel Carbon Based Nano-Architectures as Efficient Oxygen Reduction Reaction Catalysts for Fuel Cells and Li-Air Battery" is an original work carried out under the supervision of Prof. Noriyoshi Matsumi at School of Materials Science, JAIST, Japan during 2013-2016.

In the present global scenario of depleting fossil fuels and global warming, where the emission of green-house gases from the transportation and electricity generation hold the prime responsible for the global warming. A global shift from the traditional fossil fuel to more sustainable energy conversion and storage systems is the need of the hour. The applications of different types of carbon substrates to electrochemical devices, especially in the field of energy, viz., fuel cells and Li-air battery, are significant, as they project high energy density with prolonged durability. The major limiting factor that affects the efficiency of these devices is the sluggishness of the oxygen reduction reaction (ORR) at the cathode. Hence, the need for an efficient cathode material has been under continuous research.

The author's main focus in this work is to design and develop novel and facile methodologies to prepare highly active ORR catalytic material which can be readily commercialized. For this, simple strategies were adopted to tune or tailor cost effective catalytic nanostructures with very high activity. The work presented in this dissertation covers the facile and simple functionalization techniques to the carbon substrates to induce the electrolyte absorptive or interfacial charge transfer characteristics and strong metal substrate interaction characteristics of the substrate for higher ORR activity. To the best of my knowledge, the work present original results. Neither this, nor any substantially similar dissertation has been or is being submitted for any other degree, diploma or other qualifications at any university.

Badam Rajashekar

School of Materials Science

Japan Advanced Institute of Science and Technology

September 2016

Acknowledgement

Firstly, the author expresses his heartfelt gratitude to Prof. Noriyoshi Matsumi, School of Materials Science, Japan Advanced Institute of Science and Technology (JAIST), for his all-embracing support, kind guidance and timely advices throughout the journey at JAIST. I am very thankful to him for his patience, motivation and heartfelt encouragement. I would like to extend my gratitude to Asst. Prof. Raman Vedarajan, as he was the first person to reach for any suggestions. I thank him for his constant support, useful critiques and innovative ideas all through the journey.

I would like to thank the members of my review committee Prof. Masahiro Miyauchi (Tokyo Institute of Technology), Prof. Kohki Ebitani (JAIST), Assoc. Prof. Yuki Nagao (JAIST), Assoc. Prof. Toshiaki Taniike (JAIST) for spending their valuable time assessing my thesis, for their insightful comments and remarks to enhance the quality of this dissertation from various perspectives.

I would like to thank Tanaka Kikinzoku for helping in RDE experiments. I express a great appreciation for the staff members of Machine shop, JAIST for their engineering expertise in the fabrication of device for testing Li-air battery. The author is very thankful to Center for Nano Materials and Technology (CNMT), Assoc. Prof. Mikio Koyano and School of Materials Science for the technical support and instrumentation. I am very thankful to Dr. Rajalakshami Natarajan for giving an opportunity to carry out fuel cell experiments at Center for Fuel Cell Technology (ARCI) IIT Madras Research Park, India. A huge thanks will not be enough for the members of CFCT for their active collaboration and warm support during my stay in India. The author also takes this opportunity to thank all the members of Matsumi lab for their valuable inputs, support, cooperation, stimulating discussions and creating lively ambiance in JAIST.

The word ‘thanks’ will not be enough to express my gratitude to my parents, brother, wife and all the members of family for their love and relentless efforts all the time.

As a sense of gratitude, the author would like to offer everything in life to the almighty God.

Badam Rajashekar

School of Materials Science

Japan Advanced Institute of Science and Technology

September 2016

Abstract

The importance of Oxygen Reduction Reaction (ORR) as a principle reaction in various elelctrochemical applications have been well understood over the years. Fuel cells and Li-air battery working on the basis of ORR, which project a high energy density, prolonged durability with low emission of global warming gases have gained greater significance among plethora of electrochemical energy devices. Electrocatalyst plays an important role in realization of both these devices by enhancing the sluggish kinetics of ORR. The two interconnected materials forming the ORR catalyst are the porous & conducting carbon support and the active metal nanoparticles as ORR centres. A careful and strategic optimization in their designing of the substrate for enhanced activity, increased durability, simple preparation method for immediate commercialization and reduction of overall cost. In this view, the present work details the importance of substrate modification in enhancing above attributes of the catalytic activity of Pt/carbon based catalysts by tuning a) surface area of carbon based support b) ability to support the catalyst c) pore size d) charge transfer resistance and e) the ability to anchor Pt nanoparticles.

The chapters in this thesis, include strategies to tune one, more or all of the above mentioned intrinsic properties of the catalyst with very simple, facile and in some cases green processes which can possibly see the light of commercialization.

Chapter 2 deals with a novel single-pot method to exfoliate and functionalize acetylene black. The deliberate functionalization was found to enhance the intrinsic oxygen reduction efficiency along with the nucleation and growth of platinum nano-particles on the surface. The prepared material was well characterized to understand the morphology, elemental composition and electrocatalytic behaviour. The resulting material showed enormously high oxygen reduction reactivity compared to its commercial counterparts. The mass activity evaluated from the rotating disc electrode (RDE) techniques was found to be higher than the target set by the

department of energy (DOE), USA. The material also showed very encouraging results when employed as cathode material for PEMFC and Li air batteries.

Electrocatalytic materials for oxygen reduction reaction, currently dominated by platinum/carbon catalyst is marred by drawbacks such as, use of copious amount of Pt and use of "non-green" sacrificial reducing agent (SRA) during the synthesis. A single stroke remedy for these two problems has been achieved through an *in-situ* aqueous photoreduction void of even trace amounts of SRA with an enhanced activity. Reduction of $PtCl_6^{2-}$ salt to Pt nano particles on carbon substrate was achieved solely using solar spectrum as the source of energy and TiO_2 as photocatalyst. In chapter 3, it was demonstrated that this new procedure of photoreduction, decorates Pt over different types of conducting carbon allotropes with the distribution and the particle size primarily depending on the conductivity of these allotrope. The $Pt/C/TiO_2$ composite unveiled an ORR activity on par with the most efficient Pt based electrocatalyst prepared through the conventional sacrificial reducing agent aided preparation methods.

The development of novel substrates possessing high durability, strong anchoring to catalytic metal nanoparticle and low charge transfer resistance that can replace conventional carbon is of great importance. In order to improve the durability and reduce the cost of various energy devices, new methodologies are necessary. In this regard, chapter 4 highlights the preparation of a macroporous hybrid material containing a foam like polythiophene electropolymerized on to TNT. The prepared hybrid material showed very low charge transfer resistance and was further modified with novel and green photo-generated Pt nanoparticles. The material exhibited very strong metal substrate interaction which makes it highly durable during the ORR. This chapter proposes a novel macroporous organic/inorganic hybrid material as a candidate material that has a great probability to replace the conventional carbon substrates for ORR catalysts.

Table of Contents

Chapter 2

Platinum Decorated & Functionalized Defective Acetylene Black; A Promising Cathode Material for ORR

Chapter 3

Novel Sacrificial Reducing Agent Free Photo-Generation of Pt Nanoparticles on All Conducting Carbon Forms as Triple-Phase ORR Catalytic with Enhanced Activity

Chapter 4

3D Polythiophene Foam on TiO_2 Nanotube Array as a Substrate for Photo-Generated Pt Nanoparticles as an Advanced ORR Catalyst

Chapter 5

Conclusions

List of Figures

List of Tables

Chapter 1

Introduction to Oxygen Reduction Reaction (ORR) Catalysts and Devices Functioning on ORR

1.1. General Introduction to Oxygen Reduction Reaction and Its Catalyst

Oxygen, the most abundant element in the earth's crust, is very important in human life. Oxygen reduction reaction (ORR) is not only important to life processes such as biological respiration but also plays a lead role in corrosion, sensors and various electrochemical devices. It stands as one of the principle reaction for sustenance of human body by being a part in the redox reaction in the biological respiration. Aerobic respiration is the source of energy for majority of the animal kingdom (fungi to human being) in which oxygen reduction is one of the principle reaction. The following reaction shows the oxidation of glucose and the reduction of oxygen to generate carbon dioxide and water along with energy during aerobic respiration.

$$C_6H_{12}O_6\ (s) + 6\ O_2\ (g) \rightarrow 6\ CO_2\ (g) + 6\ H_2O\ (l) + \text{heat}$$

The other important area where ORR occurs naturally is the corrosion of metals. As the manufactured metals are meta-stable forms of stable and naturally occurring ores. The corrosion is the process in which these metals are transformed back to the original forms of ores. Rusting of iron is the simplest of examples for corrosion. Anodic dissolution of metals in an aqueous environment and cathodic reduction of oxidant are the principle reactions that are occurring during the process of corrosion. Oxygen reduction is a major cathodic reaction during the corrosion of metals as oxygen is one of the most abundant oxidant naturally available. Corrosion of metals is found to be one of the major challenges in the present industrialized society. Proper understanding and control over the oxygen reduction can lead us in achieving plausible solutions for the corrosion of metals.

In the present global scenario of depleting fossil fuels and global warming, the emission of green-house gases from the transportation and electricity generation hold the primary responsibility for the global warming. A global shift from the traditional fossil fuel to more sustainable energy conversion and storage systems is the need of the hour. Research community is striving for developing very efficient and durable energy conversion and storage devices like fuel cell and metal air batteries respectively so that, the urgent requirement for electric vehicles (EVs) and production sustainable energies can be met[1]. Interestingly, both of these energy devices principally work on ORR. The sluggish kinetics of ORR make the ability to control the reduction of oxygen electrocatalytically a hard shell to break. The difficulty in adsorption of oxygen onto the electrode surface, activation/cleavage of O-O bond and removal of oxide products are possibly few known reasons for the sluggish kinetics of ORR. In order to achieve high efficiencies, the ORR has to be activated closer to its thermodynamic potential i.e., with very less over potential. The highly irreversible nature of the ORR makes the introduction of electrocatalyst a must and foremost to reduce the overpotential. The list of electrocatalysts includes noble metals, alloys, carbon materials, quinone and derivatives, transition metal macrocyclic compounds, transition metal chalcogenides, and transition metal carbides. Among the long list of ORR electrocatalysts, Pt has been a universal choice due to its efficient and reliable electro-catalytic activity for ORR. The demand of high loading of ORR catalyst (usually a precious metal) due to slow kinetics increases the practical cost of the energy devise marring the realization of the EVs. A study conducted by Department of Energy (DOE), United States in 2007 showed that, 56% cost of a cell stack of fuel cell arises from the amount of platinum used. Hence, the cost of the fuel cell is directly linked to the amount of Pt used in it. To curb the high cost of these energy devices the best strategies that can be thought of are, the substantial improvement in the efficiency of the electrocatalyst and reduce the production cost of the electrocatalyst. On the other hand, the longevity or the durability of standard or advanced

electrocatalyst is a long standing concern in the scientific community as the operation conditions of the energy devices performs on ORR are very corrosive. For instance the when fuel cell test fleets in EVs have been monitored by DOE using ≥ 0.4 $mg_{Pt}cm^2$ on cathode, the stability of the catalyst fall short of the expected durability target[2]. Hence, the low cost with high performance and enhanced durability is the subject of interest in the area of electrocatalyst. The development in the material science and nanotechnology[3–6] in the recent times made a significant progress rationale designing and preparation of Pt-based ORR electrocatalysts with excellent efficiency. The emergence of nanoscale material from bulk, attractive physical and chemical properties of the material has been observed. The synergy of development in nano science and characterizing techniques opened the doors to develop low cost processes and material to address critical issues bothering the scientific world[7,8]. These new trends gradually shifted the trial-and-error methods of preparations to design and fabrication of electrocatalysts at molecular or even atomic level precision. Manipulation of the surface electronic structure and the atomic structure of the electrocatalyst were found to be the most important design principle after understanding of the ORR mechanism. So, understanding the mechanism of the ORR catalysis is very important aspect to design an efficient catalyst.

1.2. Mechanism of ORR

Electrocatalytic reduction of oxygen is structurally very sensitive and an atomic level understanding of its mechanism throws light on the intricate details in designing an efficient ORR catalyst. Though, ORR is known to be a multi-electron transfer process, many intermediates get adsorbed during its several steps mechanism and makes it more difficult to get the whole some view. In spite of the numerous investigations over a few decades the mechanism is still not very clear[9–12]. Thus, reaction pathways are more talked about than the reaction mechanism in the case of ORR. However, it is clear now that the ORR involves four net transfer of coupled proton and electrons to molecular oxygen at cathode. Based on the

nature of electrode material, catalyst and electrolyte ORR follows one/more pathways. The reduction pathways (table 1.1) involves in various electron transfer pathways such as, 1, 2 and 4 electron transfer. Each pathway has its own importance in their respective applications. For instance, 1 electron transfer is useful for clear understanding of the ORR mechanism in non-aqueous aprotic solvents, 2 electron transfer is useful in the hydrogen peroxide production and finally 4 electron transfer is very essential in the topic of discussion i.e., ORR in fuel cells and metal air batteries.

Table 1.1 Thermodynamic electrode potentials of electrochemical ORR

Electrolyte	**ORR Reactions**	**Thermodynamic Electrode Potential at Standard Conditions (V)**
Acidic aqueous solution	$O_2 + 4H^+ + 4e^- \rightarrow H_2O$	1.229
	$O_2 + 2H^+ + 2e^- \rightarrow H_2O_2$	0.70
	$H_2O_2 + 2H^+ + 2e^- \rightarrow H_2O$	1.76
Alkaline aqueous solution	$O_2 + H_2O + 4e^- \rightarrow 4OH^-$	0.401
	$O_2 + H_2O + 2e^- \rightarrow HO_2^-$	-0.065
	$HO_2^- + H_2O + 2e^- \rightarrow 3OH^-$	0.867
Non-aqueous aprotic solvent	$O_2 + e^- \rightarrow O_2^-$	Strongly dependant on the solvent used.
	$O_2^- + e^- \rightarrow O_2^{2-}$	

As aforementioned, the ORR pathway primarily depends on the electronic and atomic structure of the catalytic material used. Less active transition metal catalysts like Au and Ag involves in two electron pathway and the most electroactive catalyst Pt follows four electron pathway. Identifying the rate determining step is essential to understand the sluggish kinetics. Researchers have deliberated the possibility of three important steps which might cause the sluggish nature. They are, 1) the first electron transfer from the catalyst to the oxygen 2) the hydration of oxygen and 3) desorption of the intermediate products. Many researchers[13–17]

mentioned that the first electron transfer was the rate determining step of ORR. Anderson *et al.*, calculated the activation energies for the elemental steps of ORR using *ab initio* method[17]. The studies determined the highest activation barrier was for the first electron transfer step and the proton transfer on the Pt catalyst. Similar conclusions were made by other researchers by investigating the first electron transfer step[18,19] to be rate determining step. Janik, Taylor and Goddard gave different contradicting opinions on the sequence of electron and the proton transfer[20–22].

A more recent and widely appreciated approach has been proposed by Norskov *et al*[23–25]. The study proposed that the adsorption of intermediate species O and OH might play a crucial role during ORR on metal catalysts. Norskov in his study proposed a method for computing the free energy of all intermediates as a function of electrode potential by calculating the adsorption energy for various adsorption intermediates using DFT method. They showed that the oxygen

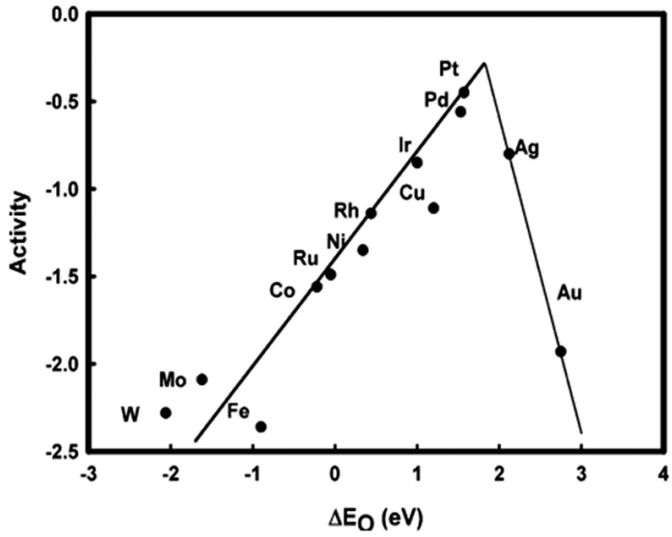

Figure 1.1 Trends in oxygen reduction activity plotted as a function of the oxygen binding energy (Ref.24)

adsorbed on the Pt(111) was very stable at high potentials which make the electron and proton transfer highly impossible. But, by lowering the electrode potential the stability of adsorbed oxygen decreases and triggers the reaction. This potential difference was suggested to be the origin of over potential for the ORR on Pt. This work also contributed in calculating the bond

energies of oxygen and hydroxyl for a series of ORR metal catalysts shown in the Figure 1.1[23]. The trend in the Figure 1.1 shows the catalytic activity of various metal catalysts in which the Pt and Pd tops the list with highest activity. In the case of metals that have the tendency to bind the adsorbed oxygen molecules very strongly, the rate determining factor is desorption of intermediates, O and OH. For the metal catalysts that weakly adsorb the oxygen molecule, the rate is limited by the transfer of electron or the dissociation of O_2 molecule.

1.3. Introduction: ORR Catalysts

In the recent years enormous amount of research has been dedicated in designing and synthesizing efficient electrocatalysts based on both computational and by developing novel extended model systems to single crystal Pt. Though most recently developed electrocatalysts include, metal and alloy based nano materials[26], various carbon based materials like, quinone and its pyrolytic derivative[27], transition metal chalcogenide[28], transition metal carbide[29], oxide, transition metal macrocyclic compounds[30,31], perovskites[31] etc, Pt based nano materials remain the most practical ones in strong acidic media.

1.3.1. Emphasis on Platinum (Pt) Based Catalysts

Based on the understanding of the ORR mechanism, the rational optimization of intrinsic reactive sites of Pt and efficiently utilizing them are widely believed strategies to develop an efficient Pt based ORR catalyst. As ORR is a surface sensitive reaction, effectively tuning the surface electronic properties and atomic arrangement of the catalyst are very crucial. Altering of the electronic properties lead to efficient adsorption behavior and thus effectively reduce the overpotential[32]. It is believed that this adsorption behavior triggers a high ORR activity[33]. Thus tuning the surface electronic properties are very crucial in enhancing the activity of Pt based catalysts. To tune the same, four possible strategies can be considered, i) single component Pt catalyst; preparation of facet controlled Pt nanocrystals that has maximum exposure to

environment so as to perform better ORR, ii) Pt bimetallic and multimetallic nanocrystals in the form of alloys, core-shell, branches or anisotropic nanocrystals towards high activity. iii) Pt nanoparticles with surface modification, iv) Pt nanoparticle decoration on active surfaces to reduce the corrosion and improve the stability. These strategies are dealt in details in the following section.

1.3.1.1. Facet Controlled Uni-metallic Pt Catalyst

Generally, ORR activity can be fine-tuned by varying the composition which modifies the electronic structure or by controlling the atomic arrangement and coordinates which determines the shape of the Pt catalyst. The later has received a lot of attention to tune the catalytic performance and its fundamental understanding. Fundamental studies on ORR using bulk Pt single crystal is greatly dependent on the shape and arrangement of the atoms (facets). Generally high-index planes exhibit better ORR catalytic activity owing to the presence of more active sites in the form high density of atomic steps, ledges and kinks[34,35]. The most common low-index Pt single crystals have been well studied in acidic medium. The order of catalytic activity is found to be in the order of surface free energy of the each facet, {110} exhibited the highest activity followed by {111} and the least activity was found to be {100} in adsorbing electrolyte like $HClO_4$. In case of H_2SO_4, the order of activity is found to be different. In this case, {100} exhibited higher activity than {111} owing to the adsorption of bisulphate anions. The systematic adsorption studies revealed that Pt {100} adsorbs less than one-third of bisulphate anions than that of {111} in the same concentration of electrolyte. Allowing higher surface area for H adsorption, Pt{111} showed a stronger bisulphate adsorption in wide potential range than that of Pt{100} owing to its surface electronic properties. The subsequent morphological studies also confirmed that the enhancement of surface area also improves the activity. Early research on shape controlled synthesis of nano particles was led by El-Sayed *et al*.[36] Variety of nano particles including tetrahedral

nanoparticles with {111} facet, nanocubes with {100} were prepared and also effort was made to make spherical nano particles. Subsequent efforts were made to prepare monodispersed Pt nanocubes with {100} termination through high temperature treatment in organic phase and study their ORR activity in H_2SO_4. ORR studies reported that the activity of the aforementioned nanocubes was twice that of commercial Pt catalyst available then[37]. The same group also reported that {100} faceted nanocubes with 7 nm size performed as a better catalyst than other morphologies. This not only demonstrated the effect of improvement in surface area of the nanoparticles but also the shape-dependency of ORR activity. This reaffirmed the results of sulphate adsorption on different facets of Pt and hence the ORR activity[38].

The stability of the generally available low index facets such as {111} and {100} surfaces bridged with {100} surface is higher than that of face-centered-cubic (*fcc*) nano crystals with high density atomic steps, ledges and kinks due to high activity. So the stable higher faceted nanocrystals with high surface activity should result in better ORR activity. Sun and coworkers have reported electrochemical preparation of well-defined surface with tetrahexahedral (THH) Pt particles with high-index planes of {730}, {210}, and {520} with high density of atomic steps, ledges and kinks[39]. Further it was also shown that these particles possessed very high electrocatalytic activity than that of Pt nanocrystals with low facets. The exponential increase in the electrocatalytic activity can be ascribed to the surface that contains high percentage of edge, corner and step sites that acts as the binding sites for the elctrocatalysis. Besides this, Xia *et al*., have demonstrated a very simple method of aqueous reduction to prepare Pt concave nanocubes exposed with high index facets of {510}, {720} and {830}. Concave nanocubes with high surface area exhibited extremely high ORR activity compared to those of cubes, cuboctahedra and commercial Pt/C that have low index planes[40]. Although a great improvement in the activity of ORR was seen in these Pt nanocrystals with high facets, the clear mechanism to understand the enhancement is still not clear. Moreover, due to the fact that

these nanocrystal are of large sizes, their mass activity is found to be far behind the other highly active ORR catalysts. Alongside their low mass activity these well faceted nanocrystal were found to be very intolerant in the fuel cell environment, thus, low durability. It was found that these highly active facets undergo changes due to the morphological transformations that are inevitable during the fuel cell operations. Along with the durability the high cost of the Pt makes the practical application of these nanocrystals as such is very limited. Hence, the combination of low cost metals with Pt was found to be working strategy to reduce the cost.

1.3.1.2. Pt Bimetallic and Multimetallic Nanocrystals

Current trend is to utilize Pt nanoparticles for ORR due to its high catalytic activity. The skyrocketing price of Pt and being a limited resource, the development of new electrocatalysts with ultra-low amount of Pt is found to be next strategies. The strategy is to alloy Pt with other low cost metals, to make core-shell type of material, forming branches or anisotropic material. The use of bimetallic systems is a very attractive and can probably be a practical strategy as these systems not only have the intrinsic properties of individual metals but also novel properties resulting from the synergy of both the metals. Moreover, the rational selection of alloying metal with Pt and well defined size, composition of these type of bimetallic and multimetallic systems can boost the ORR activity and durability along with the control over cost of the final devices.

Alloy System:

Alloy electrocatalyst with lower quantity of costlier Pt metal not only succeed in keeping the intrinsic activity of Pt but also generally result in efficient oxygen reduction when compared to activity of the individual metals present in the system[41,42]. The recent past has seen a variety of combination of Pt with other transition metal alloy systems for ORR applications. They are, Pt in combination with Pd, Au, Ag, Cu, Fe, Ni, Co and W. These alloy systems have been studied to find the higher ORR activity. The enhancement in the electrocatalytic activity is

believed to be due to the alteration in the surface electronic structure of the Pt. Simulation studies, though don't provide the information regarding the precise electronic structure but provides with the important clues for the requirement for surface structure to enhance the ORR activity. Various DFT studies reported that the alloying will alter the chemisorption properties of the Pt so as to efficiently adsorb oxygen molecules. This has been attributed to the short-range charge transfer effects (ligand effect) and long range lattice strain resulting in geometric effects[32,43]. The strain and ligand effect cause a shift of the energy centers of d-states in the Pt which affect the bond strength of the surface adsorbates and result in the modification of the chemisorption of O_2, intermediates formed and the products. To understand the role of alloying metal, various 3d transition metals have been studied. In one such study by Stamenkovic *et al.*[44] the catalytic activity of the resulting material was highly dependent on the alloying 3d metal. Metals such as Ni, Co, Fe, Ti and V were studied to correlate the ORR catalytic activity and the role of electronic structure (d-band center). A fundamental correlation has been drawn by these results studying alloy material in the form of Pt_3M (M=Ni, Co, Fe, Ti and V). The relation between the d-band center vs the specific activity and enhanced activity compared to Pt was drawn as shown in Figure 1.2.

Figure 1.2 shows a volcano type of behavior, here the ORR activity was governed by a balance

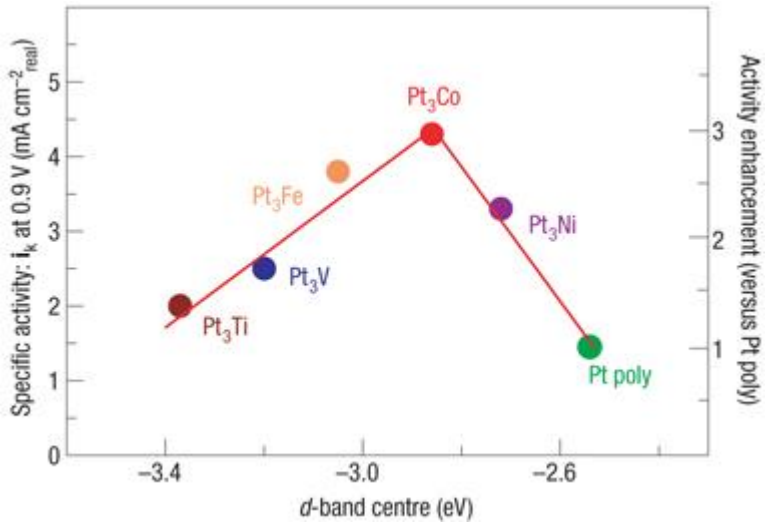

Figure 1.2 Relationships between the catalytic properties and electronic structure of Pt_3M alloys (Ref.45)

between adsorption energy of the oxygen and adsorption of blocking species. These studies gave a clue regarding the attributes of better catalyst. A better catalyst for ORR should weakly bind oxygen than that of Pt to increase the rate of intermediate removal. A better ORR catalyst ideally should lower the binding energy of oxygen species (along with intermediates) by 0.2 eV compared to that of bare Pt catalyst. Based on this fact, Ni, Co and Fe were found to be effective alloying metals to lower the binding energies.

In contrast to the above reported material with high Pt percentage, attempts were made to reduce the Pt content in the alloy preparation. In one such attempt Chen *et al.* used first-principal theoretical calculations demonstrating the tendency of W to form an alloy with less amount of Pt. Apart from formation of stable alloy, the peculiar electronic effect of 5d transition metal W to Pt has the ability to perform ORR better than that of Pt. Subsequent preparation of PtW_2 and ORR studies exhibited 4 times higher mass activity than that of Pt and found stable over 30000 potential cycles[45].

The development of material synthesis in the recent times led to a significant progress in the synthesis of various Pt-M (transition metal) alloy catalysts with tailored compositions and sizes[46,47]. The general procedures to prepare these alloy nano-material is by decomposition or reduction of metal carbonyl and metal salts or by co-reduction of alloying metal precursors[48,49]. Though the synthetic approaches have reached a stage where precise composition and size can be controlled, preparation method for each alloy is metal specific. Similar reaction conditions may not work with other metals to form alloys. In this regard to have a general preparation method Sun and co-workers have reported a simple yet general procedure to prepare Pt-M (M=Fe, Co, Ni, Cu, Zn) alloy nanoparticles[50].

In spite of the understanding of mechanism, factors effecting ORR and efforts to have general preparation methods to develop new ORR catalysts, the realization of alloy materials in commercial devices is marred by the non-retention of the initial Pt based mass activity. The

reduction of mass activity was ascribed to the leaching of non-precious metal due to the acidic environment in the diagnostic tests as well as in the final application devices. With this background a protective covering of stable Pt over the alloying material would probably result a stable and efficient bi or multi metallic catalyst.

Core-shell Nano-structures:

The leaching and dissolution of non-precious metal of the alloy systems in the acidic environment resulted in the poor stability of the bimetallic Pt electrocatalytic systems. Novel methodologies for the improvement of their stability were devised so that the advantages of the bimetallic nanostructures could be utilized. The protective layer of stable Pt nano layer over the non-precious metal core was found to be a strategy to reduce the dissolution of alloying metal and increase the stability of the catalyst. This core-shell with few atomic layers of precious Pt metal arranged over non-precious transition metal not only could induce the stability but also makes use of every Pt atom to facilitate the reaction. This strategy also resulted in the reduction of cost of the catalyst subsequently and the cost of energy device. Various core-shell nanoparticles using different core metals like, Au[51], Pd[52], Cu[53] and Ni[54] were prepared successfully by following colloidal synthesis or Under Potential Deposition (UPD)[55]. The core-shell type of material not only reduce the cost of the catalyst but also enhances the activity of ORR by reducing the binding energy for the oxygen similar to alloy materials. In addition the latest preparation techniques like physical vapor deposition, chemical or electrochemical dealloying/leaching and segregation techniques resulted in compositional and size controllable core-shell preparation methods to achieve good ORR activity. Pre-treatment method was approached for the dissolution of non-Pt metal atoms on the top most layer of the core-shell. The pre-treated core-shell was left with a rough atomic layer of Pt with low or without lateral coordination resulting in Pt-skeleton, which showed enhancement in the ORR. The thermal annealing of the core-shell resulted in the Pt-skin[56] nanostructure is another method to form

pure Pt monolayers to enhance the stability and active surface area of the ORR catalyst. Though the Pt in the form of thin shell over a non-precious metal core showed enhancement in the activity by enhanced utilization of Pt atoms, durability and reduction in the cost, the scalability of the preparation methods to commercialize these materials is one of the factors that is limiting the realization of these in practical devices. Most of the above sections deal with the 0 dimensional (0-D) platinum nano structures. These 0-D catalysts generally undergo migration, aggregation and Ostwald ripening due to high surface activity which results in the significant diminution of electrochemical active surface area (ECSA)[57]. These drawbacks gave researchers a scope to explore self-supporting high surface area catalysts with anisotropic morphologies like, nanowires[58], nanotubes[59], branched flowers and dendrites[60].

Anisotropic Nanocrystals:

These anisotropic catalysts exhibit high catalytic activity not only because of their high ECSA but also the intrinsic attributes like high density of active edges, corners and steps on the catalyst's surface. The high surface area and anisotropic properties improves the stability by limiting the migration, aggregation and Ostwald ripening compared to 0-D nanoparticles. Various reports on anisotropic nanostructures of Pt along with few bimetallic catalyst found that the activity of these materials is in fact far better than that of the 0-D Pt catalysts. The practical application of these catalyst in energy devices is impaired due to the ease of preparation in the commercial scale.

Along with the tuning of the facets of nano crystals and the strategy of formation of bi/multimetallic nanostructures, the surface modification of Pt nanoparticles with various organic, inorganic, polymers, metal clusters, molecules and ion was found to have effect on the optimization of Pt electronic structure. Thus the enhancement in the activity can be achieved. This strategy was also found to have few drawbacks like reduction in the electronic conductivity of the overall catalyst, stability of organic molecules etc. At the same time frame

scientists were also trying to modify the carbon substrate. Due to low stability issues related to diffusion of nanoparticles to form agglomerates, the Pt was decorated on to various substrates. Among many carbon substrates were very attractive due to low cost, ease of processing and availability of various tailoring techniques.

1.3.2. Understanding Carbon Supported ORR Catalysts

Despite of the different strategies to improve support less Pt based catalysts in the various morphologies ranging from nanoparticles to complex core-shell and anisotropic structures, the realization of these high catalytically active materials are limited by a number of factors. Along with migration, agglomeration, Ostwald ripening other factors like easier protocols to prepare the material in large scale to commercialize the material is yet to evolve. Till date the most reliable, universally adopted catalysts for various device applications is platinum based nanoparticles decorated on carbon substrate.

1.3.2.1. Various Carbon Supports

Metal supported on carbon substrates have been used as ORR catalyst from past many years. The catalytic application is being extended to a range of carbon substrates like activated carbon, carbon black, graphite and graphitized material. Though, there it is well known that carbon substrate has the effect on the dispersion of Pt nanoparticles on the surface[61,62], somehow not many studies are seen to compare various carbon substrate based Pt catalysts. Instead, the studies have been confined to only well know carbon substrates such as carbon blacks, graphite, fullerene and the recent carbon nanotubes (CNT) and graphene. Furnace black (Vulcan XC-72, black pearl 2000, Ketjen black etc) and acetylene black (AB) are the two major types of carbon blacks extensively used for the catalytic support. Furnace blacks are prepared from aromatic residual oil from petroleum refineries and AB is manufactured by the thermal decomposition of acetylene. All the carbon blacks are found to have very high surface area as well as adsorption properties. Along with these other carbon forms explored for the catalytic supports

are modified graphite, modified diamond, mesoporous carbon, monodispersed hard carbon, carbon and carbon cryogels. The recent development in the nano science and technology lead to the discovery of various nano dimensional carbons such as fullarenes, CNTs, graphene and quantum dots. The introduction of these carbon based materials revolutionized as active catalytic materials by itself as well as stable substrates for metal catalysts.

1.3.2.2. Preparation of Pt/C

In order to control the size and dispersivity of the Pt nano particles on to the carbon there has been a numerous types of preparation techniques of the material have been reported[63]. This includes, chemical methods, electrochemical methods, photo-chemical methods, sonochemical methods, pulsed laser deposition and microwave deposition methods. Commercially, chemical methods are widely used to make the supported catalysts. Chemical methods has been one of the well understood and the long standing technique to decorated Pt nanoparticles on to carbon substrate. Various chemical methods that are available are impregnation method, colloidal, ion exchange, vapor phase and microemulsion methods. All or most of these techniques include a reducing agent in aqueous solutions or in combination with some alcohols. In case of other methods such as sonochemical, microwave, electrochemical and photochemical methods, the variation is the change in the source of energy such as ultrasonic waves, microwaves, electrical potential or electromagnetic light spectrum respectively.

1.3.2.3. Electronic Interaction of Pt Decorated Carbon Electrocatalysts

In Pt decorated carbon catalyst systems, along with their inert behavior, carbon also triggers the galvanic potential of the system which raises the electronic density on the Pt and lowers the Fermi level. The electron transfer at the catalyst-electrolyte interface will be accelerated owing to the above electronic factors. Mitani and group, performed first principle studies on the interaction of Pt cluster with the carbon substrate. It was found from the charge density analysis that the charge transfer increase from Pt to carbon increased linearly with the size of the cluster.

The density-of-state analysis suggested that the interaction between Pt and carbon was partially ionic and partially covalent[64]. The strong metal-carbon interaction, further inhibits the dissolution of Pt during the potential cycling there by enhancing the stability. Few studies have also attempted to understand the change in the electronic states of the Pt upon decoration on the carbon substrate which modifies the ORR activity[65]. The report corroborates that, the difference in the electronic work function of the Pt (5.4 eV) and the carbon (4.7 eV) substrates is an indicative of the double layer formed. This rise in the electronic density on the Pt can be significant only if the Pt cluster size and the double layer are comparable. The studies also showed that the particle size of the catalyst has the effect on the interaction with the carbon substrate thereby the activity.

Various methodologies have been adapted to study the interaction of the Pt with the conducting carbon substrate. The techniques involved are conventional physical, spectroscopic and electrochemical techniques. For example, Electron-spin resonance (ESR) studies were able to confirm the transfer of electron from the Pt to carbon substrate[66]. Similar conclusions were brought by XPS[67] which shows that the Pt acts as an electron donor to the supporting carbon. In brief, the Pt 4f signal from XPS always gave very important information. The peak of the supported Pt catalyst showed a higher binding energy than that of the unsupported Pt[68]. In some cases particle size effect was also reported[69], i.e., the particles having a size of 1-2 nm showed a higher binding energy along with the increase in the full-with half-maxima (FWHM) of the peak due to the difference in the band structure.

Though there are no quantitative correlation for the electronic interaction and catalytic activity, the above evidences clearly note that the electronic interaction between the Pt and the carbon result in better catalytic activities along with the stability. Similar results were reported even in the case of electrooxidation reactions of CO and methanol[70].

1.3.2.4. Surface Treatment of Carbon and Its Effect on Catalytic Activity

Most common and inevitable functionalities even on the commercially available carbon materials is 'Oxygen'. Oxygen functional groups on the surface of carbon are responsible for the acid, base and redox properties of the carbon[71]. These functionalities are of great interest

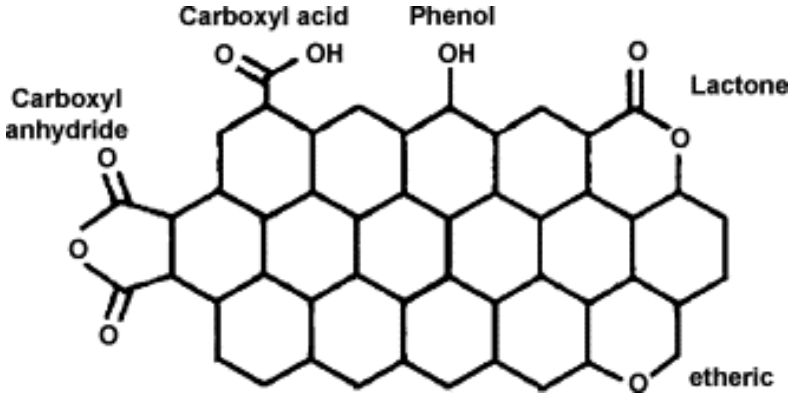

Figure 1.3 Various types of surface oxygen functional groups on carbon (Ref.73)

for the preparation of ORR catalyst using carbon support. The exact nature of the oxygen functionalities on carbon are not clear. Some of the most common functionalities found after the oxidative treatment of the carbon are carboxylic, phenolic, lactonic, etheric groups etc (Figure 1.3)[72].

A variety of chemical oxidative treatments on the surface of carbon can be performed by utilizing a spectrum of oxidants: HNO_3, H_2SO_4, H_3PO_4, O_2, O_3, K_2ClO_3, $KMnO_4$ etc. The presence of oxygen functionalities on the surface of carbon have been found to show great effect on the platinum dispersion on the carbon support. The initial studies by Prado-Burguete *et al.*[73,74] reported that, when carbon was deliberately oxidized by using oxidizing agent like H_2O_2, it resulted in more acidic functional groups leading to evolution of CO_2 at high temperature application. The hydrophilicity of the carbon increased drastically which made the surface more accessible for the metal precursor in aqueous solution. An increasing trend of Pt dispersion was seen by increasing the oxygen surface groups. Further, the introduction of less acidic groups which evolve as CO at high temperatures lead to increased dispersion of metal

on carbon. These metal dispersions were found to be having an increased interaction with the carbon substrate. It was also reported that, more stable oxygen functional groups would lead to effective anchoring between metal particles and carbon. Torres *et al.*[75] reported that the different oxidation treatment lead to different oxygen functionalities on the carbon surface. When the carbon was treated with HNO_3, high density of both strong and weak acid functionalities were formed. In case of H_2O_2 and O_3 as oxidants weaker acid functional groups were more prominent and less concentration of stronger acid groups are formed. The isotherm of H_2PtCl_6 in liquid phase at room temperature was found to have stronger interaction with the carbon with low acidic moieties and weaker interaction with strong acidic moieties. The oxidation of carbon substrate using milder oxidants would lead to moderate strength acidic functional groups and shows strong interaction with H_2PtCl_6. This strong interaction favors Pt dispersion over the carbon with enhanced anchoring effect. According to Sepulveda-Escribano *et al.*[76] the presence of oxygen functionalities improved the interaction with $[Pt(NH_3)_4]$ than that of H_2PtCl_6 metal precursors. Rodriguez-Reinoso explained this phenomenon accordingly, i) the oxidized carbon are generally negatively charged over a range of pH, the negatively charged carbon electrostatically repels same charged $PtCl_6^{2-}$ anions and interact efficiently with $[Pt(NH_3)_4]^{2+}$ cations maximizing the surface dispersion ii) similarly, when the carbon is having basic Cπ sites on its basal planes, better interaction was found by $PtCl_6^{2-}$ and positively charged Cπ sites by increasing the electrostatic attraction iii) C=O groups as anchoring centers, reduce the agglomeration and surface diffusion of metal particles across the carbon basal planes[77].

Some oxygen surface functional groups are not stable during the reduction of metal precursor. When the formation of active metal on these anchoring sites takes place, this would lead to agglomeration and diffusion over the basal planes upon sintering due to the decomposition of the weaker functional groups. Also, the presence of oxygen functional group may diminish the strength of π sites of the carbon due to electron withdrawing effect of oxygen functional groups.

Similarly the recent studies by Wei *et al.*[78] found that the thiolated carbon support found to have enhanced anchoring to the Pt nanoparticles and drastically reduce the dissolution of Pt nanoparticles at high potentials. Further, the durability of the material is enhanced and found to be stable for nearly 1500 voltammetric cycles. The enhanced activity and the stability of the catalyst was due to the increased interaction of Pt with thiolated carbon and depressed d-band center of Pt.

Not only the formation of Pt on a pretreated carbon, but also post treatment after the formation of Pt/C was also found to be enhancing the stability of Pt on carbon in few recent works. Xu *et al*.[79,80] reported that a linking of a Pt with carbon using a short chain sulfonic or phosphonic acid groups through diazonium salts formation by using 2-aminoethanesulfonic or 2-aminoethanephosphonic acid show better catalytic performance than untreated Pt/C materials. It was also found that the electrodes made using these post treated Pt/C material uses less nafion in the catalyst layers with enhanced activity than the unsulfonated catalysts[81].

Thus the pre and post treatment of the carbon and Pt/C based ORR catalysts is a very promising methodology to increase the activity and the durability of the Pt nanoparticles in harsh ORR environment.

1.3.3. Brief Introduction to Advanced Tri-Phasic and Pt-free ORR Catalysts

Although pre and post treatment of carbon or Pt/C respectively show a many fold reduction in the corrosion there by increasing the stability, they are still prone to irreversible oxidation of carbon at high potentials. However, large scale commercial applications of energy devices based on ORR are precluded by the high manufacturing cost of the catalyst. Hence, researcher have been focusing on reducing the cost of the catalyst by reducing the amount of Pt used by adapting to different variety of carbon materials, use of transition metal oxides and doping of nitrogen in carbon. Recently, the focus is on using transition metal oxides with commonly used

carbon supports or substituting the carbon by the doped metal oxides to improve the catalysts stability.

Irreversible oxidation of carbon was found to be very important factor to be eliminated which was found to have other implications like agglomeration and dissolution of Pt due to less interactions. To curb these implications various non-carbonaceous materials like WO_x, TiO_2, TiC, inium tin oxide (ITO), RuO_2-SiO_2 and TaB_2 were reported. The results indicated that the use of these materials significantly increased the activity and durability of the catalyst because of strong metal-support interaction (SMSI) between metal particles and supporting non-carbonaceous material. It is a well-known phenomenon that SMSI can drastically alters the electronic states or the Fermi level of the Pt nanoparticles that has a great influence on the ORR activity as well as the durability of the materials. Though many non-carbonaceous supports show enhanced stability during the ORR, their practical application is limited due to small specific activity and the poor conductivity of the supporting materials.

Later on researchers have moved on to using catalyst in combination of these transition metal oxide materials that showed very good SMSI in combination with the carbon material as supporting material with the Pt. Alonso-Vante *et al.*[82], investigated the substrate effect on the activity and the durability of the Pt nanoparticles on TiO_2/carbon (Vulcan XC-72 and multi walled carbon nanotubes (MWCNT). It was reported that the electrocatalytic activity of the material was enhanced owing to the SMSI. It was found that the enhanced Pt interaction with that of TiO_2/carbon hybrid material was enhanced by forming Pt-Ti interfacial alloy structure. Alongside, the interaction of Pt and carbon was also found to be improved by the presence of TiO_2.

In similar lines, several others reported that the incorporation of semiconductor oxides (e.g., TiO_2, SnO_2 or WO_3) improve the stability to the metal particles on oxide-carbon (metal oxide-carbon) composites along with improving the ORR performance[83,84]. In particular, oxide-

carbon hybrid systems like Pt/C-WO_3[85], Pt/C-TiO_2[82], and Pt/C-SnO_2[86] have been used as catalysts in fuel cells for oxygen reduction reaction (ORR) along with hydrogen and ethanol oxidation reactions. These semiconducting oxides have gathered a huge interest due to their high oxidation resistance in ORR environments, along with a SMSI that tunes the electronic and stability properties of the active material (ligand effect), resulting in the improvement of the electrocatalytic activity for the ORR compared to normal Pt/C. Sung *et al*. observed that the presence of oxide enhances the resistance to carbon monoxide poisoning due to the modification of the electronic states in the d-center of the Pt[87]. Alongside, Pt/oxide-carbon (Pt-transition metal oxide-carbon composite) was found to be very tolerant methanol[88], and the chemical stability as compared to the conventional Pt/C[86].

1.4. Introduction to Electrochemical Characterization Techniques to Evaluate ORR

1.4.1. Cyclic Voltammetry

Cyclic Voltammetry (CV) is one of the most useful electrochemical technique to evaluate the electrocatalytic activity of the material. It is a very simple technique that quickly provides qualitative information about catalysts and electrochemical reactions. Figure 1.4 shows the typical cyclicvoltammogram of the Pt/C catalyst showing hydrogen region showing hydrogen adsorption (H_{ad}), hydrogen desorption to proton and oxygen region indicating the formation Pt-oxide and reduction Pt-oxide to Pt metal.

In heterogeneous catalysis especially in ORR using Pt as electrocatalyst, the real or electro active surface area (ECSA) is one of the vital parameter that determines the catalytic activity of the material. ORR involves in charge transfer between electrode-electroactive species. So, the reaction rate and the current are in proportional to ECSA. The macroscopic or the geometrical surface area of the catalyst is different from the active surface are. The microscopic

or the active surface area of the Pt consists of steps, kinks, ledges and holes. So, the microscopic or ECSA measurements provides the exact active surface area available for electrocatalysis. For Pt catalysts, charge under the hydrogen adsorption or desorption curves is used as tool to calculate the ECSA. During the reduction cycle, protons present in the electrolyte get adsorbed on to the surface of the Pt. While, these get desorbed back in the form of protons from atoms of hydrogen.

$$H_{ad} \rightarrow H^+ + e^-$$

The number of electrons liberated during the desorption process or oxidation in the hydrogen region gives the exact number of hydrogen atoms adsorbed on to active sites present on the Pt. Hence the charge under the curve at the region of H_{ad} as shown in Figure 1.4 can be directly used for the calculation of ECSA assuming that hydrogen adsorption being a monolayer. ECSA can be calculated using the following equation.

$$ECSA = \frac{Q_H\ (\mu C/cm^2)}{Q_M X\ Pt\ loading\ (g/cm^2)}$$

Where Q_H is the charge corresponding to the hydrogen desorption peak, $Q_M = 210\ \mu C/cm^2$ is the electrical charge associated with the monolayer adsorption of hydrogen on Pt and Pt loading is the amount of Pt loaded onto the electrode.

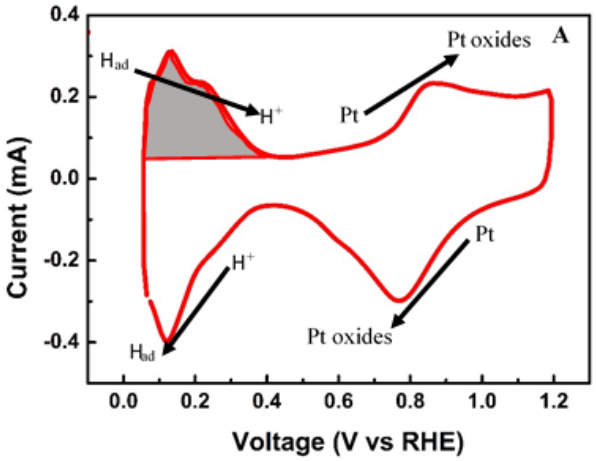

Figure 1.4 CV curve of the Pt catalyst showing the typical reactions on Pt and H_{ad} region.

1.4.2. Rotating Disc Electrode

During the electrochemical experiments especially in current vs voltage experiments, the current gets influenced or disturbed by the convection of various molecules and ions. Hence, accurate evaluation of current due to diffusing species or the species of interest is very difficult. Among various approaches the forced control of convection current or hydrodynamic voltmmetry in specific gives valuable information about the kinetics of the reaction. In ORR, the low solubility of oxygen along with above factors makes hydrodynamic voltammetry an unavoidable technique to evaluate the catalyst. Rotating disc electrode (RDE) technique stands as a powerful tool for evaluating the kinetics of the ORR catalyst. Using RDE experiment with precise control over the rotating rate of electrode (Figure 1.5 A)[89], precise qualitative control of the diffusion layer thickness can be achieved. This precision in controlling the diffusion layer will enable quantitative analysis of the kinetics and the reaction mechanism. Figure 1.5 B shows the typical ORR RDE polarization curve at different rotation rate of Pt/C showing various indicators of ORR kinetics. They are onset potential (E_{onset}), half wave potential ($E_{1/2}$) and diffusion limiting current (I_l).

To determine the mechanism with which the ORR electrocatalyst operates is very crucial to evaluate the catalyst. The numbers of electrons transferred per O_2 molecule was calculated with well-known Koutecky– Levich equation.

$$\frac{1}{I} = \frac{1}{i_k} + \frac{1}{i_L} \qquad (1)$$

$$i_L = 0.620nFACD^{2/3}\nu^{-1/6}\omega^{1/2} \qquad (2)$$

Where, i_k represents the kinetic current for the oxygen reduction happening at the surface of the electrode, i_L is the Levich current for the oxygen reduction reaction by a diffusion controlled process in other words it can be called as diffusion-limited current, n is the number of electrons involved in the reduction of oxygen, F is the Faraday constant (96,485 C mol^{-1}), A is the area

of the RDE used (0.196 cm^2), D is the diffusion coefficient of the dissolved oxygen in electrolyte(1.93×10^{-5} cm^2s^{-1}), C is the concentration of dissolved oxygen (1.26×10^{-6} mol cm^{-3}), v is the kinematic viscosity of the electrolyte (10.09×10^{-3} cm^2 s^{-1}), ω is the rotation rate of

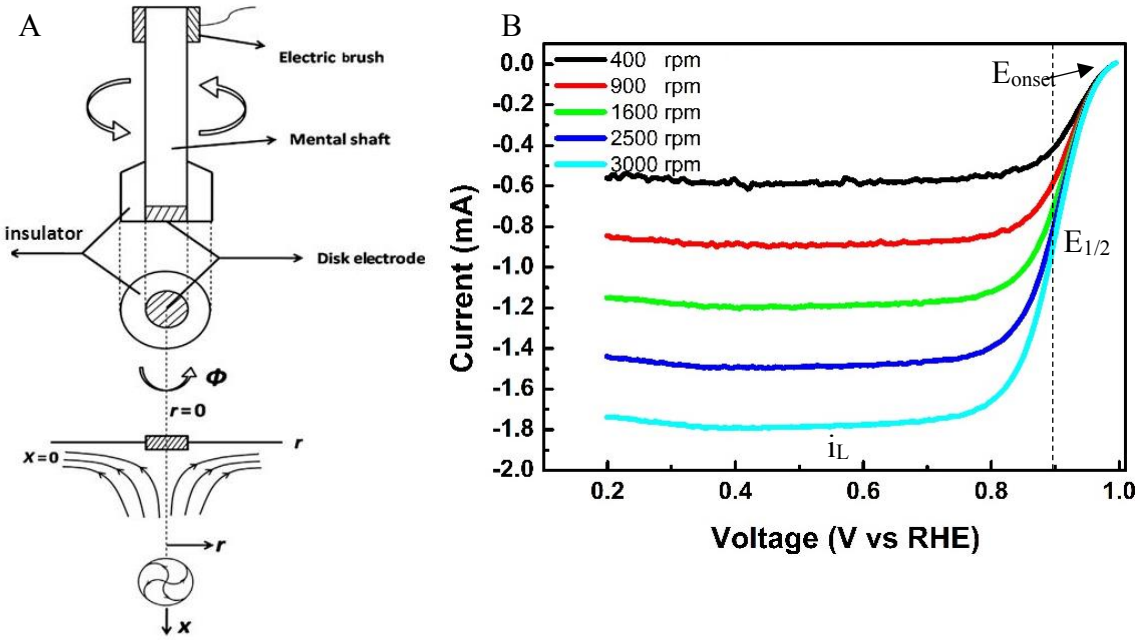

Figure 1.5 Schematic of the RDE and the electrolyte flow(Ref. 90) (A) typical ORR polarization curves showing various kinetic parameters that can be determined from the curve (B)

electrode.

1.4.3. Electrochemical Impedance Spectroscopy

As the ORR is a reaction that occurs at the interface of catalyst and the electrolyte, so the interfacial studies are very crucial in understanding the electrocatalytic activity of the electrode. Electrochemical impedance spectroscopy (EIS) stands as one of the very important diagnostic tool to evaluate the interfacial properties of the catalyst. The well-known Ohm's law is valid only for one circuit element i.e., ideal resistor. The complex circuit elements that are common cannot be understood by the simple Ohm's law. Hence, to evaluate more general and complex circuit parameters, EIS is used. Impedance like resistance is the ability to obstruct the flow of electrons. In an EIS experiment, in the case of ORR catalyst analysis, a minute sinusoidal perturbation is applied to the potential difference between the working electrode and the

reference electrode, and current associated is analyzed in the frequency domain in terms of impedance. Generally, the sinusoidal variation is applied at the open-circuit voltage of the half cell. As EIS is a complex term it consists of both real (Z_{real}) and imaginary (Z_{im}) impedance.

$$Z(\omega) = \frac{E}{I} = Z_0(cos\emptyset + jsin\emptyset)$$

Here, Z(ω) is the impedance at certain frequency ω, E is the small potential applied, I is the response current, ϕ is the shift in the phase in the response signal and j is the complex function. If the real and the imaginary parts of impedance are plotted in X and Y axis respectively, the resulting plot is called as Cole-Cole plot or Nyquist plot. The typical Nyquest plot for carbon based material is seen in Figure 1.6 A. These resistances include the resistance of electrode materials and the catalyst. The semi-circle is also influential in evaluating the charge transfer resistance. While the impedance at the lower frequencies are controlled by the diffusion coefficient. The real impedance at the left most part of the Nyquist plot is largely controlled by the ionic and electrical conductivity of the material. The typical Nyquist plot and the equivalent circuit evaluating various elements for the Pt-carbon[90] are shown in Figure 1.6 B.

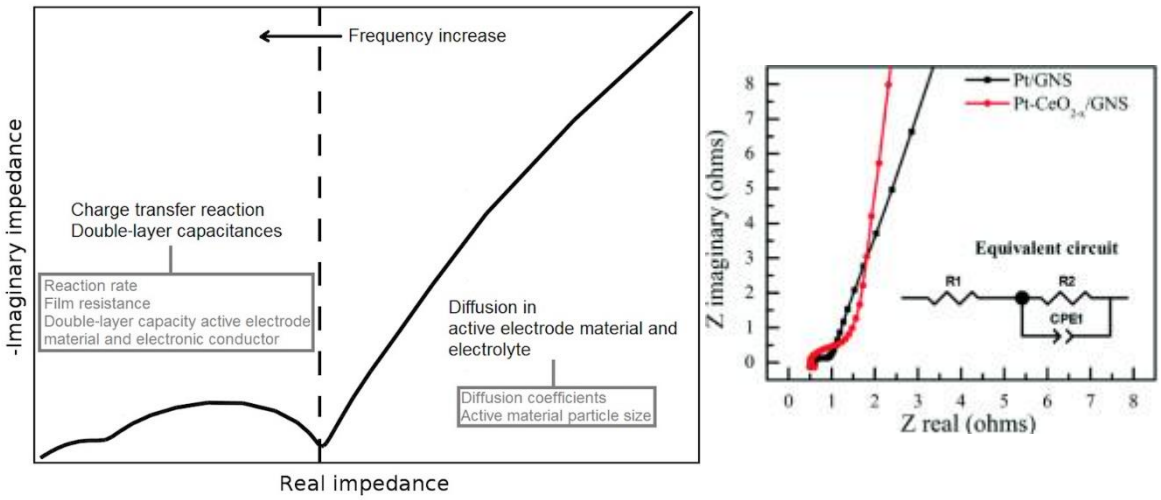

Figure 1.6 Typical Nyquist plot and contribution to various properties (A) and Nyquist plot of Pt-carbon and the corresponding equivalent circuit (Ref. 91).

1.5. Introduction to Devices Functioning on ORR

Devices functioning on ORR can be broadly divided into two kinds. They are, energy conversion and energy storage devices. The flagship devices for these two kinds are fuel cells and metal air batteries, respectively.

1.5.1. Fuel Cell

Generally energy conversion devices convert the chemical energy of fuel into direct current electricity (DC). Typically energy conversion from fuel to electricity is a multistep energy conversion process. They are,

a) Combustion of fuel to generate heat (conversion from fuel to heat)
b) This heat is used in conversion of water to steam
c) Steam is then used to run a turbine (conversion of thermal energy to mechanical)
d) Finally the turbine runs to generate electricity (conversion of mechanical energy to electrical energy)

Fuel cell by-passes all these steps and generates electricity from fuel in a single step. This makes the fuel cell very attractive. Thus, a fuel cell is a device that converts chemical energy of the fuel to electrical energy in a single step. The working of fuel cell is analogous to a battery being recharged with fresh reactants. The construction of fuel cell is similar to that of battery comprising a positive anode and negative cathode sandwiching an electrolyte which is an ionic conductor (Figure 1.7). The fuel cell is very different from other energy conversion technologies (heat engines) which work on raising the temperature of the working fluid. For any heat engine, the maximum efficiency is defined by Carnot process and limited by Carnot efficiency limitation. It is the maximum efficiency of the heat engine which can be calculated if the temperature extremes are known.

$$\text{Carnot efficiency} = \frac{T_H - T_L}{T_H}$$

Here, T_H is the absolute high temperature and T_L is the absolute low temperature.

Whereas, the theoretical efficiency of a fuel cell is defined as the ratio of two thermodynamic properties.

$$\text{Fuel cell efficiency} = \frac{\Delta G^0}{\Delta H^0}$$

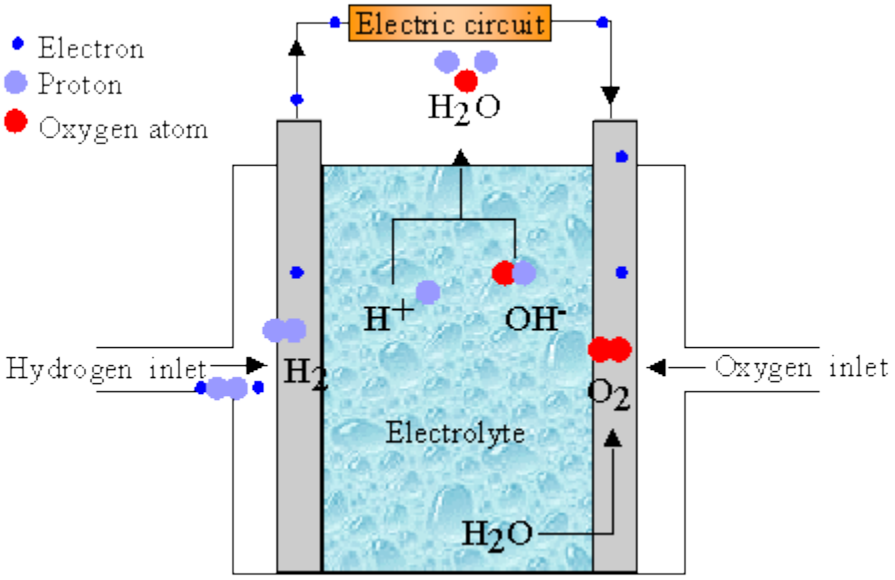

Figure 1.7 Schematic representation of fuel cell

Where, ΔG^0 is the Gibbs free energy or the chemical energy and ΔH^0 is the enthalpy or the total heat energy of the fuel. Theoretical efficiency of the heat engine increases if the temperature is increased in contrast, the Gibbs free energy decreases with increase in temperature with enthalpy being largely unchanged. Thus, the fuel cell's efficiency decreases on increasing the temperature.

The purpose of fuel cell is to convert chemical energy of the fuel into electrical energy. Most of the fuel cells work on hydrogen as fuel. When hydrogen is fed to fuel cell, it gets oxidized by giving away one of its electron to the anode to form a proton. The electron from the anode provides the current externally. Oxygen at the cathode gets reduced with the electrons that are generated at the anode to complete the electrical circuit. The positively charged hydrogen ion

travels through the electrolyte to react with the negatively charged oxygen atoms to form water. Fuel cells are broadly classified into six different types basing on the type of electrolyte that is used. All of there have different characteristics with differing advantages and disadvantages. Figure 1.8[91] summarizes the six types of fuel cells and operation conditions.

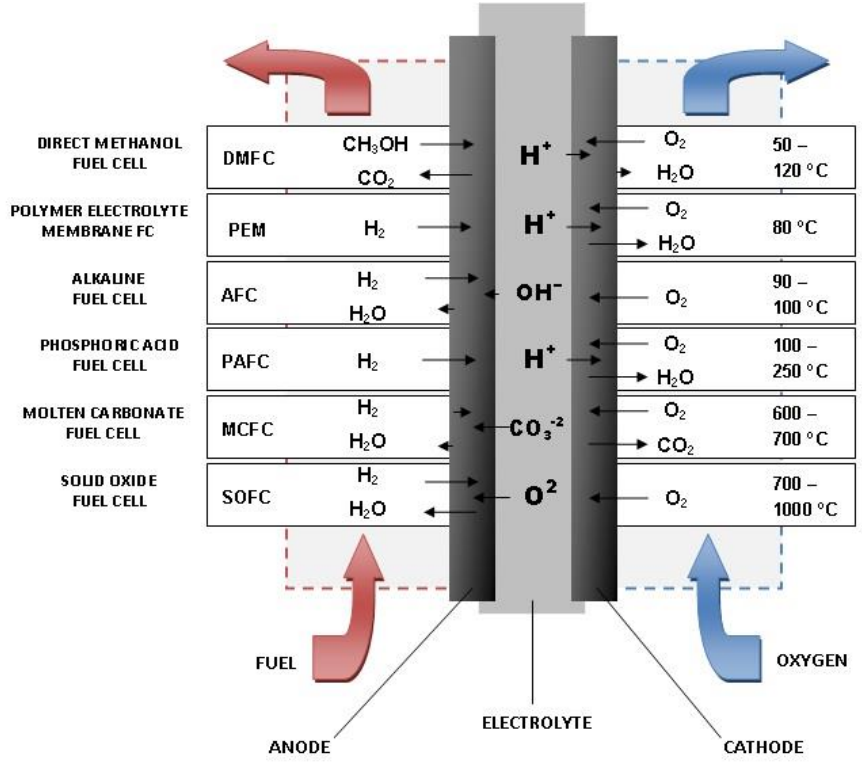

Figure 1.8 Various types of fuel cells and their operation conditions (Ref. 92)

Proton Exchange Membrane Fuel Cell:

In the recent years, proton exchange membrane fuel cell (PEMFC) has attracted lot of attention and is considered to be a promising candidate for portable application and electric vehicles. The attention is owing to its high energy density, minimum/no emission, relatively low operation temperatures and less corrosion problems.

The PEM fuel consists of a polymer membrane which is impermeable to gases and permeates only protons hence the name of PEMFC(Figure 1.9)[92]. The polymer membrane acts as the electrolyte sandwiched between two porous electrically conducting electrodes (usually carbon cloth or paper) which is coated with the catalyst (generally Pt/C). The electrochemical reaction

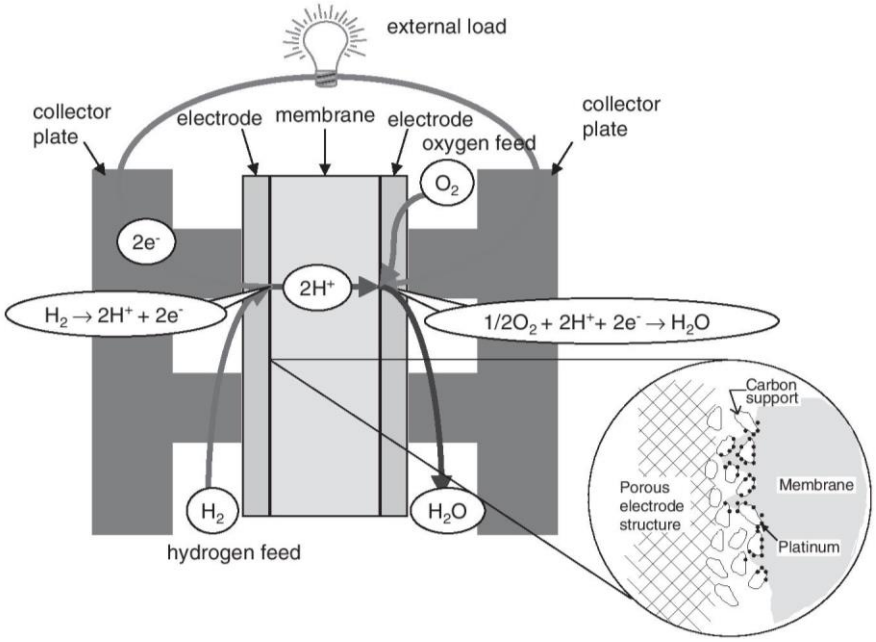

Figure 1.9 Schematic explaining the working of PEMFC (Ref. 93)

at both the ends happens at the interface of electrolyte and the membrane. The electrochemical reaction that happens at the anode is the oxidation of hydrogen generating the proton and an electron and the oxygen is reduced at cathode with the electron that is generated at the anode travels externally to complete the circuit. The complete reduction of oxygen generates H_2O through a four electron process and the partial reduction to produce peroxide through a two electron process. The partial reduction is the main cause for the reduction of efficiency of the PEMFC.

The following are the reactions that happens at the anode and cathode,

$$H_2 \rightarrow 2H^+ + 2e^- \qquad E^0 = 0\ V\ vs\ SHE$$

$$\frac{1}{2}O_2 + 2H^- + 2e^- \rightarrow H_2O \qquad E^0 = 1.23\ V\ vs\ SHE$$

The oxygen reduction reaction at cathode is the rate determining reaction for the fuel cell. The sluggish kinetics of the ORR causes large over-potential that hampers the performance of the fuel cell. Thus a highly active ORR electrocatalyst which enhances the performance of the PEMFC is the need of the hour.

1.5.2. Metal Air Batteries

Rise in the global warming pushed the world to think of green energy with less emission. This leads to the development of several renewable energy sources like solar, wind, hydropower and other renewable energy sources. The development of high energy storage systems is very essential to store the energy which is generated from these technologies. Various energy storage technologies available at present can be classified into four types; mechanical, electrical, electrochemical and chemical. Various interesting features like pollution free operation, high round trip efficiency, durability and low/no maintenance makes electrochemical energy storage very popular amongst others. Owing to their intrinsic properties mentioned above, batteries are the most renowned energy storage technology. The energy storage systems can be assessed by some basic parameters, such as energy density (Wh/L), specific energy (Wh/kg), power density (W/L), specific power (W/kg), cyclability, safety and cost. Along with the storage of energy, batteries are also used for powering various portable devices. In a futuristic view to replace fossil fuels with other alternatives for emission less electric vehicles (EVs), batteries are most reliable. To realize the EVs, batteries with high specific energy and power for long driving range and high acceleration respectively are prerequisites. To replace gasoline which has the theoretic specific energy of 13000 Wh/kg and energy conversion efficiency of 12.6% achieved i.e., 1700 Wh/kg is still long way to be replaced with the best of available battery technology with specific energy of 100 – 200 Wh/kg. Therefore, novel strategies to develop higher energy densities are desirable. At this juncture, the beginning of metal air battery marked a leap in the energy density as one of its cathode is air and is not stored. Various metal air batteries have been developed such as lithium-air, zinc-air, magnesium-air, and aluminum-air batteries. These are found to be very promising for the generation of EVs because the oxygen from air which

is one of the reactant is not stored inside the battery but directly utilizes from the atmosphere. Amongst all, lithium air battery shows the highest theoretical energy density almost equal to that of gasoline i.e. oxidation of 1 kg of lithium metal releases around 11680 Wh/kg. The present day metal air batteries such as zinc air battery achieved 40-50% of their theoretical density. In similar lines a safe assumption of completely developed Li air battery can be made to have 1700 Wh/kg which is 14.5% of its theoretical energy density (Figure 1.10)[93].

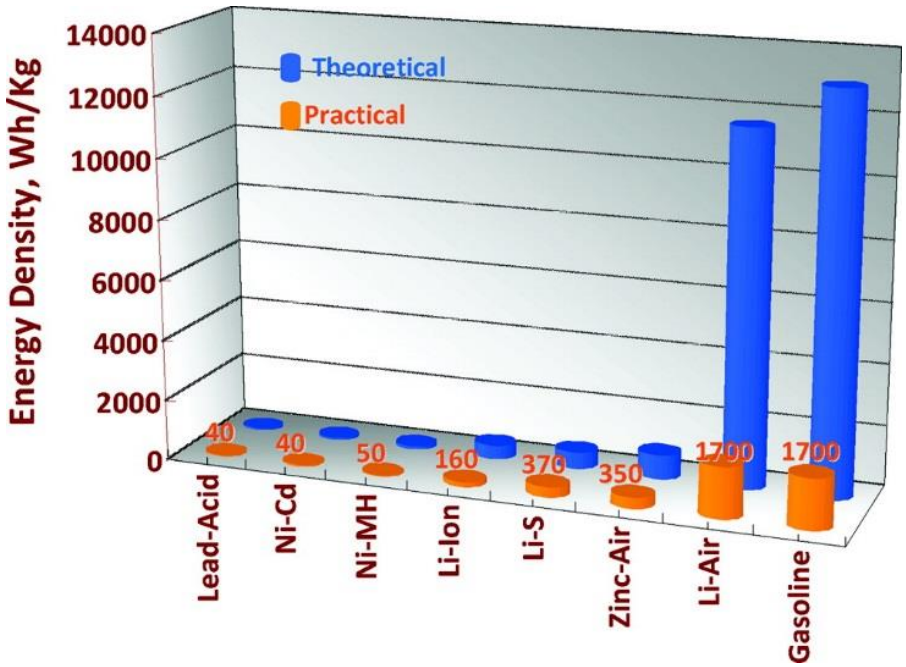

Figure 1.10 The gravimetric energy densities (Wh/kg) for various types of rechargeable batteries compared to gasoline (Ref. 94).

Typical Li air battery consists of Li metal as anode, porous carbon with catalyst as supporting the reduction of gaseous cathode oxygen and an ionically conducting electrolyte. Depending the type of electrolyte used there are four types of Li air batteries shown in Figure 1.11.

The four types of electrolytes used along with lithium salt are;

i. Non-aqueous (aprotic) solvents

ii. Aqueous solvents

iii. Hybrid (aqueous/non-aqueous) solvents and

iv. All solid-state electrolyte

The electrochemical reactions at cathode majorly depends on the electrolyte used. The following are the electrochemical reactions that are taking place both anode and cathode.

Anode:

$Li \leftrightarrow Li^+ + e^-$

Cathode:

$Alkaline\ O_2 + 2H_2O + 4e^- \leftrightarrow 4OH^-\ (E_0 = 3.43\ V\ vs\ Li/Li^+)$

$Acid\ O_2 + 4e^- + 2H^+ \leftrightarrow 2H_2O\ (E_0 = 4.26\ V\ vs\ Li/Li^+)$

$Nonaqueous\ 2Li^+ + 2e^- + O_2 \leftrightarrow Li_2\ O_2\ (E_0 = 2.96\ V\ vs\ Li/Li^+)$

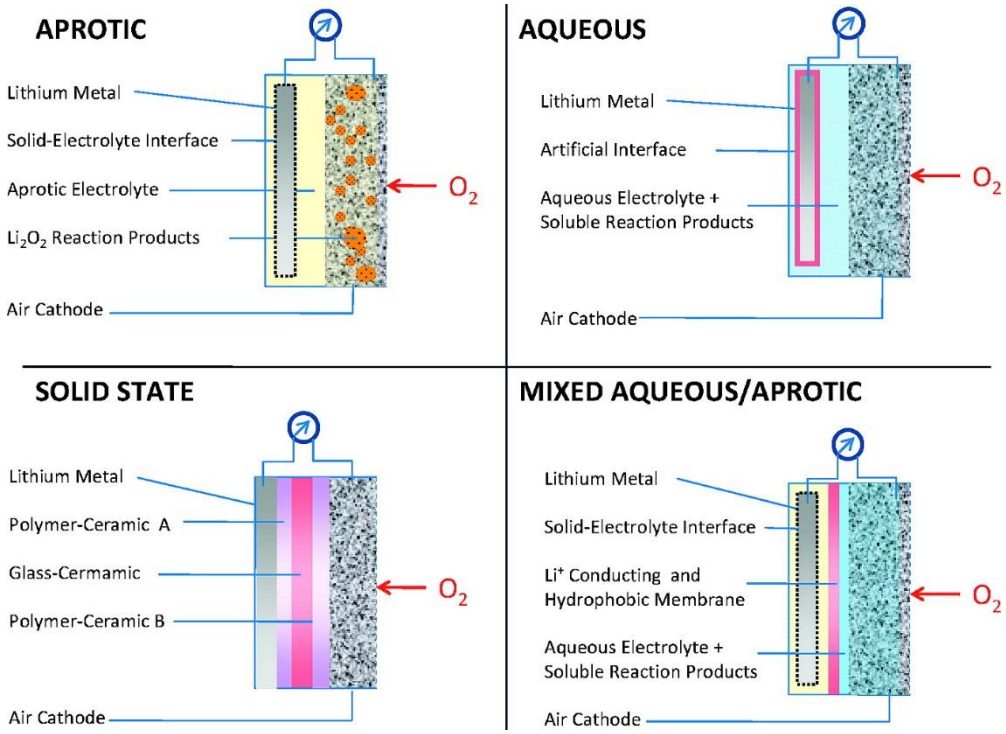

Figure 1.11 Four different architectures of Li-air batteries, which all assume the use of lithium metal as the anode (Ref. 94).

In the recent years, the nonaqueous systems were found to be a practical idea for rechargeable and safe lithium air batteries. As seen above, the principle reaction at cathode is very crucial to achieve rechargeable batteries. The reduction of oxygen (ORR) at cathode is the rate determining step of the lithium air battery which decides the rate of charge and discharge and the specific energy of the rechargeable battery. The formation and decomposition Li_2O_2 is the prerequisite for the practical rechargeable battery. It was found that the use of inefficient

catalyst will lead to the formation of insoluble LiO_2. Though there are various challenges that needs to be solved before realization of commercial Li air battery, optimization of ORR catalyst being the most crucial challenge amongst all.

1.6. Problems Associated in Designing and Commercialization of ORR Catalysts

Fuel cells and Li-air battery due to their high energy density, prolonged durability with low emission of global warming gases have gained greater significance among many electrochemical devices. The similarity in working of fuel cells and metal air batteries is that the ORR happens at the cathode end. Electrocatalyst plays an important role in realization of both these devices due to the sluggish kinetics of ORR. The sluggish kinetics cause overpotential at the cathode which is responsible for major voltage loss in PEMFC and low round trip efficiency of the Li air battery. Hence, the need for an efficient cathode material has been under constant research.

The two interconnected materials forming the ORR catalyst are the porous carbon support and the metal nanoparticles at which ORR actually happens. So the support and the catalytic particles need a careful and strategic optimization.

The durability of the fuel cell and the cyclability of the Li air battery are largely dependent on the carbon support that is used. The development of nanoscience and technology lead the researchers to develop various carbon based allotropes such as carbon blacks, nanostructured carbon, functionalized carbon, diamond like carbon, graphite, fullerenes, carbon nanotubes, graphene and various 3D carbon architectures. Though there are various types of carbon materials the following are the challenges that are still needed to be solved to realize the material as well as the energy device commercially. They are, 1) high surface area 2) low oxidation of carbon at operation potentials of fuel cell and metal air batteries 3) optimizing a trade-off between the functionalization, conductivity and durability 4) ability to anchor the

catalyst 5) pore size to enhance the percolation of air (oxygen) and formation and decomposition of Li_2O_2 in fuel cells and Li air battery respectively 6) as ORR occurs at the interface of electrolyte and the catalyst, lowering the charge transfer resistance plays a key role in improving the kinetics of the ORR and 7) last but not the least the arduous preparation procedures and the cost of processing.

The performance of the devices gets greatly influenced by the improvement of the catalytic behaviour of the catalyst due to improvement in the kinetics of the ORR. The challenges in the designing the ORR catalytic nanostructures are 1) durability of catalyst, weak interaction of the catalyst to the substrate leads to the dissolution and agglomeration of the particles 2) optimization particle size, low particle sizes usually enhance the electrochemically active surface area but agglomerates to form clusters on cycling or on longer run 3) the cost of the catalyst (Pt) is more than 75% of the cost of the device, high cost of Pt poses a great challenge and give a great scope for research 4) non-greener and multi-step methods of catalyst preparation.

The above are challenges that gives a lot of scope for research in the area of ORR catalyst to enhance the activity of the fuel cells and metal air batteries.

1.7. Novel Methodologies in Tackling the Problems Associated

The above challenges gives a lot of scope for the improvement of catalyst as well as the clues to tackle various challenges. Most of the above challenges can be tackled by using two novel methodologies. They are,

1.7.1. Need for Novel Substrates for ORR Catalysts

The advancement in the field of material science and nano-technology has led to the discovery of many novel carbon material in varied dimensional orders, such as fullerene, carbon nano-tubes (CNT), graphene, carbon blacks etc., as an effective support for ORR catalyst. The

attributes looked for an efficient ORR catalyst of choice are a) should possess high surface area of carbon support b) ability to support the catalyst c) high pore size d) negligible charge transfer resistance and e) high cyclability. All the aforementioned properties also affect the kinetics of cathode reaction. The wonder material, 'graphene' though shows amazing performance is hindered from commercialization due to its arduous process of preparation. Though bulk preparation of graphene based materials were made using various chemical procedures, the reduction in the conductivity and durability of the graphene oxide and reduced graphene oxide (graphene equivalent) found to be not a feasible method. Hence, looking for an alternative material with high electronic conductivity, high surface area, decent trade-off between the functional groups to form SMSI and durability is the need of the hour.

1.7.2. Need for Novel Methods to Prepare ORR Catalysts

Pt based carbon catalyst possesses unique and high electrocatalytic activity of oxygen reduction reaction as well as hydrogen adsorption and desorption which also are important parameters to evaluate the catalyst. However, large scale commercial applications are precluded by the high manufacturing cost of the catalyst. High cost can be correlated not only to the cost of Pt alone but also the efficient methods to make the catalysts. The general methods which are used for the decoration of metal nanoparticles on to carbon substrates are basically carried out by employing a sacrificial reducing agents (SRA) like alcohols or other reducing agents at elevated temperatures, which are against the green approach. Hence alternative methodologies not only to make efficient catalyst but to make catalyst efficiently are the need of the hour.

References:

(1) Bruce, P. G.; Freunberger, S. A.; Hardwick, L. J.; Tarascon, J.-M. Li-O_2 and Li-S batteries with high energy storage. *Nat. mater.,* 2012, *11*, 19–29.

(2) http://www.hydrogen.energy. gov/pdfs/review11/tv001_wipke_2011_o.pdf - Google Search, 2016.

(3) Bell, A. T. The impact of nanoscience on heterogeneous catalysis. *Science*, 2003, *299*, 1688–1691.

(4) Li, Y.; Somorjai, G. A. Nanoscale advances in catalysis and energy applications. *Nano lett.*, 2010, *10*, 2289–2295.

(5) Zaera, F. New challenges in heterogeneous catalysis for the 21st century. *Catalysis Letters*, 2012, *142*, 501–516.

(6) Zaera, F. The new materials science of catalysis: Toward controlling selectivity by designing the structure of the active site. *J. Phys. Chem. Lett.*, 2010, *1*, 621–627.

(7) Weckhuysen, B. M. Heterogeneous catalysis: Catch me if you can! *Nat. chem.*, 2009, *1*, 690–692.

(8) Somorjai, G. A.; Frei, H.; Park, J. Y. Advancing the frontiers in nanocatalysis, biointerfaces, and renewable energy conversion by innovations of surface techniques. *J.Am.Chem. Soc.*, 2009, *131*, 16589–16605.

(9) Macia, M. D.; Campina, J. M.; Herrero, E.; Feliu, J. M. On the kinetics of oxygen reduction on platinum stepped surfaces in acidic media. *J.Electroanal.Chem.*, 2004, *564*, 141–150.

(10) Markovic, N. M.; Gasteiger, H. A.; Ross Jr, P. N. Oxygen reduction on platinum low-index single-crystal surfaces in sulfuric acid solution: rotating ring-Pt (hkl) disk studies. *The*

J.Phys.Chem., 1995, *99*, 3411–3415.

(11) Hsueh, K. L.; Gonzalez, E. R.; Srinivasan, S. Electrolyte effects on oxygen reduction kinetics at platinum: a rotating ring-disc electrode analysis. *Electrochim.Acta*, 1983, *28*, 691–697.

(12) Perez, J.; Villullas, H. M.; Gonzalez, E. R. Structure sensitivity of oxygen reduction on platinum single crystal electrodes in acid solutions. *J.Electroanal.Chem.*, 1997, *435*, 179–187.

(13) Zhang, T.; Anderson, A. B. Oxygen reduction on platinum electrodes in base: Theoretical study. *Electrochim. Acta*, 2007, *53*, 982–989.

(14) Anderson, A. B.; Roques, J.; Mukerjee, S.; Murthi, V. S.; Markovic, N. M.; Stamenkovic, V. Activation energies for oxygen reduction on platinum alloys: Theory and experiment. *J. Phys-Chem. B*, 2005, *109*, 1198–1203.

(15) Albu, T. V.; Anderson, A. B. Studies of model dependence in an ab initio approach to uncatalyzed oxygen reduction and the calculation of transfer coefficients. *Electrochim. Acta*, 2001, *46*, 3001–3013.

(16) Anderson, A. B.; Albu, T. V. Catalytic effect of platinum on oxygen reduction an ab initio model including electrode potential dependence. *J. Electrochem. Soc.*, 2000, *147*, 4229–4238.

(17) Anderson, A. B.; Albu, T. V. Ab initio approach to calculating activation energies as functions of electrode potential: trial application to four-electron reduction of oxygen. *Electrochem. Commun.*, 1999, *1*, 203–206.

(18) Toda, T.; Igarashi, H.; Uchida, H.; Watanabe, M. Enhancement of the electroreduction of oxygen on Pt alloys with Fe, Ni, and Co. *J. Electrochem. Soc.*, 1999, *146*, 3750–3756.

(19) Hartnig, C.; Koper, M. T. Molecular dynamics simulation of the first electron transfer step in the oxygen reduction reaction. *J. Electroanal. Chem.*, 2002, *532*, 165–170.

(20) Sha, Y.; Yu, T. H.; Merinov, B. V.; Shirvanian, P.; Goddard III, W. A. Oxygen hydration

mechanism for the oxygen reduction reaction at Pt and Pd fuel cell catalysts. *J. Phys. Chem. Lett.*, 2011, *2*, 572–576.

(21) Yeh, K.; Janik, M. J. Density functional theory-based electrochemical models for the oxygen reduction reaction: Comparison of modeling approaches for electric field and solvent effects. *Journal of Computational Chemistry*, 2011, *32*, 3399–3408.

(22) Janik, M. J.; Taylor, C. D.; Neurock, M. First-principles analysis of the initial electroreduction steps of oxygen over Pt (111). *J. Electrochem. Soc.*, 2009, *156*, B126–B135.

(23) Nørskov, J. K.; Rossmeisl, J.; Logadottir, A.; Lindqvist, L. R. K. J.; Kitchin, J. R.; Bligaard, T.; Jonsson, H. Origin of the overpotential for oxygen reduction at a fuel-cell cathode. *J. Phys-Chem. B*, 2004, *108*, 17886–17892.

(24) Stamenkovic, V.; Mun, B. S.; Mayrhofer, K. J.; Ross, P. N.; Markovic, N. M.; Rossmeisl, J.; Greeley, J.; Nørskov, J. K. Changing the activity of electrocatalysts for oxygen reduction by tuning the surface electronic structure. *Angew. Chem. Int. Ed. Engl.*, 2006, *118*, 2963–2967.

(25) Tripković, V.; Skúlason, E.; Siahrostami, S.; Nørskov, J. K.; Rossmeisl, J. The oxygen reduction reaction mechanism on Pt (111) from density functional theory calculations. *Electrochim. Acta*, 2010, *55*, 7975–7981.

(26) Yu, W.; Porosoff, M. D.; Chen, J. G. Review of Pt-based bimetallic catalysis: from model surfaces to supported catalysts. *Chem. Rev.,* 2012, *112*, 5780–5817.

(27) Fournier, J.; Lalande, G.; Guay, D.; Dodelet, J. Activation of Various Fe-Based Precursors on Carbon Black and Graphite Supports to Obtain Catalysts for the Reduction of Oxygen in Fuel Cells. *J. Electrochem. Soc.*, 1997, *144*, 218–226.

(28) Gao, M.; Gao, Q.; Jiang, J.; Cui, C.; Yao, W.; Yu, S. A Methanol-Tolerant Pt/$CoSe_2$ Nanobelt Cathode Catalyst for Direct Methanol Fuel Cells. *Angew. Chem. Int. Ed. Engl.*, 2011, *123*, 5007–5010.

(29) Esposito, D. V.; Chen, J. G. Monolayer platinum supported on tungsten carbides as low-

cost electrocatalysts: opportunities and limitations. *Energy & Environmental Science*, 2011, *4*, 3900–3912.

(30) Dodelet, J.P. Oxygen reduction in PEM fuel cell conditions: heat-treated non-precious metal-N4 macrocycles and beyond. *N4-macrocyclic metal complexes*, Springer Science & Business Media, 2007, 83-139.

(31) Suntivich, J.; May, K. J.; Gasteiger, H. A.; Goodenough, J. B.; Shao-Horn, Y. A perovskite oxide optimized for oxygen evolution catalysis from molecular orbital principles. *Science*, 2011, *334*, 1383–1385.

(32) Strasser, P.; Koh, S.; Anniyev, T.; Greeley, J.; More, K.; Yu, C.; Liu, Z.; Kaya, S.; Nordlund, D.; Ogasawara, H. Lattice-strain control of the activity in dealloyed core–shell fuel cell catalysts. *Nat. Chem.*, 2010, *2*, 454–460.

(33) Kitchin, J. R.; Nørskov, J. K.; Barteau, M. A.; Chen, J. G. Modification of the surface electronic and chemical properties of Pt (111) by subsurface 3d transition metals. *J. Chem. Phys.*, 2004, *120*, 10240–10246.

(34) Li, J.-B.; Huang, T.-S.; Chen, A.-C.; Sun, S.-G.; Tian, Z.-W. Electrocatalytic properties of Pt(111), Pt(332), Pt(331) and Pt(110) single crystal electrodes towards ethylene glycol oxidation in sulphuric acid solutions. *Journal of Electroanalytical Chemistry*, 1992, *340*, 213–226.

(35) Blakely, D. W.; Somorjai, G. A. Mechanism of catalysis of hydrocarbon reactions by platinum surfaces. *Nature*, 1975, *258*.

(36) Narayanan, R.; El-Sayed, M. A. Catalysis with transition metal nanoparticles in colloidal solution: nanoparticle shape dependence and stability. *Jour. Phys. Chem. B*, 2005, *109*, 12663–12676.

(37) Wang, C.; Daimon, H.; Lee, Y.; Kim, J.; Sun, S. Synthesis of monodisperse Pt nanocubes and their enhanced catalysis for oxygen reduction. *J. Am. Chem. Soc.*, 2007, *129*,

6974–6975.

(38) Wang, C.; Daimon, H.; Onodera, T.; Koda, T.; Sun, S. A General approach to the size- and shape-controlled synthesis of platinum nanoparticles and their catalytic reduction of oxygen. *Angew. Chem. Int. Ed. Engl.*, 2008, *47*, 3588–3591.

(39) Wang, Z. L.; Ding, Y.; Sun, S.-G.; Zhou, Z.-Y.; Tian, N. Synthesis of tetrahexahedral platinum nanocrystals with high-index facets and high electro-oxidation activity. *Science*, 2007, *316*, 732–735.

(40) Yu, T.; Kim, D. Y.; Zhang, H.; Xia, Y. Platinum concave nanocubes with high-index facets and their enhanced activity for oxygen reduction reaction. *Angew. Chem. Int. Ed. Engl.*, 2011, *50*, 2773–2777.

(41) Greeley, J.; Stephens, I. E. L.; Bondarenko, A. S.; Johansson, T. P.; Hansen, H. A.; Jaramillo, T. F.; Rossmeisl, J.; Chorkendorff, I. N. J. K.; Nørskov, J. K. Alloys of platinum and early transition metals as oxygen reduction electrocatalysts. *Nat. Chem.*, 2009, *1*, 552–556.

(42) Stamenkovic, V. R.; Fowler, B.; Mun, B. S.; Wang, G.; Ross, P. N.; Lucas, C. A.; Marković, N. M. Improved oxygen reduction activity on Pt_3Ni (111) via increased surface site availability. *Science*, 2007, *315*, 493–497.

(43) Kitchin, J. R.; Nørskov, J. K.; Barteau, M. A.; Chen, J. G. Role of strain and ligand effects in the modification of the electronic and chemical properties of bimetallic surfaces. *Phys. Rev. Lett.*, 2004, *93,* 156801(1) -156801(4).

(44) Stamenkovic, V. R.; Mun, B. S.; Arenz, M.; Mayrhofer, K. J.; Lucas, C. A.; Wang, G.; Ross, P. N.; Markovic, N. M. Trends in electrocatalysis on extended and nanoscale Pt-bimetallic alloy surfaces. *Nat. Mat.*, 2007, *6*, 241–247.

(45) Dai, Y.; Ou, L.; Liang, W.; Yang, F.; Liu, Y.; Chen, S. Efficient and superiorly durable Pt-lean electrocatalysts of Pt− W alloys for the oxygen reduction reaction. *J. Phys. Chem. C.*, 2011, *115*, 2162–2168.

(46) Zhang, J.; Fang, J. A general strategy for preparation of Pt 3d-transition metal (Co, Fe, Ni) nanocubes. *J. Am. Chem. Soc.*, 2009, *131*, 18543–18547.

(47) Wang, C.; Chi, M.; Li, D.; van der Vliet, D.; Wang, G.; Lin, Q.; F. Mitchell, J.; More, K. L.; Markovic, N. M.; Stamenkovic, V. R. Synthesis of Homogeneous Pt-bimetallic nanoparticles as highly efficient electrocatalysts. *ACS Catalysis*, 2011, *1*, 1355–1359.

(48) Kim, J.; Rong, C.; Liu, J. P.; Sun, S. Dispersible ferromagnetic FePt nanoparticles. *Adv. Mat.*, 2009, *21*, 906–909.

(49) Kang, Y.; Murray, C. B. Synthesis and electrocatalytic properties of cubic mn−pt nanocrystals (nanocubes). *J. Am. Chem. Soc.* **2010**, *132*, 7568–7569.

(50) Yu, Y.; Yang, W.; Sun, X.; Zhu, W.; Li, X.-Z.; Sellmyer, D. J.; Sun, S. Monodisperse MPt (M= Fe, Co, Ni, Cu, Zn) nanoparticles prepared from a facile oleylamine reduction of metal salts. *Nano lett.*, 2014, *14*, 2778–2782.

(51) Zhao, D.; Xu, B. Enhancement of Pt utilization in electrocatalysts by using gold nanoparticles. *Angew. Chem. Int. Ed. Engl.*, 2006, *118*, 5077–5081.

(52) Wang, Y.; Toshima, N. Preparation of Pd-Pt bimetallic colloids with controllable core/shell structures. *J. Phys. Chem. B*, 1997, *101*, 5301–5306.

(53) Zhou, S.; Varughese, B.; Eichhorn, B.; Jackson, G.; McIlwrath, K. Pt–Cu core–shell and alloy nanoparticles for heterogeneous NOx reduction: anomalous stability and reactivity of a core–shell nanostructure. *Angew. Chem. Int. Ed. Engl.*, 2005, *117*, 4615–4619.

(54) Chen, Y.; Liang, Z.; Yang, F.; Liu, Y.; Chen, S. Ni–Pt core–shell nanoparticles as oxygen reduction electrocatalysts: effect of Pt shell coverage. *J. Phys. Chem. C*, 2011, *115*, 24073–24079.

(55) Sasaki, K.; Naohara, H.; Cai, Y.; Choi, Y. M.; Liu, P.; Vukmirovic, M. B.; Wang, J. X.; Adzic, R. R. Core-protected platinum monolayer shell high-stability electrocatalysts for fuel-cell cathodes. *Angew. Chem. Int. Ed. Engl.*, 2010, *49*, 8602–8607.

(56) Wang, C.; Chi, M.; Li, D.; Strmcnik, D.; Van der Vliet, D.; Wang, G.; Komanicky, V.; Chang, K.-C.; Paulikas, A. P.; Tripkovic, D. Design and synthesis of bimetallic electrocatalyst with multilayered Pt-skin surfaces. *J. Am. Chem. Soc.*, 2011, *133*, 14396–14403.

(57) Bagotsky, V. S. *Fuel Cells*; John Wiley & Sons, Inc, 2012, 227.

(58) Sun, S. H.; Yang, D. Q.; Villers, D.; Zhang, G. X.; Sacher, E.; Dodelet, J.-P. Template- and surfactant‐free room temperature synthesis of self‐assembled 3d pt nanoflowers from singl-crystal nanowires. *Adv. Mater.*, 2008, *20*, 571–574.

(59) Alia, S. M.; Zhang, G.; Kisailus, D.; Li, D.; Gu, S.; Jensen, K.; Yan, Y. Porous platinum nanotubes for oxygen reduction and methanol oxidation reactions. *Adv. Func. Mater.*, 2010, *20*, 3742–3746.

(60) Lim, B.; Jiang, M.; Camargo, P. H.; Cho, E. C.; Tao, J.; Lu, X.; Zhu, Y.; Xia, Y. Pd-Pt bimetallic nanodendrites with high activity for oxygen reduction. *Science*, 2009, *324*, 1302–1305.

(61) Ralph, T. R.; Hogarth, M. P. Catalysis for low temperature fuel cells. *Platinum Metals Review*, 2002, *46*, 117–135.

(62) Hall, S. C.; Subramanian, V.; Teeter, G.; Rambabu, B. Influence of metal–support interaction in Pt/C on CO and methanol oxidation reactions. *Solid State Ionics*, 2004, *175*, 809–813.

(63) Esmaeilifar, A.; Rowshanzamir, S.; Eikani, M. H.; Ghazanfari, E. Synthesis methods of low-Pt-loading electrocatalysts for proton exchange membrane fuel cell systems. *Energy*, 2010, *35*, 3941–3957.

(64) Cuong, N. T.; Chi, D. H.; Kim, Y.-T.; Mitani, T. Structural and electronic properties of Ptn (n = 3, 7, 13) clusters on metallic single wall carbon nanotube. *Physica Status Solidi (B)*, 2006, *243*, 3472–3475.

(65) Skundin, A. M.; Bagotzky, V. S. Electrocatalysts on supports—I. Electrochemical and

adsorptive properties of platinum microdeposits on inert supports. *Electrochim. Acta*, 1984, *29*, 757–765.

(66) Hillenbrand, L. J.; Lacksonen, J. W. The Platinum-on-carbon catalyst system for hydrogen anodes: II. chemical requirements of the carbon surface. *J. Electrochem. Soc.*, 1965, *112*, 249–252.

(67) Coloma, F.; Sepúlveda-Escribano, A.; Fierro, J. L. G.; Rodríguez-Reinoso, F. Crotonaldehyde hydrogenation over bimetallic Pt-Sn catalysts supported on pregraphitized carbon black. Effect of the preparation method. *Applied Catalysis A: General*, 1996, *148*, 63–80.

(68) Shukla, A. K.; Ravikumar, M. K.; Roy, A.; Barman, S. R.; Sarma, D. D.; Arico, A. S.; Antonucci, V.; Pino, L.; Giordano, N. Electro-oxidation of methanol in sulfuric acid electrolyte on platinized‐carbon electrodes with several functional‐group characteristics. *J. Electrochem. Soc.*, 1994, *141*, 1517–1522.

(69) Eberhardt, W.; Fayet, P.; Cox, D. M.; Fu, Z.; Kaldor, A.; Sherwood, R.; Sondericker, D. Photoemission from mass-selected monodispersed Pt clusters. *Phys. Rev. Lett.*, 1990, *64*.

(70) Dicks, A. L. The role of carbon in fuel cells. *J. Power Sources*, 2006, *156*, 128–141.

(71) Harrison, B.; Dodgson, I. L.; Cooper, S. J.; Cameron, D. S.; Jenkins, J. W. Carbons as supports for precious metal catalysts. *Catalysis Today*, 1990, *7*, 113–137.

(72) Yu, X.; Ye, S. Recent advances in activity and durability enhancement of Pt/C catalytic cathode in PEMFC: Part I. Physico-chemical and electronic interaction between Pt and carbon support, and activity enhancement of Pt/C catalyst. *J. Power Sources*, 2007, *172*, 133–144.

(73) Lecea, C. S.-M. D.; Rodriguez-Reinoso, F.; Linares-Solano, A.; Prado-Burguete, C. Effect of carbon support and mean Pt particle size on hydrogen chemisorption by carbon-supported Pt ctalysts. *J. Catalysis*, 1991, *128*, 397–404.

(74) Lecea, C. S.-M. de; Rodríguez-Reinoso, F.; Linares-Solano, A.; Prado-Burguete, C. The

effect of oxygen surface groups of the support on platinum dispersion in Pt/carbon catalysts. *J. Catalysis*, 1989, *115*, 98–106.

(75) Torres, G. C.; Jablonski, E. L.; Baronetti, G. T.; Castro, A. A.; de Miguel, S. R.; Scelza, O. A.; Blanco, M. D.; Pen˜a Jiménez, M. A.; Fierro, J. L. G. Effect of the carbon pre-treatment on the properties and performance for nitrobenzene hydrogenation of Pt/C catalysts. *Appl. Cat. A: General*, 1997, *161*, 213–226.

(76) Sepúlveda-Escribano, A.; Coloma, F.; Rodríguez-Reinoso, F. Platinum catalysts supported on carbon blacks with different surface chemical properties. *Appl. Cat. A: General*, 1998, *173*, 247–257.

(77) Rodríguez-reinoso, F. The role of carbon materials in heterogeneous catalysis. *Carbon*, 1998, *36*, 159–175.

(78) Chen, S.; Wei, Z.; Guo, L.; Ding, W.; Dong, L.; Shen, P.; Qi, X.; Li, L. Enhanced dispersion and durability of Pt nanoparticles on a thiolated CNT support. *Chem. Commun.*, 2011, *47*, 10984–10986.

(79) Xu, Z.; Qi, Z.; Kaufman, A. Advanced Fuel Cell Catalysts: Sulfonation of Carbon-Supported Catalysts Using 2-Aminoethanesulfonic Acid. *Electrochem. Solid-State Lett.*, 2003, *6*.

(80) Qi, Z.; Kaufman, A.; Xu, Z. High performance carbon-supported catalysts for fuel cells via phosphonation. *Chem. Commun.*, 2003, 878–879.

(81) Xu, Z.; Qi, Z.; Kaufman, A. Superior catalysts for proton exchange membrane fuel cells: sulfonation of carbon-supported catalysts using sulfate salts. *Electrochem. Solid-State Lett.*, 2005, *8*.

(82) Ma, J.; Habrioux, A.; Guignard, N.; Alonso-Vante, N. Functionalizing effect of increasingly graphitic carbon supports on carbon-supported and TiO_2–carbon composite-supported Pt nanoparticles. *J. Phys. Chem. C*, 2012, *116*, 21788–21794.

(83) Ishihara, A.; Ohgi, Y.; Matsuzawa, K.; Mitsushima, S.; Ota, K. Progress in non-precious metal oxide-based cathode for polymer electrolyte fuel cells. *Electrochim. Acta*, 2010, *55*, 8005–8012.

(84) Zhang, X.; Zhu, H.; Guo, Z.; Wei, Y.; Wang, F. Sulfated SnO2 modified multi-walled carbon nanotubes – A mixed proton–electron conducting support for Pt catalysts in direct ethanol fuel cells. *J. Power Sources*, 2011, *196*, 3048–3053.

(85) Saha, M. S.; Banis, M. N.; Zhang, Y.; Li, R.; Sun, X.; Cai, M.; Wagner, F. T. Tungsten oxide nanowires grown on carbon paper as Pt electrocatalyst support for high performance proton exchange membrane fuel cells. *Journal of Power Sources*, 2009, *192*, 330–335.

(86) Du, C.; Chen, M.; Cao, X.; Yin, G.; Shi, P. A novel CNT@SnO_2 core–sheath nanocomposite as a stabilizing support for catalysts of proton exchange membrane fuel cells. *Electrochem. Commun.*, 2009, *11*, 496–498.

(87) Lee, K.-S.; Park, I.-S.; Cho, Y.-H.; Jung, D.-S.; Jung, N.; Park, H.-Y.; Sung, Y.-E. Electrocatalytic activity and stability of Pt supported on Sb-doped SnO_2 nanoparticles for direct alcohol fuel cells. *J. Catalysis*, 2008, *258*, 143–152.

(88) Xiong, L.; Manthiram, A. Synthesis and characterization of methanol tolerant Pt/TiOx/C nanocomposites for oxygen reduction in direct methanol fuel Cells. *Electrochim. Acta*, 2004, *49*, 4163–4170.

(89) Xing, W.; Yin, G.; Zhang, J. *Rotating electrode methods and oxygen reduction electrocatalysts*, Elsevier, 2014, 171-183.

(90) Zhang, L.; Shen, Y. One-Pot Synthesis of Platinum–ceria/graphene nanosheet as advanced electrocatalysts for alcohol oxidation. *ChemElectroChem*, 2015, *2*, 887–895.

(91) Electrodeposition of Functional Coatings on Bipolar Plates for Fuel Cell Applications – A Review | InTechOpen, 2016.

(92) Barbir, F. *PEM Fuel Cells: Theory and practice*; Academic Press, 2012.

(93) Girishkumar, G.; McCloskey, B.; Luntz, A. C.; Swanson, S.; Wilcke, W. Lithium− air battery: promise and challenges. *J. Phys. Chem. Lett.*, 2010, *1*, 2193–2203.

Chapter 2

Platinum Decorated & Functionalized Defective Acetylene Black; A Promising Cathode Material for ORR

2.1. Abstract

Exploring novel carbon substrates for enhancing the dispersion and activity of the metal catalyst and commercially viable simple preparation method is a very crucial area of research in the field of energy materials for fuel cells and Li-air battery. In this regard the present chapter deals with a novel single-pot method to exfoliate and functionalize acetylene black. The deliberate functionalization was found to enhance the intrinsic oxygen reduction efficiency along with the nucleation and growth of platinum nano-particles on the surface. The prepared material was well characterized to understand the morphology, elemental composition and electrocatalytic behaviour. The resulting material showed enormously high oxygen reduction reactivity compared to its commercial counterparts. The mass activity evaluated from the rotating disc electrode (RDE) techniques was found to be higher than the target set by the department of energy (DOE), USA. The material also showed very encouraging results when employed as cathode material for PEMFC.

2.2. Introduction

The global scenario of energy depletion has led to an aggressive outlook for different electrochemical devices, particularly for the ones that use renewable energy. The applications of different types of carbon to electrochemical devices, especially in the field of energy, viz., fuel cells and Li-air battery, are significant, as they project high energy density with prolonged durability. The major limiting factor that affects the efficiency of these devices is the sluggishness of the oxygen reduction reaction (ORR) at the cathode. Hence, the need for an efficient cathode material has been under continuous research. The advancement in the field of material science and nano-technology has led to the discovery of many novel carbon materials in various dimensional orders, such as fullerenes, CNTs, graphene, and carbon black, as an effective support for ORR. These attributes render them as suitable material for the ORR with a high surface area, an ability to support the catalyst, high pore size, negligible charge transfer resistance, and high cyclability[1,2]. All the aforementioned properties also affect the kinetics of the cathode reaction. Graphite, which is currently used in many commercially available electrochemical devices, suffers from disadvantages, such as a low surface area and high charge transfer resistance. Among all the carbon materials, the new material, 'graphene', is superior to the other carbon material for many applications. However, its arduous preparation methods hinder its commercialization. Hence, to reap the benefits of the high energy density devices, there is a need for a novel carbon material with enhanced inherent properties. Recently, researchers have started to revisit acetylene black (AB) as a carbon support for a range of applications[3,4]. Uchida *et al*.[5,6] reported the tremendous activity of AB as a carbon support for proton exchange membrane fuel cells and direct methanol fuel cells. Generally, graphite is used as a cathode material along with carbon black, such as acetylene black (AB), as a binder. Although graphite has better conductivity, acetylene black (AB) can override graphite because of its properties, such as (i) low resistivity in the presence of an electrolyte and an active

electrode material by itself, (ii) ability to absorb and retain a significant volume of electrolyte without reducing its ability to mix with the active material, (iii) high surface area and (iv) low cost compared to its counterparts. AB can become a prospective material for use as an active electrode material by tuning the inherent properties of AB. However, the poor cyclability of AB cannot be overlooked. Preliminary experiments by us indicated the enormous potential of AB as an efficient cathode material. Hence, it was concluded that the properties of AB could be enhanced by modifying the surface with a facile procedure to improve its ability to support the catalyst, reduce the charge transfer resistance, increase its surface area by exfoliating its graphitic layers, and increase its durability. This work presents a simple methodology to make a unique functionalized carbon material. This study also demonstrates the importance of functionalization or defects on the surface of AB to achieve the well dispersed nucleation of Pt over FAB along with enhanced substrate interaction. This functionalization led to an improvement in the overall distribution of Pt-nanoparticles (Pt-np) impregnated over the surface of AB. Also the decorated Pt-nanoparticles were formed as a protective shield against the easy degradation of AB to improve the cyclability of the catalyst.

2.3. Experimental Section

2.3.1. Single Pot Method for Exfoliation and Functionalization of Acetylene Black

1 g of acetylene black (AB) was taken in a round bottom flask, to this around 10 mL of 3:1(volume ratio) conc.H_2SO_4 and conc.HNO_3 mixture was added in a way, such that the entire amount of AB was immersed completely in the acid mixture. The solution was ultrasonicated for 3 hrs at room temperature. The solution was then poured in to 100 mL of distilled water and the mixture was filtered using nylon filter membrane with 0.1 μm pore size. The filtrate was copiously washed with distilled water to remove the acidic contaminants, further the content was washed with methanol and air dried for few minutes. This was then dried at 100 ^oC in a vacuum oven for 2 hrs to get functionalized acetylene black (FAB).

2.3.2. Platinum Decoration onto the Surface of FAB

Chemical reduction method was used for the decoration of Pt nanoparticles (Pt-np) on the surface of FAB. In this method 90 mg of AB or FAB was added to a round bottom flask containing (3.27 mL for obtaining 19 wt% of Pt depositions and 6.55 mL for obtaining 41 wt% of Pt deposition) aqueous solution of 0.0443 M H_2PtCl_6, 8.84 mL of de-ionised water and 40 mL of ethylene glycol. This mixture was ultrasonicated for 4 hrs to ensure uniform dispersion of FAB in ethylene glycol–water solution. After the FAB was uniformly dispersed in the ethylene glycol - water mixture, it was heated at 120 ^oC for 24 hrs with constant stirring. Finally, the 19% (wt/wt) Pt–np decorated FAB (19 wt% Pt-FAB) and 41 wt% Pt-FAB was filtered using 0.1 μm pore sized nylon membrane under vacuum and washed with water and methanol. Then the obtained solid was dried under vacuum at 100 ^oC for 2 hrs.

2.3.3. Physical and Chemical Characterization

The diffraction pattern of the material was characterized by powder X-ray diffraction technique (Smart Lab X-Ray Diffractometer , Rigaku) with Cu Kα radiation (λ = 0.1541 nm, over the 2θ range of 10−70° with a step size of 0.05°). Elemental analysis of the material was studied using X-ray photoelectron spectroscopy (XPS) technique performed on S-probe^{TM} 2803 instrument. The morphological characterization was done by using High Resolution Transmission Electron Microscopy (HR-TEM) instrument Hitachi model H-7650. TEM sample was prepared by dropping a methanolic solution containing well dispersed composite on a carbon coated copper grid. Raman scattering experiment was performed to analyze the defects on FAB and was experiments were conducted on T64000, HORIBA-JY instrument. To find out the exact weight percentage of Pt present in Pt-FAB, Inductively Coupled Plasma Mass Spectrometry (ICP-MS) measurements were done.

2.3.4. Electrochemical Characterization

The electrocatalysts were characterized in conventional three electrode system. Glassy carbon

electrode coated with the Pt-FAB was used as working electrode, a Pt wire and Reversible Hydrogen Electrode (RHE) were used as counter and reference electrodes in all the experiments unless otherwise it is mentioned. All the experiments were conducted in 0.1 M $HClO_4$ electrolyte saturated with nitrogen at 30 ^oC for cyclicvoltammetry (CV) experiments and electrochemical impedance spectroscopic analysis. Prior to ORR measurements using RDE the electrolyte was saturated with oxygen at 30 ^oC. A stable CV was obtained before starting the RDE experiment. In RDE experiments the electrode was rotated at 400 to 3000 rpm and subjected to linear sweep voltammetry (LSV) between 0.05 and 1.00 V with respect to RHE at a scan rate of 20 mV s^{-1}.

2.4. Results and Discussion

2.4.1. Physical and Chemical Characterization

To evaluate the percentage of Pt decorated on to AB, FAB ICP-MS was performed and it was found that the percentage of Pt was 18.9 wt% and 41.4 wt%. Thus the materials are named as 19 wt% Pt-FAB and 41 wt% Pt-FAB.

X-ray powder diffraction (XRD) was used to examine the crystallinity of carbon and Pt-nps. Figure 2.1 shows the XRD pattern of AB and 19 wt% Pt-FAB. The XRD of AB is featured by two typical peaks at 25.70 and 43.00^o 2θ, corresponding to (002) and (100). The XRD pattern for the Pt-FAB showed strong peaks at 39.60, 46.20, 67.60, and 81.40^o 2θ, which correspond to Pt(111), (200), (220) and (311), respectively. The presence of the crystalline planes of face-centred-cube (fcc) structure demonstrated the decoration of crystalline Pt-nps. The average particle size of the spherical Pt-nps (also observed by TEM) was calculated using Scherrer's equation:

$$D = \frac{0.89\lambda}{\beta cos\theta}$$

where D is the diameter of the particle, λ is the X-ray wave length of 0.154 nm, θ is Bragg

angle and β is the full width at half-maximum (FWHM) of the XRD pattern of Pt(220)[7]. The calculated average particle size was 3.09 nm for 19 wt% Pt-FAB and 10.3 nm for 41 wt% Pt-FAB.

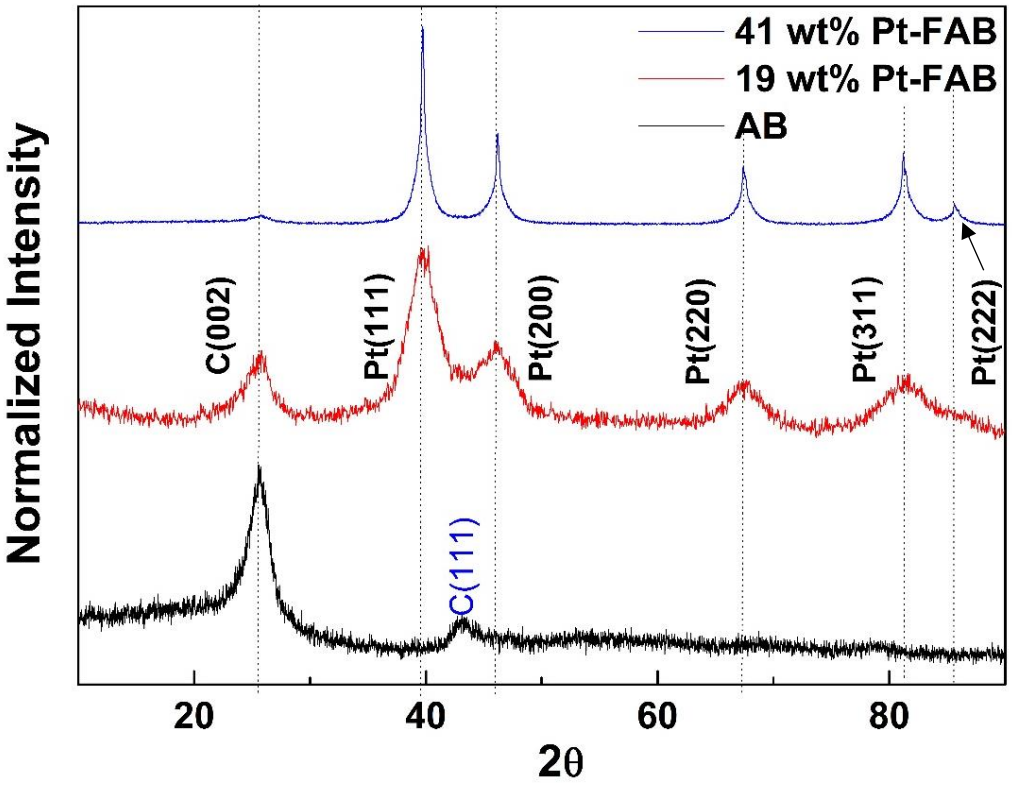

Figure 2.1 XRD pattern of AB, 19 wt% Pt-FAB and 41 wt% Pt-FAB

TEM analyses of AB, Pt-AB and Pt-FABs shed light on the dispersivity of the nanoparticles, particle size distribution and the exfoliation characteristics of the AB. The multi-layered and interconnected morphology of untreated AB can be seen in (Fig. 2.2 A-B). When the Pt deposition was performed onto the AB substrate, agglomeration and non-uniform distributed Pt depositions was observed in TEM as seen in Fig.2.2 C-D without any induced oxygen functional groups. The effect of functionalization and exfoliation can be clearly seen from the

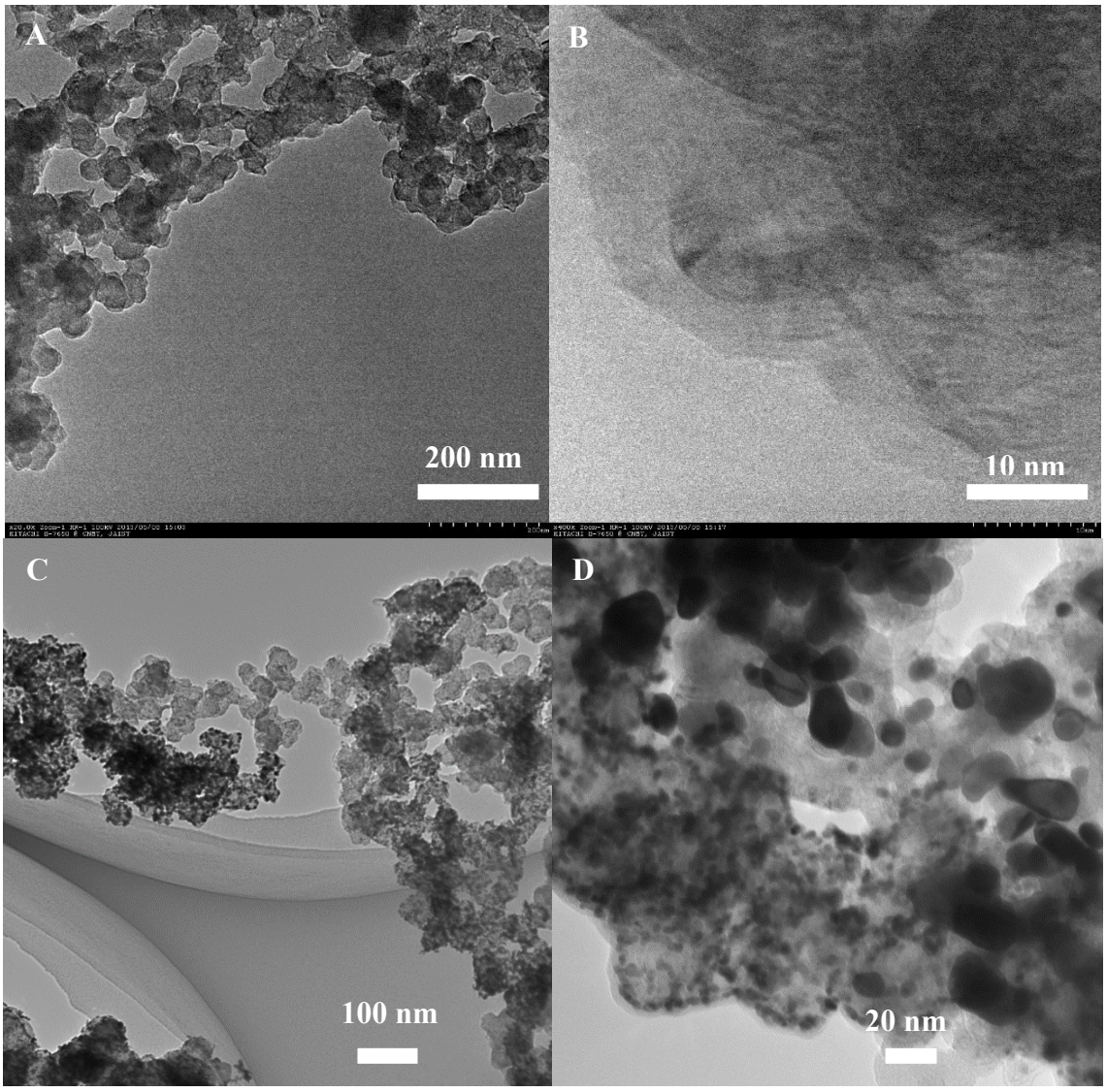

Figure 2.2 TEM images of AB (A-B) Pt-AB (C-D)

micrographs of Pt-AB (Fig. 2.3 A-D) exhibiting a well dispersed, graphene-like transparent features. Further, the Pt-nps were studded uniformly over the surface of FAB in concentric circles, which can be attributed to the circular grains of AB[8]. The grain boundaries being

predominately activated compared to the bulk of the grain might be the reason for such an observation. This was not a localized but an average phenomenon noted in all the batches of synthesis. The average size of the Pt particles in 19 wt% Pt-FAB (Fig. 2.3 A-B) were in the range of 3 nm and that in 41 wt% Pt-FAB (Fig. 2.3 C-D) were in the range of 8 nm. The results obtained in TEM reiterated the particle size calculated from XRD using Scherrer's equation. The effect of improved hydrophilicity due to the incorporation of oxygen functional groups can be appreciated by comparing the TEM images of the Pt decorated AB (Fig. 2.2 C-D) and FAB (Fig. 2.3 A-D). The nucleation of Pt nps was found to be enhanced due to the acid treatment on AB.

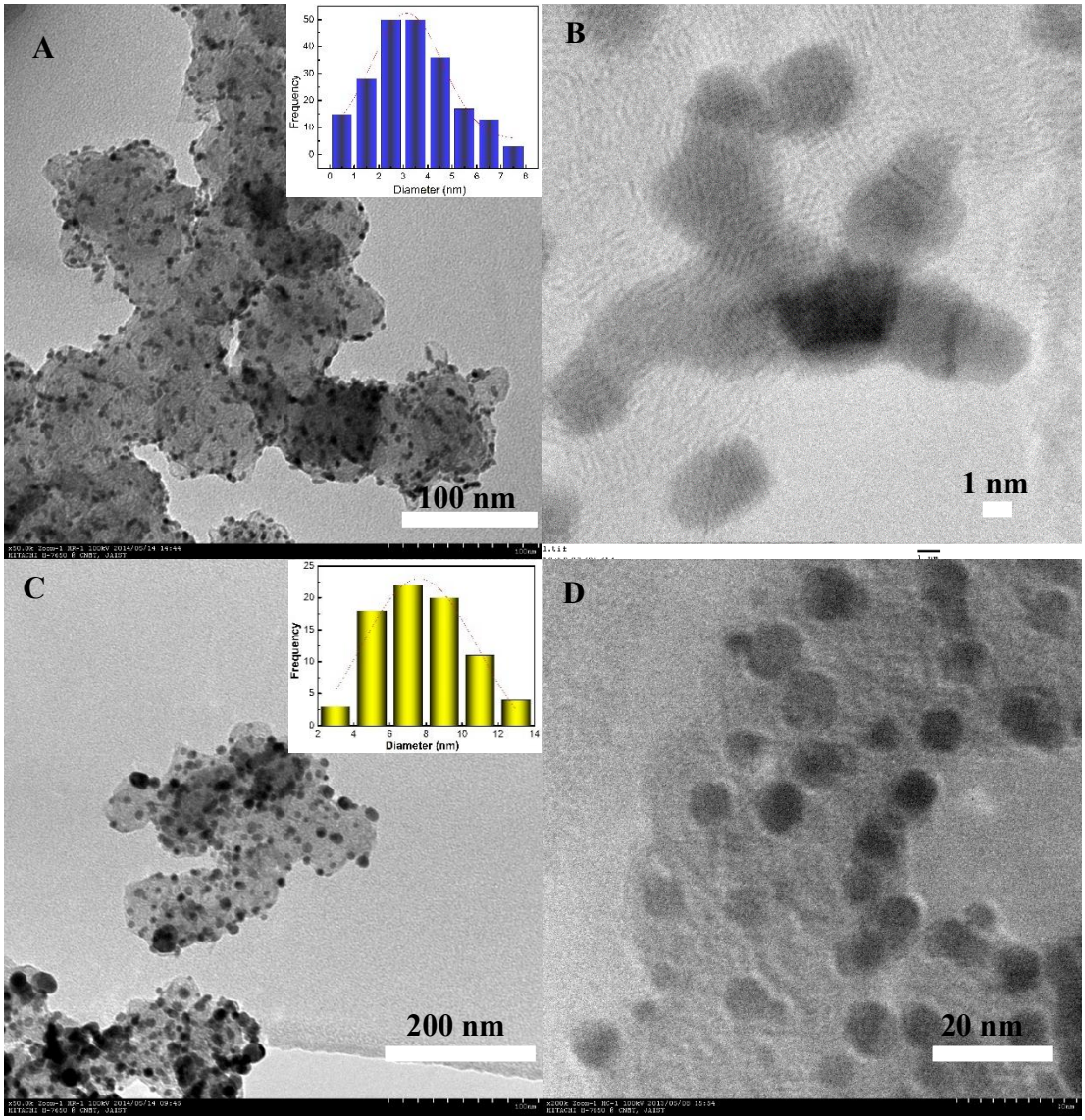

Figure 2.3 TEM micrographs of 19 wt% Pt-FAB (A-B). 41 wt% Pt-FAB (C-D).

Raman analysis of AB and 19 wt% Pt-FAB (Fig. 2.4. A-B) exhibited a typical spectra for carbonaceous materials. A blue shift of 5 cm^{-1} was observed in the D-band of 19 wt% Pt-FAB compared to AB. Further, an increase in the I_D/I_G ratio and in the full width half maxima (FWHM) for the D band at 64.0 cm^{-1} for AB to 69.5 cm^{-1} for 19 wt% Pt-FAB confirmed the increase in the number of defects, which can be attributed to the deliberate oxidation of the carbon material[9].

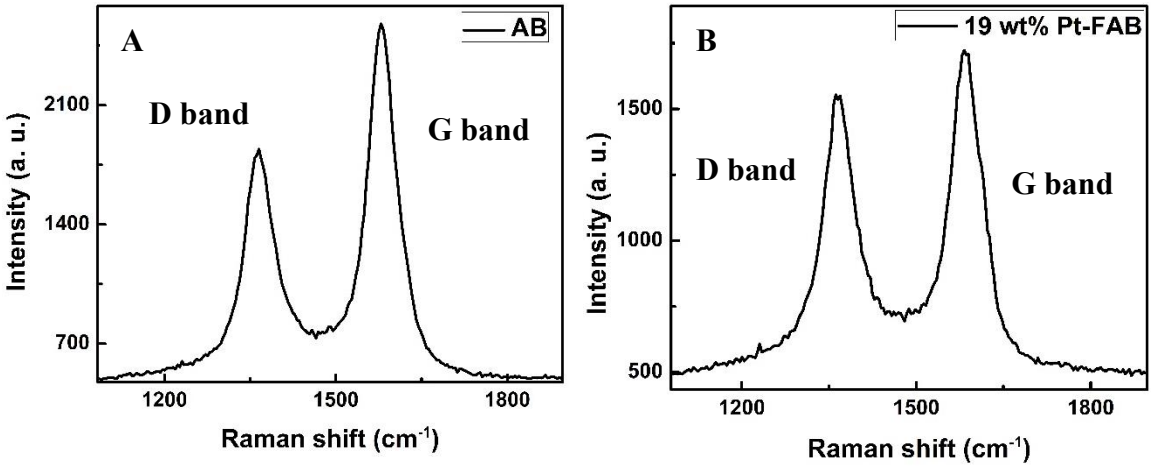

Figure 2.4 Raman spectra of AB (A) and 19 wt% Pt-FAB (B)

X-ray photo electron spectroscopy (XPS) was performed to analyse the elemental composition of the materials under study. The survey spectra of AB, FAB, 19 wt% Pt-FAB and 41 wt% Pt-FAB are shown in Figure 2.5. Figure 2.5 A shows the survey spectrum of AB showing the peaks for C 1s and O 1s. Analysing the area under the curve, it was observed that approx. 2 at% (atomic percent) of oxygen was present due to functional groups. After the exfoliation and functionalization, amount of oxygen increased to 10 at% which can be attributed to various oxygen functional groups that were deliberately introduced onto FAB as observed in Figure 2.5 B. Figure 2.5 C and D shows the typical spectra for a Pt/C consisting typical peaks for Pt, C and O.

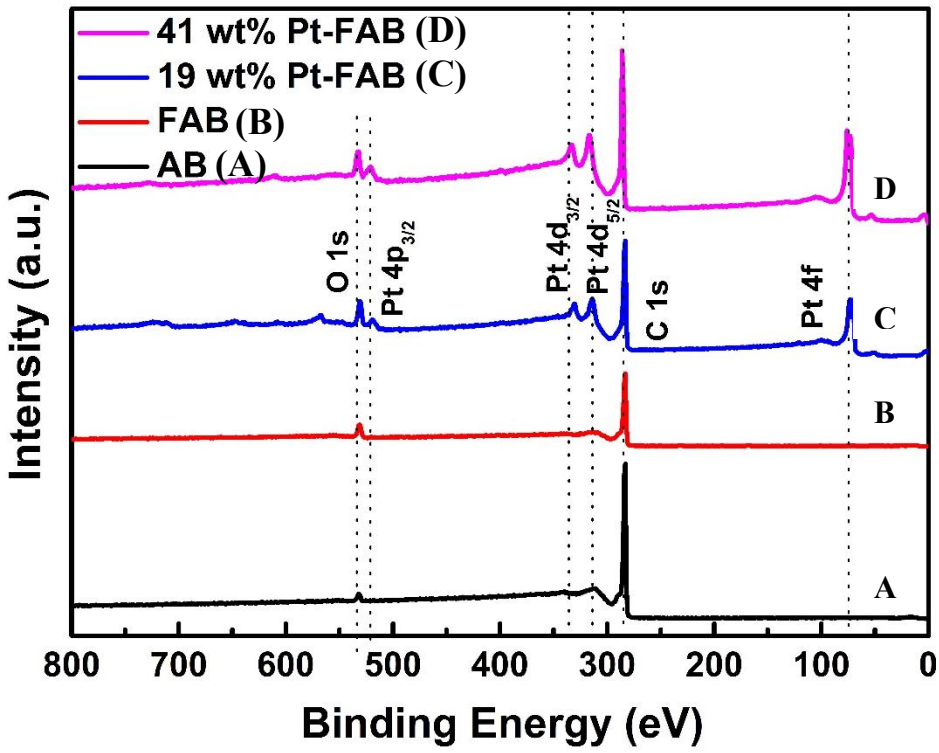

Figure 2.5 XPS survey spectrum of AB, FAB, 19 wt% Pt-FAB and 41 wt% Pt-FAB

Further to evaluate the deliberate oxidation of the surface of AB to form FAB, high resolution C 1s peak was observed. Deconvolution of the C(1s) peak revealed the formation of –COOH groups on the surface of FAB. As shown in Figure 2.6, FAB consists of the following types of carbons: C (284.6 eV), C–OH bonds (285.1 eV), carbonyl C (C=O, 286.0 eV), and carboxylate carbon (O–C=O, 286.7 eV). It can also be observed that the sp2 carbon at% increased significantly while the –C-O at% is decreased up on Pt decoration. This behavior can be attributed to the co-reduction of various easily reducible functional group during the process of decoration of Pt nps onto FAB through chemical reduction method.

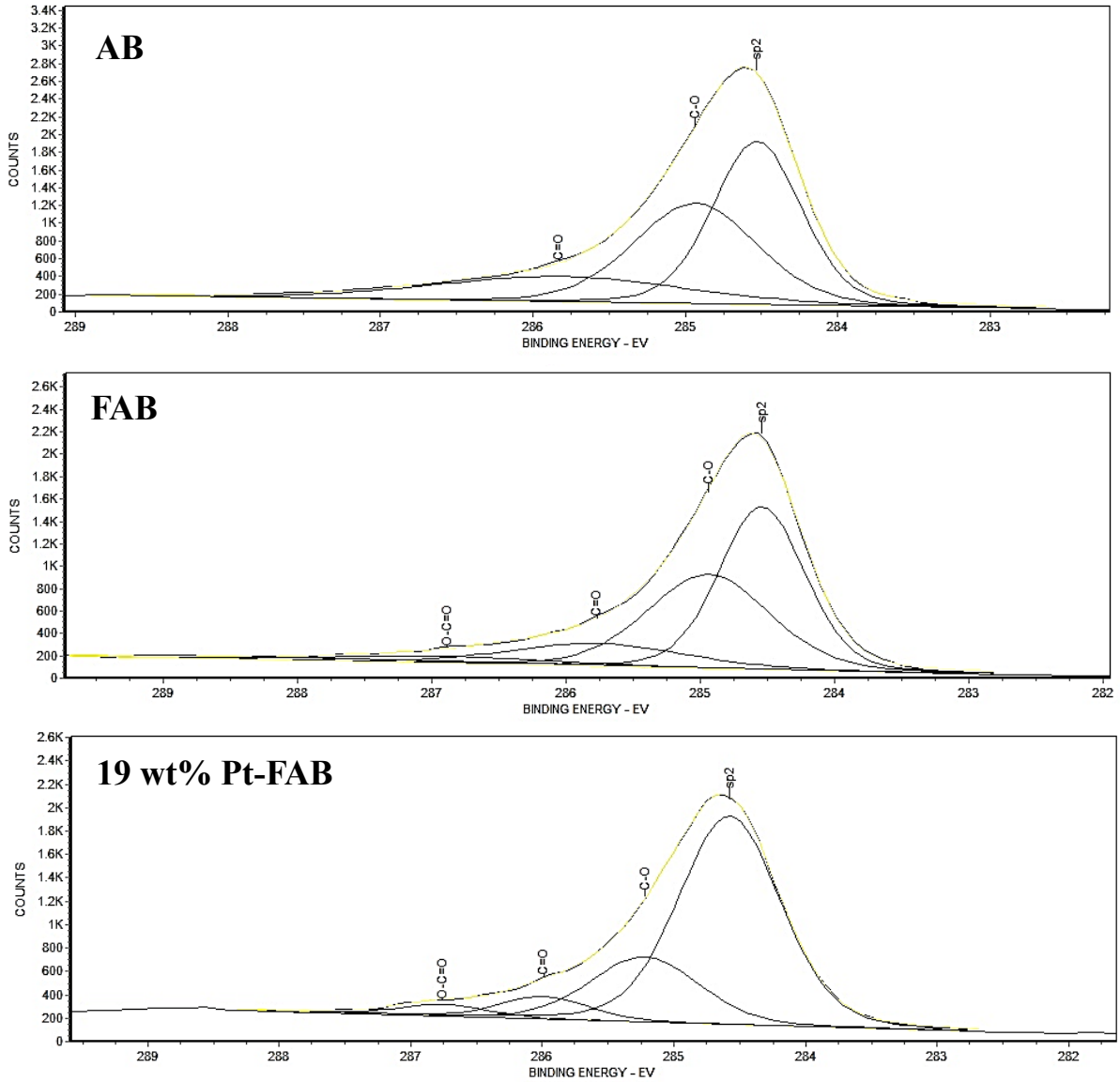

Figure 2.6 Core level XPS spectra of C 1s and its deconvolution in AB, FAB and 19 wt% Pt-FAB

XPS was further employed to analyze the valence states of Pt in the prepared catalyst. High resolution of local scan of Pt 4f peak provided valuable information of various oxidation states of the Pt present over the FAB. Deconvoluted spectra of Pt 4f of 19 wt% Pt-FAB and 41 wt% Pt-FAB are shown in Figure 2.7 A & B consisting of 3 doublet peaks. The first and the most intense doublet of 19 wt% Pt-FAB was found at 71.4 and 74.8 eV which can be ascribed to Pt^0 valence state. The second doublet at 72.3 and 75.6 eV can be assigned to Pt^{II} state and the third doublet at 73.7 and 77 eV was due to Pt^{IV} valence state. In the case of the 41 wt% Pt-FAB the

Pt^0 peak was found to be at 71.5, Pt^{II} at 72.5 and Pt^{IV} was found at 73.9 eVs. The Pt^0 peak was shifted by 0.4 eV in the case of 19 wt% Pt-FAB and 0.5 eV in the case of 41 wt% Pt-FAB compared to typical Pt^0 found in Pt/C. The shift can be ascribed to the strong anchoring of Pt to the oxygen functional groups with which the nucleation could have possibly taken place. The composition of Pt in 19 wt% Pt-FAB was analyzed to be containing 56.4 at% of Pt^0, 23.8 at% of Pt^{II}, and 19.8 at% of Pt^{IV}. While, 41 wt% Pt-FAB consisted of 50.0 at% of Pt^0, 25.0 at% of Pt^{II} and 25.0 at% of Pt^{IV}. The Pt^0 state in both the cases was found to be the predominant valence state.

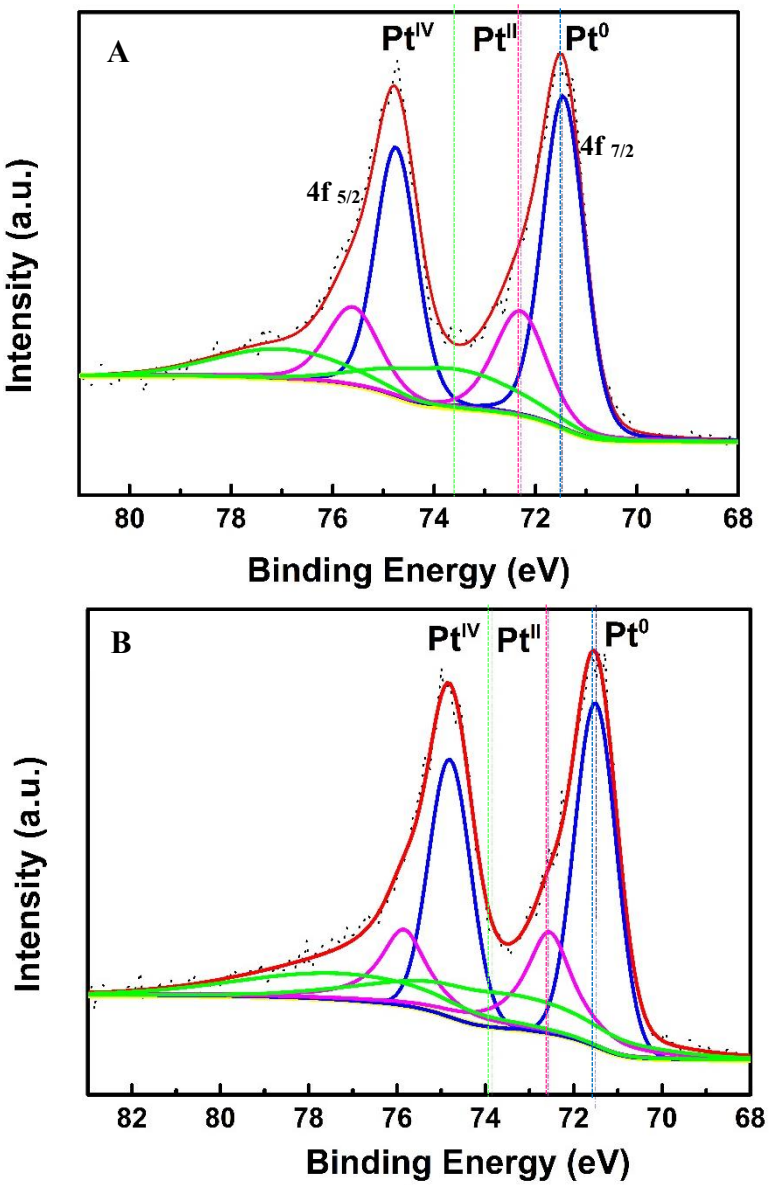

Figure 2.7 Deconvolution of Pt 4f peak of 19 wt% Pt-FAB (A) and 41 wt% Pt-FAB (B) showing Pt^0, Pt^{II} and Pt^{IV} valence states.

2.4.2. Electrochemical Characterization

Cyclic voltammetry (CV) is one of the most useful electrochemical technique to evaluate the electrocatalytic activity of the material. CV forms a versatile technique that quickly provides qualitative information about catalysts and electrochemical reactions. CV was performed to understand the electrocatalytic activity of the materials under study. Preliminary CV studies for AB and FAB revealed the inherent ORR activity of AB and on further exfoliation of the AB to FAB along with more defects in the form of oxygen functionalities, the ORR electrocatalytic activity was improved.

Figure 2.8 shows cyclic voltammograms of AB and FAB are noteworthy because of their impressive ORR activity even without a metal loading. Many researchers have shown in the

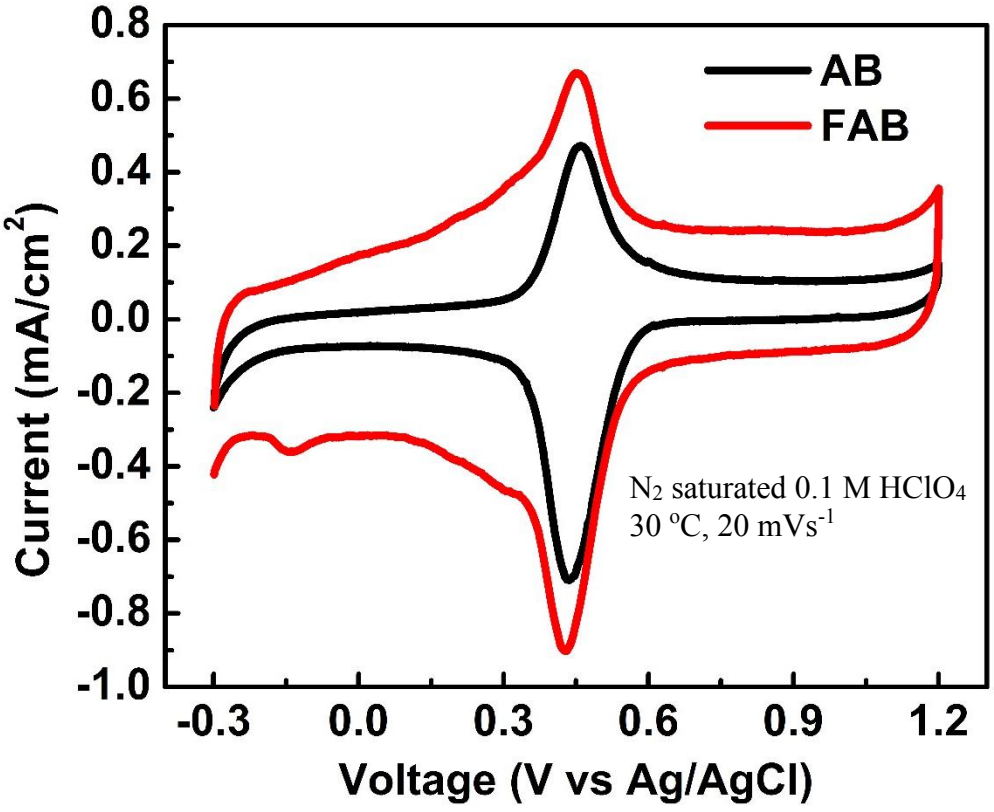

Figure 2.8 Cyclic voltammograms of AB and FAB showing ORR activity

past that the presence of a hetero atom, which creates a partial charge on the carbon atoms, can perform ORR and OER even without catalytic metal atoms[10,11]. An increase in the oxygen functionalities increases the ORR activity, which can be confirmed without doubt by the intensity of the ORR current in cyclic voltammetry. The oxygen functionalities not only act as

the active sites for ORR, but also play a major role as nucleation sites and anchoring sites[12] for the formation of metal-nps. The main differences between AB and FAB are (i) an increased double layer capacitance, which can be attributed to the exfoliation leading to higher surface area which in turn leads to higher double layer capacitance, as observed from the region, 0.2–0.4 V, in the voltammogram; (ii) increase in the ORR peak intensity of FAB; and an apparent increase in the ORR current of FAB was observed compared to AB. The current increased from 0.139 mA of the latter to 0.177 mA for FAB.

Further CV was employed to evaluate the electrocatalytic ORR activity and electrochemical surface area (ECSA) of 19 & 41 wt% Pt-FAB. The obtained results were compared with one of the best commercial ORR catalyst, TEC10E50E (50 wt% of Pt). CV measurements were carried out in nitrogen saturated 0.1 M $HClO_4$(aq.) using Pt wire as the counter electrode, glassy carbon electrode coated with thin-film of the material understudy as the working electrode. The amount of Pt that was present on the GC was around 3.76 µg for 19 wt% Pt-FAB while in the case of 41 wt% Pt-FAB and TEC10E50E it was 2.45 and 3.98 µg respectively. All the experiments were carried out at a potential scan rate of 50 mV s^{-1} (RHE). Fig. 2.9 A-C shows the cyclic voltammograms of 19 and 41 wt% Pt-FAB in comparison with TEC10E50E. The voltammograms exhibited the electrochemical fingerprints of Pt in the electrode. The typical peaks of hydrogen adsorption and desorption at 0.05 to 0.41 V, Pt oxidation peak at 0.85 V and ORR at 0.75 V were apparent.

During the reduction cycle in the CV, protons present in the electrolyte get adsorbed on to the surface of the Pt. While, these get desorbed back in the form of protons from atoms of hydrogen.

$$H_{ad} \rightarrow H^+ + e^-$$

The electrochemically active surface are (ECSA) was determined using hydrogen desorption peak (shown in Fig.2.9 A) from the CV. Adsorption of reactants and the catalytic reaction rates are prominently dependant of ECSA. The ECSA in the present case was calculated using a

well-established estimate using the following equation.

$$ECSA = \frac{Q_H\ (\mu C/cm^2)}{Q_M X\ Pt\ loading\ (g/cm^2)}$$

Where Q_H is the charge corresponding to the hydrogen desorption peak, $Q_M = 210\ \mu C/cm^2$ is the electrical charge associated with the monolayer adsorption of hydrogen on Pt and Pt loading is the amount of Pt loaded onto the electrode. Figure 2.9. D compares the ECSA calculated for all the three samples under study. ECSA of 19 wt% Pt-FAB was found to be around 67.2 $m^2\ g^{-1}$, while that of 41 wt% Pt-FAB was found to be 30.5 $m^2\ g^{-1}$ and the ECSA of the TEC10E50E commercial catalyst was 77.0 $m^2\ g^{-1}$. The low ECSA in the case of 41 wt% Pt-FAB can be attributed to larger Pt particle size.

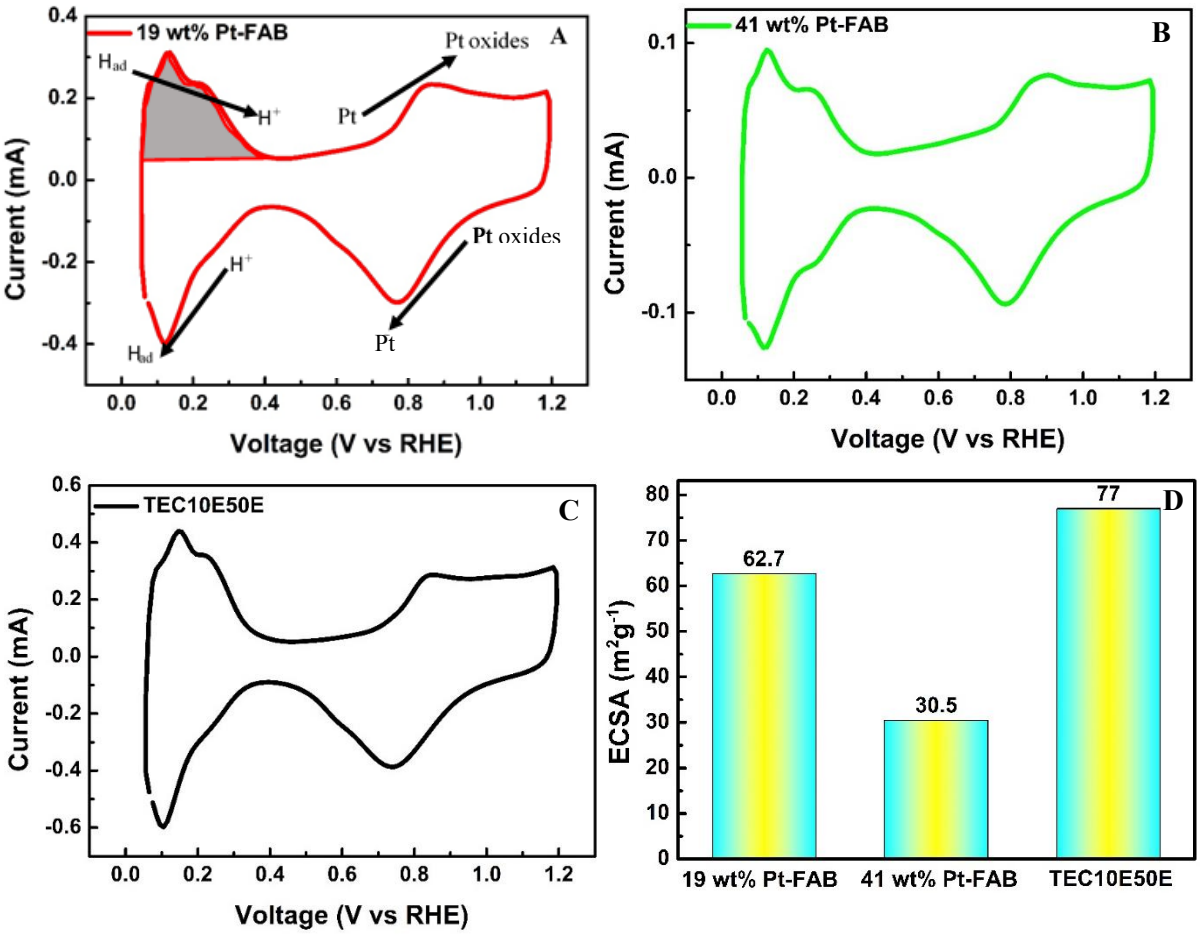

Figure 2.9 Cyclic voltammograms of 19 wt% Pt-FAB (A), 41 wt% Pt-FAB (B) and TEC10E50E (C) and ECSA of Pt-FAB samples in comparison with TEC10E50E (D)

Rotating disc electrode (RDE) method was performed to understand the kinetics of the as prepared ORR electrocatalyst. This method was found to be a powerful tool to evaluate various

kinetic parameters of the electrocatalysts. It is well known that electrocatalytic ORR can happen in two different routes in acidic medium i.e., less efficient two electron process and an efficient four electron process. To determine the mechanism with which the ORR electrocatalyst operates is very crucial to evaluate the catalyst. The numbers of electrons transferred per O_2 molecule was calculated with well-known Koutecky– Levich equation.

$$\frac{1}{I} = \frac{1}{i_k} + \frac{1}{i_L} \quad (1)$$

$$i_L = 0.620nFACD^{2/3}\nu^{-1/6}\omega^{1/2} \quad (2)$$

Where, i_k is the kinetic current for the oxygen reduction at the surface of the electrode, i_L is the Levich current for the electrode reaction of the oxygen by a diffusion controlled process in other words it can be called as diffusion-limited current, n is the number of involved in the reduction of oxygen, F is the Faraday constant (96,485 C mol^{-1}), A is the area of the RDE used (0.196 cm^2), D is the diffusion coefficient of the dissolved oxygen in electrolyte (1.93×10^{-5} cm^2s^{-1}), C is the concentration of dissolved oxygen (1.26×10^{-6} mol cm^{-3}), ν is the kinematic viscosity of the electrolyte (10.09×10^{-3} cm^2 s^{-1}), ω is the rotation rate of electrode.

Figure 2.10 A, C and E shows the liner sweep voltammograms (LSV) of both the Pt-FAB based materials and the reference material (TEC10E50E). LSV was performed from 0.2 V to 1.0 V vs RHE at 20 mV/s scan rate in O_2 saturated 0.1 M $HClO_4$ aq. at 30 ºC. The RDE measurements were done at rotation speed of 400, 900, 1600, 2500 and 3600 rpm. The linear sweep voltammograms showed typical profiles with the mixed kinetic and diffusion region at around 0.8 to 1 V vs RHE and diffusion limiting current at around 0.2 to 0.8 V vs RHE. Corresponding Koutecky-Levich plots (KL) for all the samples at rotation speeds of 900, 1600, 2500 and 3600 rpm are shown in Figure 2.10 B, D & F for diffusion limiting current at 0.80, 0.85 and 0.90 V. I^{-1} and $\omega^{-1/2}$ plots exhibited good linear relationship at all the potentials. The linearity and the parallel behaviour of the KL plots corroborate first order kinetics with respect to O_2 in mixed kinetic-diffusion controlled region. The intercept from the KL plot was used to find the kinetic

current and subsequently the number of electrons taking part in ORR.

The calculated number of electrons for the ORR was found to be ~ 4 for all the samples under study. The half-wave ($E_{½}$) potential for all the catalysts were determined by comparing the LSV at 1600 rpm (Figure 2.11 A). The $E^{½}$ of 19 wt% Pt-FAB was found to be 0.90 V which was on

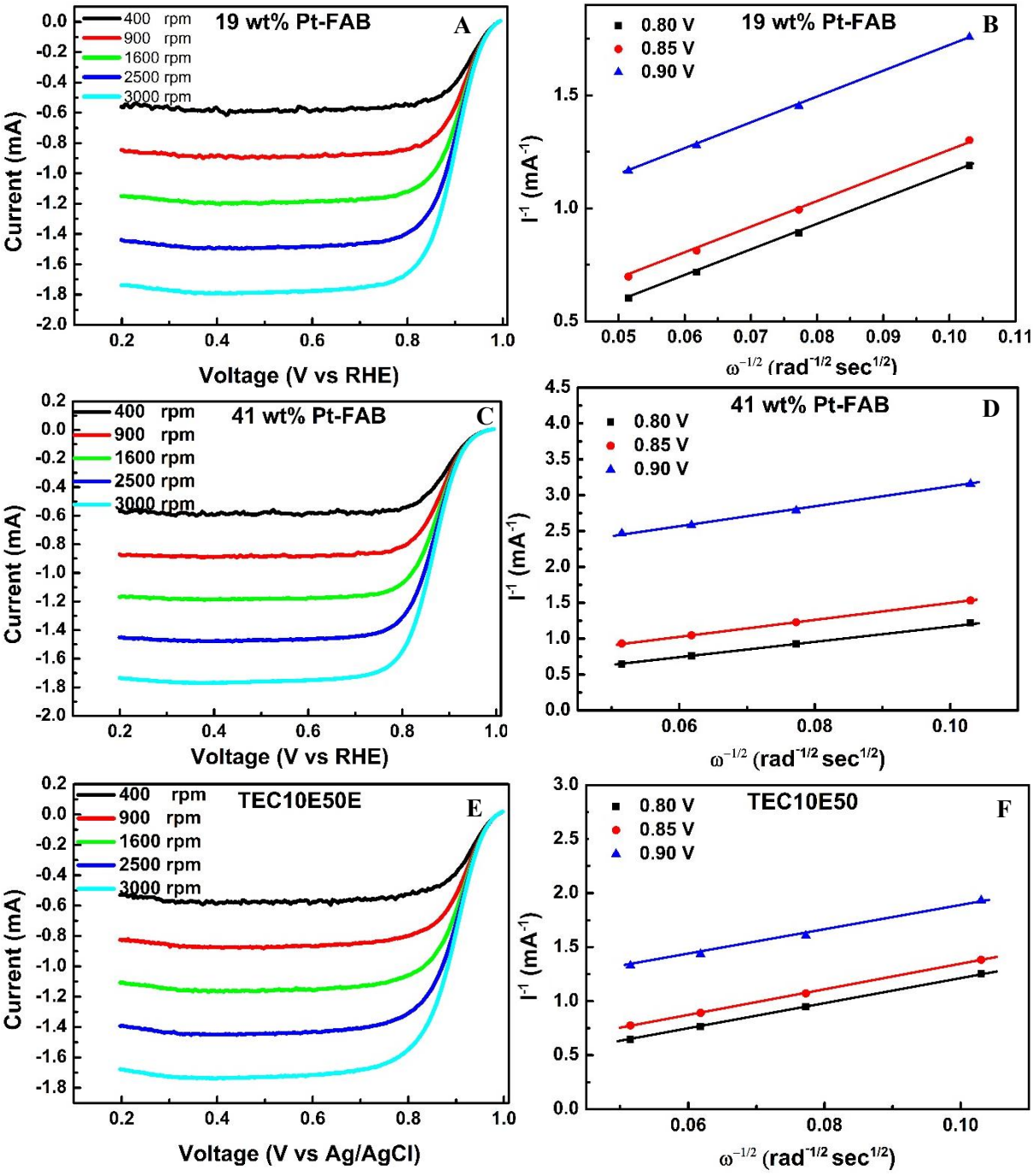

Figure 2.10 Linear sweep voltammetry curves using RDE for 19 wt% Pt-FAB (A), 41 wt% Pt-FAB (C) and TEC10E50E (E) at 30 °C in oxygen saturated 0.1 M $HClO_4$ aq. at scan rate of 20 mV/s at different rotation speeds (400, 900, 1600, 2500, 3600 rpm) and respective Koutecky-Levich plots (B, D, E) at 0.80, 0.85 and 0.90 V.

par with the commercial catalyst. The $E^{1/2}$ for 41 wt% Pt-FAB was determined to be 0.88 V. Further, the kinetic current thus obtained from the KL plot was normalized with ECSA and Pt loading on the electrode to determine the specific activity (SA) and mass activity (MA). The surface activity and the mass activity of all the samples at 0.9 V vs RHE are summarized in Figure 2.11 B. Specific activity (SA) of both the Pt-FAB materials was found to be 1.63 times that of TEC10E50E. The mass activity of 19 wt% Pt-FAB was found to be 1.32 times that of the reference material. The department of energy (DOE) USA, set a target of 440 Ag^{-1} at 0.90 V vs RHE for Pt based catalysts by year 2020. The MA of the 19 wt% Pt-FAB crossed the target limit and achieved high MA of 467.3 Ag^{-1}.

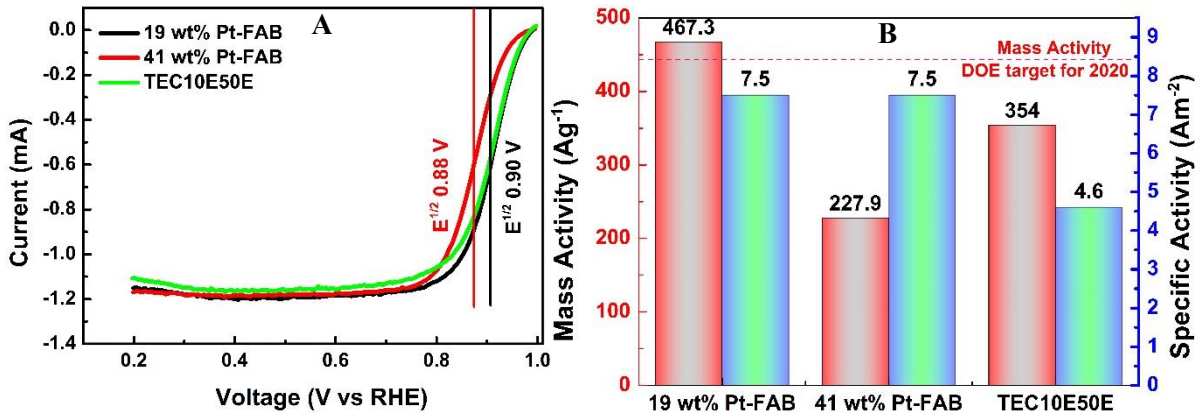

Figure 2.11 Comparison of RDE plots of 19 wt% Pt-FAB and 41 wt% Pt-FAB with TEC10E50E (A) MA and SA of the Pt-FAB at 0.9 V vs RHE(B)

One of the attractive aspects of AB, which makes it an efficient cathode material, is its interaction with the electrolyte, i.e., its ability to absorb and retain a significant volume of electrolyte. The interaction with electrolyte helps to reduce the interface boundaries, which in turn affects the overall catalytic performance of the electrode[13,14]. Hence, interfacial studies are vital to validate the catalytic performance of the electrode, which can be understood by electrochemical impedance studies. The electrochemical impedance spectroscopy (EIS) studies for the AB, FAB and Pt-FAB based catalysts were performed using conventional three electrode system using Pt wire as the counter electrode and Ag/AgCl reference electrode in nitrogen

saturated 0.1 M $HClO_4$ aq. at open circuit potential. These results were benchmarked with the commercial 20 wt% Pt-Vulcan XC-72 (Pt/C). This commercial catalyst contained similar type and amount of carbon as the material under study. EIS results presented in Figure 2.12 exhibited typical spectra of carbon and ORR catalysts[15]. However, fitting with an equivalent circuit (Figure 2.12 B inset) revealed a unique behavior unlike the conventional Pt/C catalyst. In addition to charge transfer at the Pt/C interface, two additional elements contributed to the impedance each owing to the high absorptivity of AB. The double layer formed at the interface of glassy carbon can be classified into two elements. One of these elements can be attributed to the electrolyte absorption over AB layer (R4), the other can be attributed to the direct influence of the electrolyte on the surface of the GC (R3). R_{sol} represents the resistance of the electrolyte and χ^2 is the error of the theoretical fitting. A schematic representation explaining

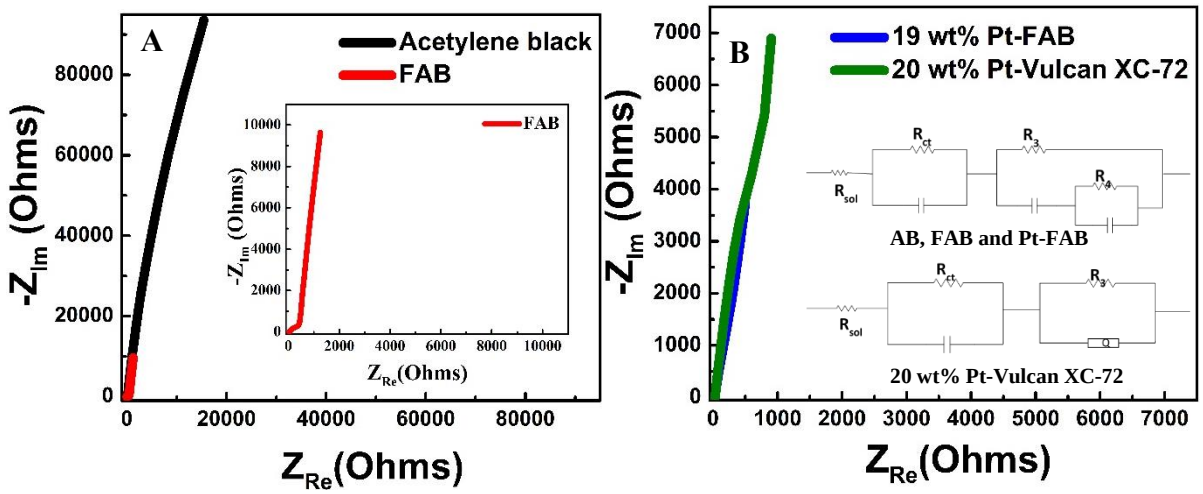

Figure 2.12 Nyquist plot of (A) AB and FAB (B) 19 wt% Pt-FAB and 20 wt% Pt-Vulcan XC-72, equivalent circuits for all the materials are given in inset.

all the elements is shown in Figure 2.13. Table 2.1 lists charge transfer resistance (R_{CT}) values along with the other elements of the equivalent circuit for all the four AB related materials in comparison with 20 wt% Pt-Vulcan XC-72. The charge transfer resistance of the AB based material was observed to be nearly 20 times less than that of the commercial Pt/C. The extremely high catalytic efficiency of the Pt-FAB materials can be ascribed to the low charge transfer resistance.

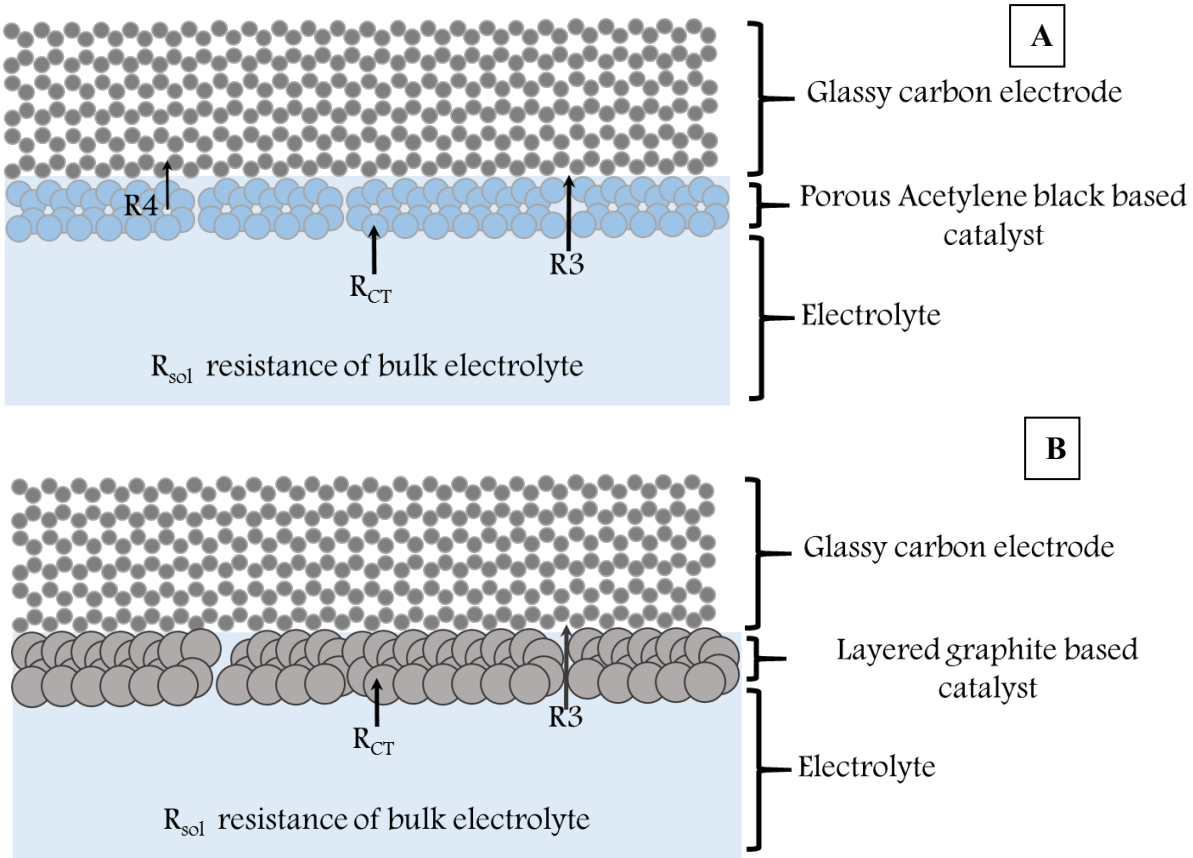

Figure 2.13 Pictorial representation explaining the elements of equivalent circuits for 19 wt% Pt-FAB and 20 wt% Pt-Vulcan XC 72.

Table 2.1 Comparison of values of elements in the equivalent circuits.

	AB	FAB	19% Pt-FAB	41% Pt-FAB	20%Pt-Vulcan XC-72
$R_{sol}(\Omega)$	41.66	38.11	52.94	31.55	31.65
$R_{CT}(\Omega)$	**37.89**	**33.99**	**22.82**	**20.10**	**378.8**
R3(Ω)	96.38	454.90	2408	3359	5.62E4
R4(Ω)	4.1E5	7.0E4	2.0E4	6.9E4	
χ^2	10^{-4}	10^{-4}	10^{-4}	10^{-5}	10^{-4}

Further, the durability of the material was investigated by subjecting the materials to 500 cycles of a potential scan in the potential range of -0.25 to 1.3 V vs Ag/AgCl with the scan rate of 20 mV s^{-1} using similar procedure as CV mentioned earlier. The cyclability of the material had increased substantially through Pt-np decoration onto the FAB. The charge-density at peak potential of ORR region was studied before and after 500 cycles. The charge density for 19 wt% Pt-FAB had decreased from 3.00 mA cm^{-2} to 1.75 mA cm^{-2} and 41 wt% Pt-FAB from 3.7 mA cm^{-2} to 2.7 mA cm^{-2} before and after 500 potential cycles. It was also observed that the durability increased with increasing the amount of Pt-np. Figure 2.14 A. shows the cyclability of 19 and 41 wt% of Pt-FAB. By increasing the Pt loading from 19 to 41 wt%, the cyclability increased by almost 25%. The durability test for Pt-FAB and commercial Pt/C was also conducted and it was found that charge density of 20 wt% Pt-Vulcan XC-72 was 0.71 mA cm^{-2}. In contrast, 19 wt% Pt-FAB was found to show 60% more ability in reducing oxygen (Coulombic efficiency) even after 100 potential scans Figure 2.14 B.

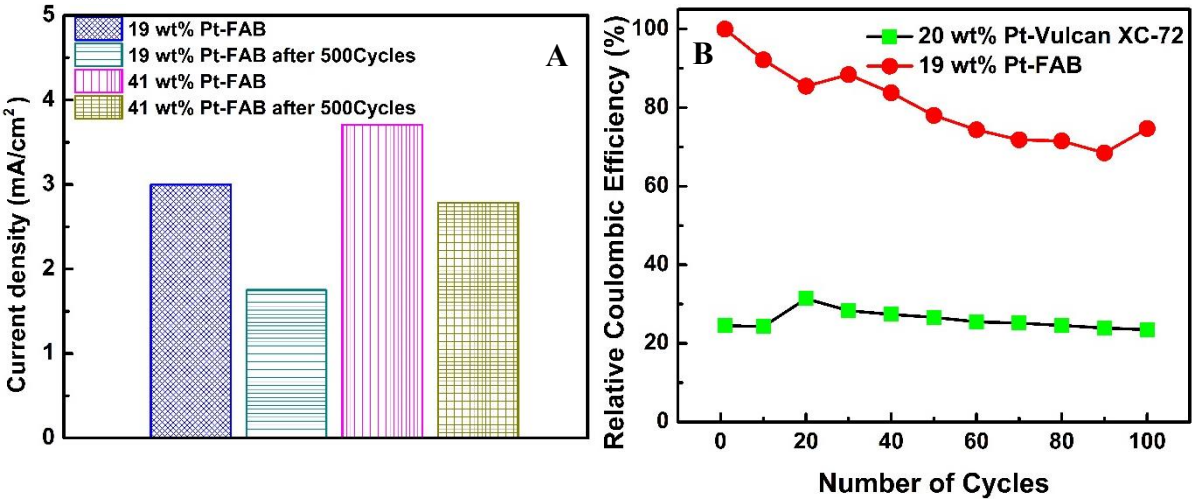

Figure 2.14 Durability of 19 wt% Pt-FAB and 41 wt% Pt-FAB (A) and coulombic efficiency of 19 wt% Pt-FAB in comparison with 41 wt% Pt-FAB (B)

2.5. Application of Catalyst in Proton Exchange Membrane Fuel Cell (PEMFC)

After systematic electrochemical characterizations of Pt-FAB based material to study the efficiency of ORR catalysts, 19 wt% Pt-FAB was used for application as cathode material in PEMFC. The high electrocatalytic efficiency of 19 wt% Pt-FAB compared to other materials under study and the lesser use of Pt prompted the selection of this material for PEMFC studies. To study the performance of the catalyst, a PEMFC single cell was assembled according to conventional Membrane Electrode Assembly (MEA) architecture. A typical MEA consists of both anode and cathode separated by a polymer electrolyte. Both the electrodes were made up of three layers viz., a backing layer, a gas diffusion layer, and a catalyst layer. The 19 wt% Pt-FAB catalyst layer was uniformly coated with the catalyst ink (prepared by dispersing required amount of catalyst in IPA and 5 wt% nafion solution) over the carbon cloth (gas diffusion layer). Commercial Pt/C (Arora Matthey) was used as anode catalyst maintaining platinum loading of 0.25 mg cm^{-2}. 19 wt% Pt-FAB was used as ORR catalyst and the platinum loading of 0.5 mg cm^{-2} was maintained. The effective electrode area was set to be 30 mm^2. The MEA was fabricated by sandwiching a commercial 212 CS membrane (Nafion based) in between anode and the cathode. The MEA was pre-treated by hot-pressing at 130 °C and 70 bar for 4 min. As-prepared MEA was tested for single cell fuel cell tests by fixing it between two graphite flow field plates facilitating serpentine fuel flow over the MEA. The performance of the fuel cell was studied under 2:1 (air:hydrogen) and 1:1 (oxygen:hydrogen) configurations at 40, 50, 60 and 70 °C with relative humidity of 90% without any back pressure.

The performance of the fuel cell can be characterized by studying the voltage drop across the external load and plotting the resulting current vs potential (IV or polarization) curve. The polarization curves represents the rate of the chemical reactions in terms of current, while the driving force of the reaction in terms of voltage. Figure 2.15 shows the typical polarization

curve with various operating regimes of the fuel cell. Generally no current flow occurs at open circuit region. When a load resistance is applied, electrons (current) flows across positive and negative electrodes through the external circuit and this is balanced by an ionic current passing through the electrolyte. With the application of large load resistances, the rapid drop in the voltage occurs with increasing current. The rapid voltage drop initially can be attributed to the activation over potential which acts as the barrier for the electron transfer reactions taking place at the anode and cathode. With further decrease in the load resistance, the voltage decreases almost linearly with increase in the current. This is termed as the "ohmic polarization region" which is ascribed to internal resistance offered by the electrolyte to ion flow. The voltage at ohmic region is the desirable operating voltage for the fuel cell. With further decrease in the external resistance, the region referred to concentration polarization region manifests, where the current reaches a limiting value due to limited or slow mass transfer of reactants to the electrode/electrolyte interface.

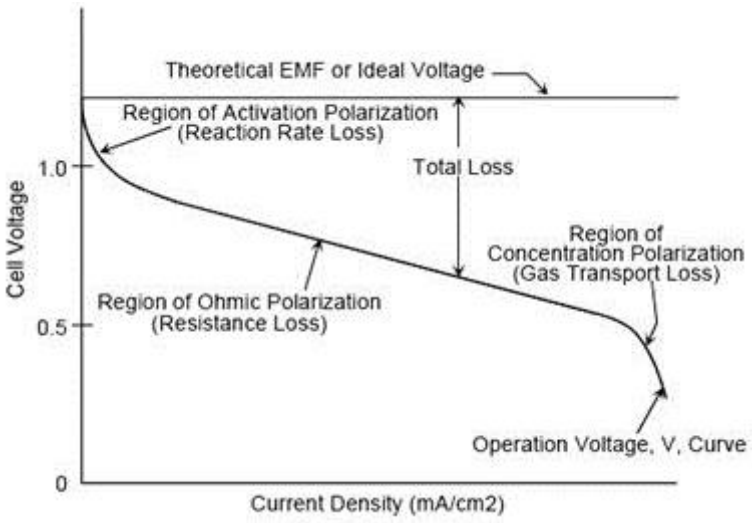

Figure 2.15 Typical polarization curve of PEMFC

The polarization curves for the fuel cell with 19 wt% Pt-FAB as cathode at four different temperatures under two different gas flow conditions are shown in Figure 2.16. Figure 2.16A shows the polarization curves when 2:1 (air and hydrogen) flow is used at cathode and anode end respectively, whereas, Figure 2.16B for 1:1 (oxygen and hydrogen) flow.

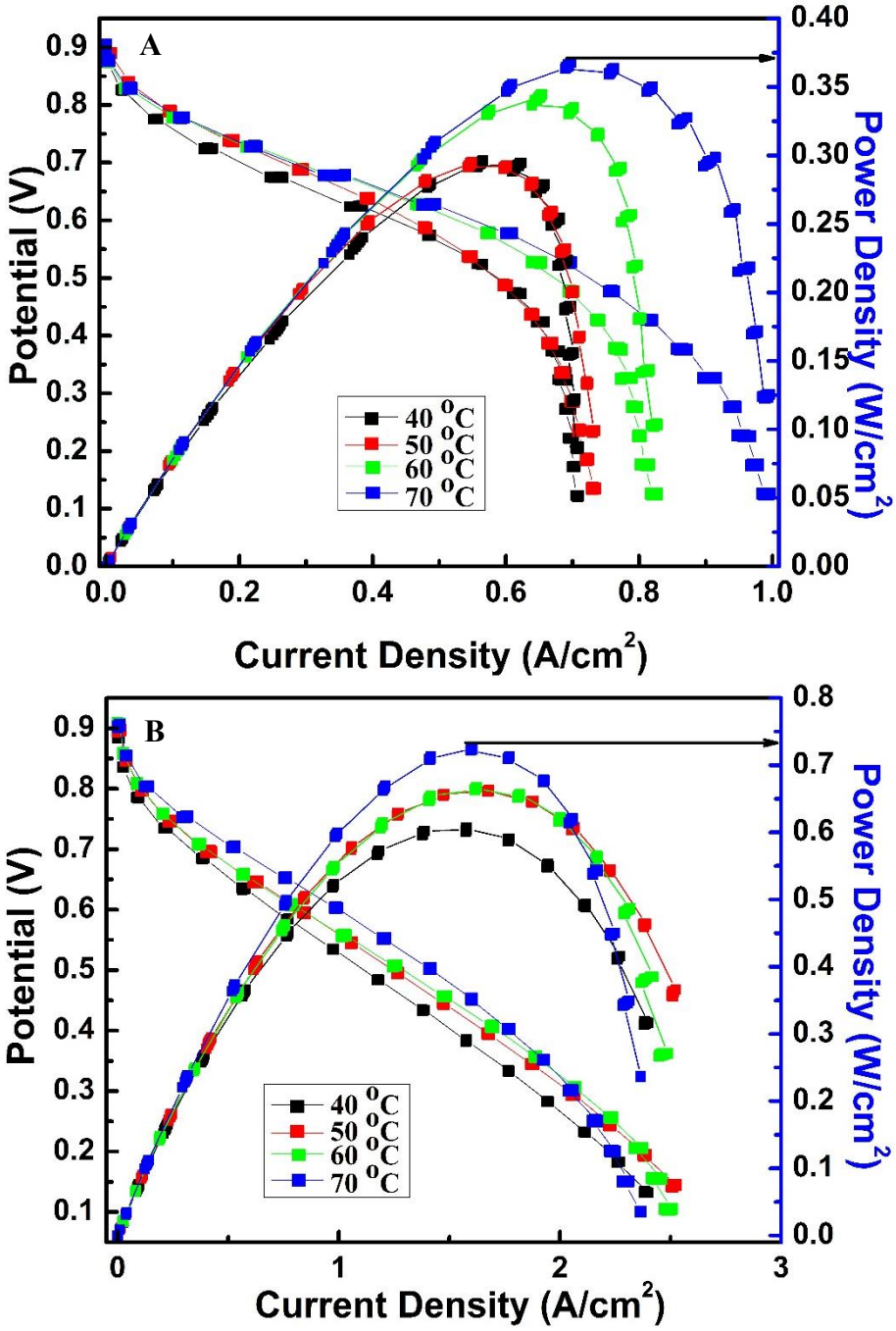

Figure 2.16 Polarization curves of 19 wt% Pt-FAB in 2:1 (air:hydrogen) condition (A) and in 1;1 (oxygen:hydrogen) condition (B)

The achieved current densities of 19 wt% Pt-FAB at 0.6 V was found to be 553.49 and 1002.0 mA cm^{-2} in air and oxygen at cathode end, respectively. The highest power densities were found to be 349.43 and 727.05 mW cm^{-2} in air and oxygen atmospheres, respectively.

In summary, the superior ECSA, SA and MA of 19 wt% Pt-FAB can be ascribed to the following reasons i) the improved interaction of Pt with the FAB which was evident with a shift in the Pt^0 peak in the XPS of the material. The improved interaction has a direct role in modifying the electronic states of the metal which has direct implication on the adsorption of oxygen to hasten the kinetics of ORR ii) recently it was reported that the edges of graphite are catalytically more active for ORR. So, the catalytic material with more active sites at the edges must show better activity. The method of preparation of the material under study in the present chapter enhances the Pt decoration at the edges which is clearly visible in TEM iii) the most important factor that determines the kinetics at rate determining step of electron transfer to the oxygen is the charge transfer resistance of the material. The extremely low charge transfer resistance enables easier charge transfer at rate determining step which inturn enhances the efficiency of the ORR iv) uniformly decorated Pt nanoparticle of ~3 nm average size which is less than other commercial counterparts also plays an important role in enhancing the efficiency of the catalyst.

2.6. Application of Catalyst in Lithium-air Battery

Li-air battery has been receiving a great deal of interest in the recent times owing to its very high theoretical specific energy comparable to gasoline. A preliminary effort has been made to study the performance of the Pt-FAB catalyst for Li-air battery application.

Preparation of Electrode: The slurry was prepared by taking 10 mg of 19 wt% Pt-FAB, 1 mg polyvinylidene fluoride (average Mw 534,000) and was uniformly dispersed in solution of 450 µl of isopropyl alcohol and 50 µl of N-Methyl-2-pyrrolidone by ultrasonicating for nearly 30 mins. This mixture was brush coated onto carbon cloth of 18 mm diameter maintaining the Pt loading at ~5 $mgcm^{-2}$ (similar loading to that of cathode used in PEMFC). The electrode was first air dried and later dried at 100 ^{o}C under vacuum for overnight.

Constant Pressure Oxygen Chamber: For maintaining the pressure of oxygen, a leak proof constant oxygen pressure chamber was designed and fabricated. Figure 2.17 shows the chamber, it consists of a pressure gauge, oxygen inlet and outlet for precisely maintaining the pressure pressure of oxygen inside the chamber and a safety valve to ensure from any unintentional pressure built-up inside the chamber leading to explosion.

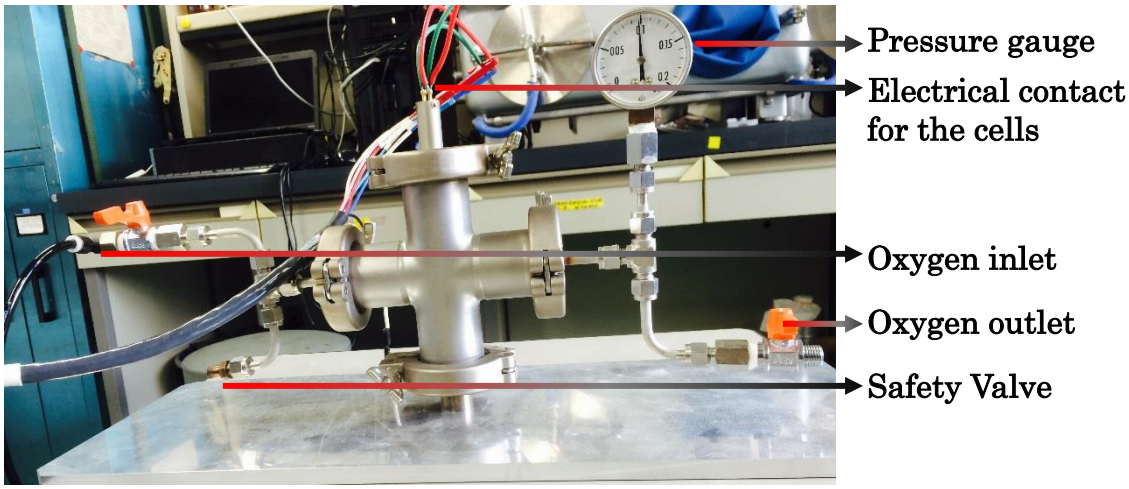

Figure 2.17 Constant pressure oxygen chamber for Li-air battery characterization

Coin cell Setup: Coin cell configuration (Figure 2.18) was used for studying the charge discharge characteristics of the electrocatalyst. A 20 mm coin cell of CR2025 Li-ion battery model was used for the studies. The above coin cell was modified such that oxygen percolation to the air electrode was ensured. The modified coin cell consisted of a "bottom can" with a hole of 15 mm covered with Ni mesh enabling the diffusion of oxygen. A typical non-aqueous battery cell set up was consisted of Li metal anode (15 mm diameter), a glass fiber filterpaper dipped in tetraethylene glycol dimethyl ether containing 0.1 M of Bis(trifluoromethane)sulfonimide lithium salt (LiTFSI) electrolyte as separator and 19 wt% Pt-FAB coated porous carbon cloth as cathode supporting material.

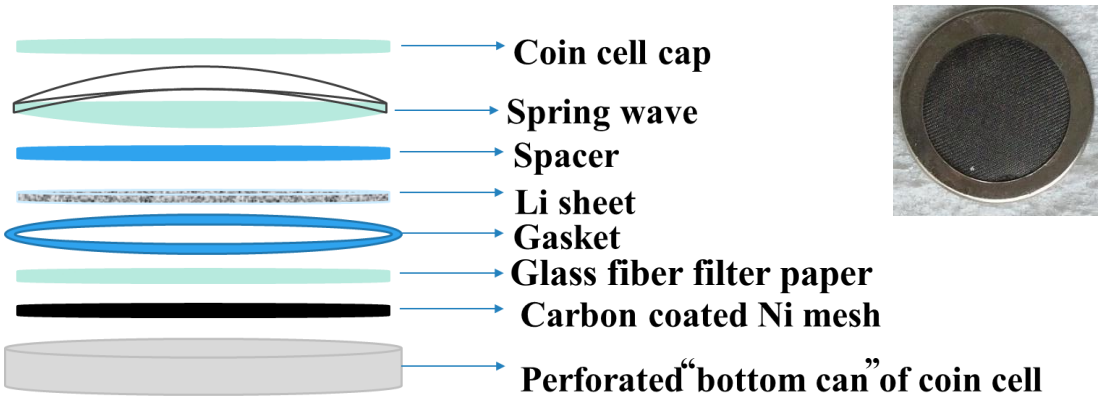

Figure 2.18 Coin cell configuration showing various components and the inset shows the perforated bottom can of the coin cell

Charge-discharge studies: The constructed coin cell was kept to stabilize for 3 hrs in the oxygen pressure chamber for attaining stable open circuit potential (OCP) for 3 hrs. An OCP of 3.1 V was observed. The cell was operated in 1 atm of O_2 and Galvanostatic charge discharge was performed. The initial discharge was done by withdrawing 0.1 mA and the charging was performed by withdrawing 0.06 mA. The first charge discharge cycle of the constructed Li-air battery is shown in Figure 2.19 A. Discharge capacity was found to be 1125 $mAhg^{-1}$ (with respect to Pt weight) with the discharge voltage of 2.7 V and a charge capacity if 620 $mAhg^{-1}$ with the charge voltage between 3.7 to 3.8 V. For the second cycle of charge discharge of the above cell was charging and discharging were performed by withdrawing 0.06 mA. The charge

discharge cycle is shown in Figure 2.19 B. The discharge capacity was to be 1041 $mAhg^{-1}$ with the discharge potential of 2.7V and the charge capacity was about 931 $mAhg^{-1}$ with the charging potential of 3.6 V to 3.7 V. The preliminary result indicate the successful fabrication of Li-air battery as well as the potential Pt-FAB material as a candidate material for Li-air battery application.

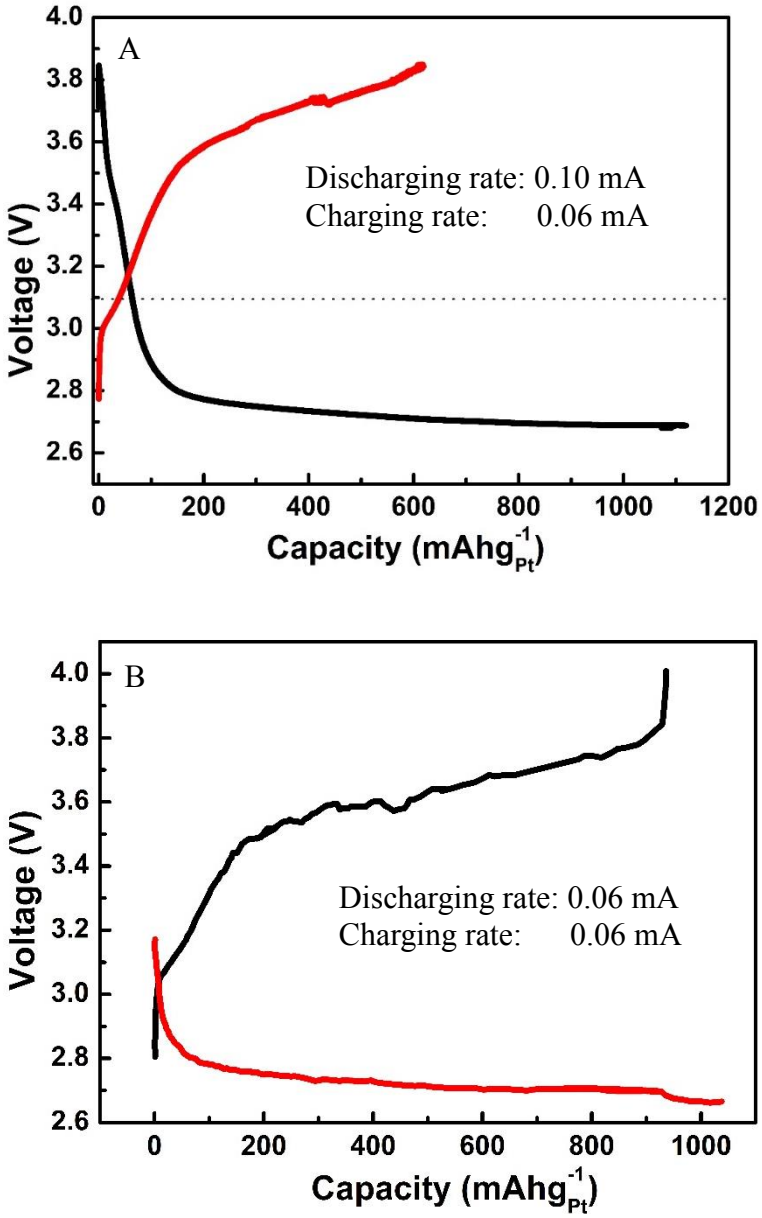

Figure 2.19 Preliminary charge discharge profile of first cycle (A) second cycle (B) of the Pt-FAB based Li-air battery

2.7. Other Electrocatalytic (Methanol Oxidation) Properties of Acetylene Black Based Catalysts

Direct methanol fuel cell (DMFC) has been considered as a plausible energy conversion source for portable electronic devices and electric vehicle because of various features, including high energy conversion efficiency, low exhaust, and ease of handling as a liquid fuel. Generally, fuel cell catalysts are under strongly oxidizing conditions, high oxygen concentration and high potentials. The development of efficient catalysts for electroxidation of methanol has been a hot topic for many researchers.

The thermodynamic standard equilibrium potential for complete electrooxidation of methanol to CO_2 is found to be $E^\circ = 0.02V$. But, due to slow kinetics, the potential is sometimes shifted to few hundreds of millivolts even when very active catalyst like platinum is used.

$$CH_3OH + H_2O \rightarrow CO_2 + 6H^+ + 6e^-$$

Total methanol oxidation to CO_2 gives six electrons, however various side products are produced in parallel side reactions.

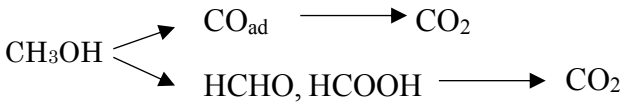

The electrooxidation catalyst must enable two important processes a) dissociation of C-H bond and b) is to facilitate the oxidation of intermediate side products for which the dissociation of water is must, as water is the source of other oxygen to generate CO_2. In Pt based electro catalysts, the interaction with water is possible at potential above 0.4 – 0.45 V vs RHE, which makes the electrooxidation of methanol with Pt based catalyst possible only above 0.45 V vs RHE.

From the vast amount of available literature, it is understood that the catalyst support plays an important role in both catalytic activity and durability of the supported catalysts. Currently,

various carbon nano structures (graphite, graphene and CNTs) are commonly used as substrate for the catalyst. The factors like, surface area, electronic conductivity, and appropriate pore structure play a major role in determining the catalytic activity. Carbon supported Pt catalyst is the most widely used anode catalyst for methanol oxidation reaction (MOR) in direct methanol fuel cells (DMFCs). However, under the working conditions of DMFCs, oxidation of carbon leads to the dissolution of Pt nanoparticles (NPs) decorated on conventional carbon nano structures resulting in the agglomeration of NPs and/or removed from the carbon due to the weak anchoring between Pt and carbon.

The durability of the carbon and the catalyst are the important problems of concern. From the above sections it was very clear that Pt-FAB based materials showed enhanced activity and durability which play an important role in MOR also.

This section deals with the characterization of Pt-FAB based catalysts for its electrocatalytic activity and durability for MOR in comparison to commercial counterparts. Electrochemical measurements were carried out in conventional 3 electrode system, a film of prepared material on glassy carbon electrode was used as working electrode, Pt chip as counter electrode and Ag/AgCl as reference electrode. Electrolyte consists of 0.5 M methanol in 0.5 M H_2SO_4 aq. The potential was scanned in between -0.30 V to 1.2 V vs Ag/AgCl. The Figure 2.19 shows the normalized cyclic voltammograms exhibiting the methanol oxidation peak (I_f) and reduction of intermediates formed as (I_r). The catalytic efficiency of the MOR catalysts can be compared using the important parameters like methanol oxidation onset potential, the oxidation current and the value of I_f/I_r. A good electrocatalyst should have low over potential, high oxidation current and higher I_f/I_r. The ratio, I_f/I_r enables the extent of poisoning of the catalyst with the intermediates formed (CO) which further reduces the MOR efficiency. Onset potential of 19 and 41 wt% Pt-FAB was found to be 0.28 mV while that of commercial Pt/C was found to be at 0.42 mV vs Ag/AgCl. The value of I_f/I_r was found to be in the order of 19 wt% Pt-FAB

(1.21) > 20 wt% Pt-Vulcan XC-72 (1.01) > 41 wt% Pt-FAB (0.63), which means the 19 wt% Pt-FAB has got very less generation of intermediate species and high efficiency for complete methanol oxidation to CO_2. Further the mass activity (MA) was calculated from the CV which gives a clear idea of probable output from the fuel cell. The MA of 19 wt% Pt-FAB was found to be 321.5 $mAmg^{-1}$ which is around 1.85 times that of the commercial counterpart. The mass activity of 41 wt% Pt-FAB was found to be 219.5 $mAmg^{-1}$. As mentioned before improving the durability or the long term use of the catalyst for MOR is most important area of research. The durability of the materials under study was analyzed by subjecting the catalyst to chronoamperometry at peak potential of the MOR i.e at 0.68 V vs Ag/AgCl in nitrogen saturated 0.5 M methanol in 0.5 M H_2SO_4 aq. for 25 mins. The normalized chronoamperogram can be seen in Figure 2.19 B. It is clear that the normalized current decays with time and reaches a steady state. Commercial Pt/C reached to almost 1 $mAmg^{-1}$ after 4 mins while the 41 wt% Pt-FAB initially showed higher current but later reached a steady state with nearly 9 $mAmg^{-1}$ at the end of 25 mins. 19 wt% Pt-FAB showed highest durability and showed nearly 3 times higher current at the end of 25 mins. All the attributes of the catalyst are tabulated in

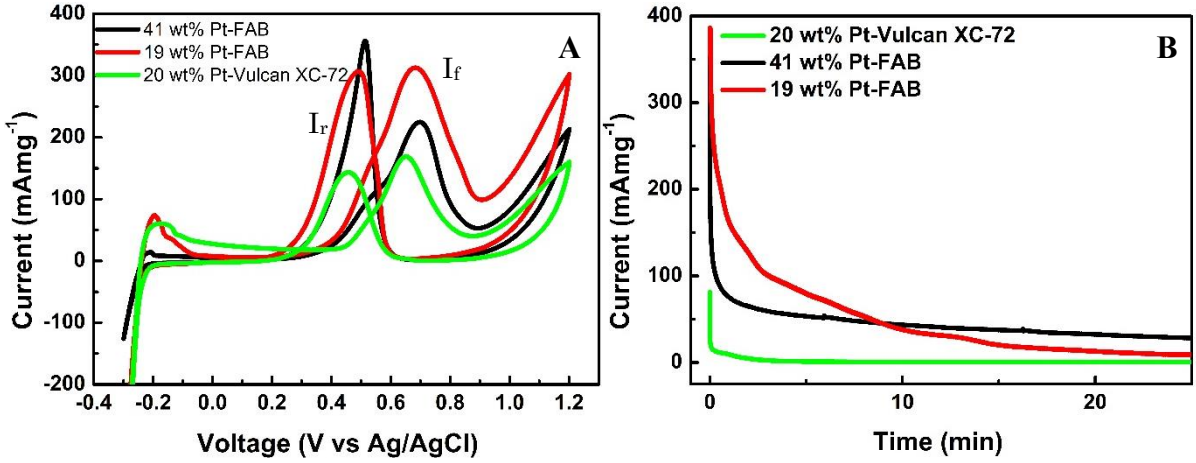

Figure 2.20 Normalized CV (A) and chronoamperograms (B) of 19 and 41 wt% Pt-FAB catalysts in comparison with 20 wt% Pt-Vulcan XC-72

table 2.

Highest mass activity and I_f/I_r of 19 wt% Pt-FAB can be attributed to its high ECSA. The XPS

data aforementioned clearly states that the D-center of the Pt in Pt-FAB was modified enabling a low energy of adsorption which makes the overpotential very less while keeping the Pt/C intact with less degradation. Thus, the durability of the material was very high which was reiterated in the chronoamperomtric studies. These studies suggests that Pt-FAB can be a very promising catalyst for MOR in DEMFC.

Table 2.2 Comparison of different parameters for MOR of Pt-FAB catalysts and commercial counterparts

Electrode	Pt Loading (mg/cm^2)	I_F (mA)	I_R (mA)	Ratio I_F/I_R	Mass Activity (mA/mg)	Onset Potential (mV)
19 wt% Pt-FAB	0.108	6.61	5.45	**1.21**	**321.5**	**0.28**
41 wt% Pt-FAB	0.259	11.3	17.8	0.630	219.5	0.30
20% Pt-Vulcan XC-72	0.056	1.45	1.43	1.01	173.6	0.42

2.8. Conclusion

A novel disordered graphene like material was prepared using AB as starting material with a facile single pot method which can be easily scaled up. Surface modification with oxygen functional groups enabled effective nucleation Pt-np uniformly all over the substrate and enhanced anchoring with the substrate. The presence of functional groups further enhanced the absorption properties of catalyst which reduced the charge transfer resistances to a great extent. All the above factors synergistically showed extremely high electrocatalytic activity which reached the DOE target for year 2020. The present work also answers the long standing problem of low durability of AB based catalysts. The application of Pt-FAB in PEMFC also showed enhanced activity. Further MOR results reveal the high catalytic activity and durability of the Pt-FAB catalyst. The above results and observations showed that Pt-FAB is a promising catalytic material not only in fuel cells but also stands tall for its application in metal air batteries.

References

(1) Park, M.; Sun, H.; Lee, H.; Lee, J.; Cho, J. Lithium-air batteries: survey on the current status and perspectives towards automotive applications from a battery industry standpoint. *Adv. Ener. Mater.*, 2012, *2*, 780–800.

(2) Xiao, J.; Wang, D.; Xu, W.; Wang, D.; Williford, R. E.; Liu, J.; Zhang, J.-G. *J. Electrochem. Soc.,* **2010**, *157*, A487–A492.

(3) Zhang, B.; Lai, C.; Zhou, Z.; Gao, X. P. Preparation and electrochemical properties of sulfur–acetylene black composites as cathode materials. *Electrochim. Acta*, **2009**, *54*, 3708–3713.

(4) Shin, H. C.; Cho, W. I.; Jang, H. Electrochemical properties of carbon-coated $LiFePO_4$ cathode using graphite, carbon black, and acetylene black. *Electrochim. Acta*, **2006**, *52*, 1472–1476.

(5) Uchida, M.; Fukuoka, Y.; Sugawara, Y.; Ohara, H.; Ohta, A. Improved preparation process of very-low-platinum-loading electrodes for polymer electrolyte fuel cells. *J. Electrochem. Soc.*, **1998**, *145*, 3708–3713.

(6) Uchida, M.; Aoyama, Y.; Tanabe, M.; Yanagihara, N.; Eda, N.; Ohta, A. Influences of both carbon supports and heat-treatment of supported catalyst on electrochemical oxidation of methanol. *J. Electrochem. Soc.*, **1995**, *142*, 2572–2576.

(7) Li, Y.; Gao, W.; Ci, L.; Wang, C.; Ajayan, P. M. Catalytic performance of Pt nanoparticles on reduced graphene oxide for methanol electro-oxidation. *Carbon* **2010**, *48*, 1124–1130.

(8) Wissler, M. Graphite and carbon powders for electrochemical applications. *J. Power Sources* **2006**, *156*, 142–150.

(9) Ferrari, A. C.; Robertson, J. Interpretation of Raman spectra of disordered and amorphous carbon. *Phys. Rev. B*, 2000, *61*.

(10) Wang, S.; Iyyamperumal, E.; Roy, A.; Xue, Y.; Yu, D.; Dai, L. Vertically aligned bcn nanotubes as efficient metal-free electrocatalysts for the oxygen reduction reaction: a synergetic effect by co‐doping with boron and nitrogen. *Angew. Chem. Int. Ed. Engl.*, **2011**, *50*, 11756–11760.

(11) Yang, L.; Jiang, S.; Zhao, Y.; Zhu, L.; Chen, S.; Wang, X.; Wu, Q.; Ma, J.; Ma, Y.; Hu, Z. Boron-Doped Carbon Nanotubes as Metal-Free Electrocatalysts for the Oxygen Reduction Reaction. *Angew. Chem. Int. Ed. Engl.*, **2011**, *123*, 7270–7273.

(12) Zhou, Y.-G.; Chen, J.-J.; Wang, F.; Sheng, Z.-H.; Xia, X.-H. A facile approach to the synthesis of highly electroactive Pt nanoparticles on graphene as an anode catalyst for direct methanol fuel cells. *Chem. Commun.* **2010**, *46*, 5951–5953.

(13) Kim, M.; Park, J.-N.; Kim, H.; Song, S.; Lee, W.-H. Low-Pt-loading acetylene-black cathode for high-efficient dye-sensitized solar cells. *J. Power Sources* **2006**, *163*, 93–97.

(14) Cai, F.; Liang, J.; Tao, Z.; Chen, J.; Xu, R. The preparation of Pt/C catalysts using various carbon materials for the cathode of PEMFC. *J. Power Sources* **2008**, *177*, 631–636.

(15) Bondarenko, A. S.; Stephens, I. E. L.; Hansen, H. A.; Pérez-Alonso, F. J.; Tripkovic, V.; Johansson, T. P.; Rossmeisl, J.; Nørskov, J. K.; Chorkendorff, I. The Pt (111)/electrolyte interface under oxygen reduction reaction conditions: an electrochemical impedance spectroscopy study. *Langmuir* **2011**, *27*, 2058–2066.

Chapter 3

Novel Sacrificial Reducing Agent Free Photo-Generation of Pt Nanoparticles on All Conducting Carbon Forms as Triple-Phase ORR Catalytic with Enhanced Activity

3.1. Abstract

Electrocatalytic materials for oxygen reduction reaction, currently dominated by platinum/carbon catalyst is marred by drawbacks such as, use of copious amount of Pt and use of "non-green" sacrificial reducing agent (SRA) during the synthesis. A single stroke remedy for these two problems has been achieved through an *in-situ* aqueous photoreduction void of even trace amounts of SRA with an enhanced activity. Reduction of $PtCl_6^{2-}$ salt to Pt nano particles on carbon substrate and TiO_2 photocatalyst was achieved solely using solar spectrum as the source of energy. Here, we demonstrate that this new procedure of photoreduction, decorates Pt over different types of conducting carbon allotropes with the distribution and the particle size primarily depending on the conductivity of these allotrope. The $Pt/C/TiO_2$ composite unveiled an ORR activity on par with the most efficient Pt based electrocatalyst prepared through the conventional sacrificial reducing agent aided preparation methods.

3.2. Introduction

The importance of ORR has been well understood over the years. However, the catalyst driving the ORR has not quenched the desires of the global demand. In general, Pt based carbon catalysts, one of the most widely employed ORR catalyst, are prepared by employing polyols and/or other reducing agents and are subjected to elevated temperatures. The use of these procedures stray outside the "green-way". Lookout for alternative green procedures has recently ended up in exploiting photo-reduction processes. Alongside 'green' aspect, large scale commercial applications are precluded by the high manufacturing cost of the ORR catalyst. Hence, researcher have been focusing on reducing the cost of the catalyst by decreasing the amount of Pt used, by adapting to a variety of carbon materials, use of transition metal oxides and doping of nitrogen in carbon. The year 2015, has seen more developments and attempts to improve the ORR activity by the addition of a metal oxide such as MoO_x[1], TiO_x[2] and CeO_x[3,4], on the Pt/C catalyst. Incidentally some or most of these metal oxides fall in the category of photo-catalyst. Generation of charges on impingement of light, characteristic to any photo-catalyst, can potentially involve in various photo-physical phenomenon like trapping of charges, radiative and non-radiative charge recombination along with interfacial charge transfer. The interfacial charges are available for further redox reactions of the molecules adsorbed onto the surface of the photo-catalyst.

In this regard, TiO_2 nanostructures have been studied in-depth and have proven to be an excellent choice for photocatalytic reduction of many materials ranging from fullerenes[5], inorganic[6] and many organic compounds[7]. Here, the high conducting band of TiO_2 (approx. -0.5 V vs NHE at 7.00 pH) enables controlled reduction of chemical species, which is highly necessary. This validates the thermodynamic feasibility to transfer the photo-generated charges, especially electrons to any conducting carbon for further reduction of metal salts[8]. In the recent past among many strategies to control the recombination of electron–hole, carbon-TiO_2 hybrid

are more looked upon due to its efficiency[9–16]. The control of recombination in TiO_2/C hybrid is achieved owing to the placement of the conduction band of carbon marginally lower than that of TiO_2 allowing a predominant passage of electrons from conduction band of TiO_2. This process of interfacial charge transfer to the pre-adsorbed conducting carbons, was found to be a working alternative to control the rapid recombination of the photo-generated charges of TiO_2[17]. This spill-over of electrons from the conduction band, when happens on a highly conducting matrix, the electrons tend to travel over the conducting matrix until it finds a suitable reducing species (Figure 3.1). Recently, a few researchers[18–20] tapped these photo-electrons for recovering few transition metals from industrial wastes in aqueous media without any added SRA. Yunteng *et al.*,[21] and Ian *et al.*,[22] contributed significantly in photo-reducing the metals salts to metal nanoparticles on to carbon substrates. However, they added a determined amount of SRA and was not a facile reaction to scale them up industrially.

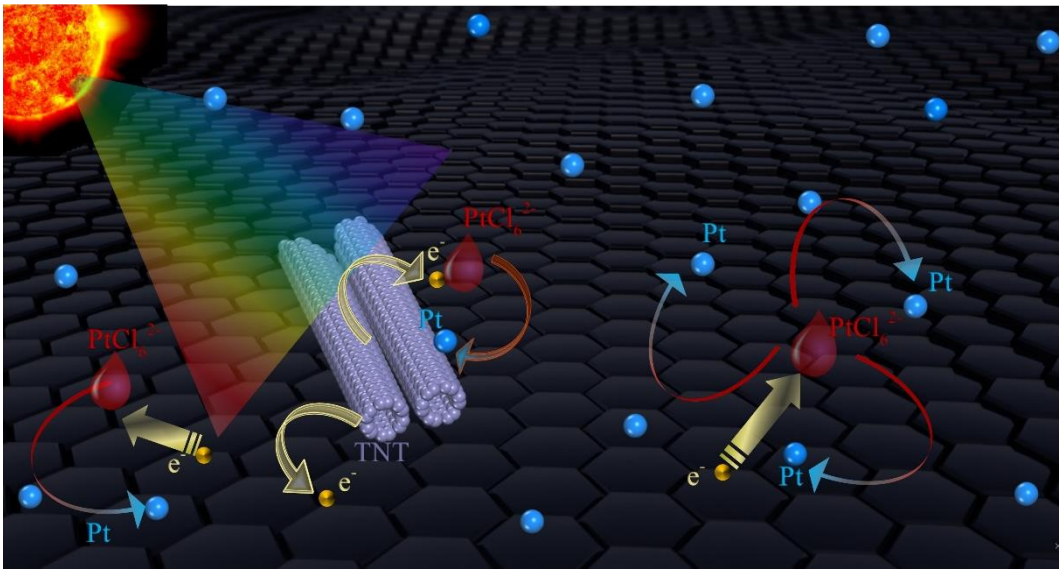

Figure 3.1 Schematic representation of the photo-reduction process

This chapter details a novel and facile photochemical reaction tapping the photo-electron generated by semiconductor when irradiated with simulated solar light. The photo-electron is successfully tapped onto carbon which further reduces chloroplatinic acid to nano particles of

high electrocatalytic activity. The process is void of any SRA, pH adjustment or increase in temperature. This chapter highlights the successful photo-reduction of metal salts to metal nano particles on to any electron conducting substrate using TiO_2 nano structures as photo catalysts. Along with the novelty in the method, this system also confirms the enhanced electro-catalytic activity with high durability by employing three component (Pt-carbon-TiO_2) system.

3.3. Experimental section

3.3.1. Preparation of Electrocatalyst by Novel Photo-reduction Process.

Two different types of TiO_2 photo-catalysts were used in the synthetic procedures, one was commercial TiO_2 obtained in anatase phase from Sigma Aldrich in the form of powder and other being homemade titania nanotubes (TNT). TNT was prepared by general anodization method. Ti chip used for the anodization process was polished 600 grit roughness and the oxide layer was removed by washing the chip in hydrofluoric acid:nitric acid:water (1:3:16 volume ratio) mixture. This chip was degreased by washing the Ti chip in methanol. Cleaned titanium metal strip was anodized at DC voltage of 50 V along with constant ultra-sonication for two and a half hour in an aqueous ethylene glycol solution containing 0.5 wt.% NH_4F using a platinum strip as cathode. In order to get the TNTs as a whole length tube without any damage, a peeling-off technique was introduced during the synthesis procedure. This was done by adapting a 15 minutes quiet period after 45 minutes from the commencement of the application of DC voltage and ultra-sonication followed by continuation of anodization for 1 hr and 30 minutes. After the TNT were grown on the Ti strip, it was washed with methanol and was ultra-sonicated in water to peel out the TNT in whole and was sintered at 300 ^oC to make the TiO_2 into a single anatase phase and eliminate all the organic contaminations.

For the photo-reduction process, graphite, graphene oxide (GO) or multiwalled carbon nanotubes (CNTs) weighing 90 mg was ultrasonicated in deionized water for nearly 2 hrs to

obtain a uniform dispersion. To this uniform dispersion, 10 mg (10 wt%) of TiO_2 (anatase commercially obtained from Sigma Aldrich) or homemade TiO_2 nano tubes (TNT) was introduced and ultrasonicated for 15 min. 800 µL of 0.045M aq. chloroplatinic acid (H_2PtCl_6) solution was added to this mixture and was irradiated by a simulated solar light for 5 hrs under constant stirring. The material was filtered, washed with deionized water and dried under vacuum overnight at room temperature. Different composite materials by varying the carbon substrate and photo-catalyst were made (shown in the scheme 3.1), they were, Photo-Pt-Graphite-TiO_2, Photo-Pt-GO-TiO_2, Photo-Pt-CNT-TiO_2 and Photo-Pt-CNT-TNT.

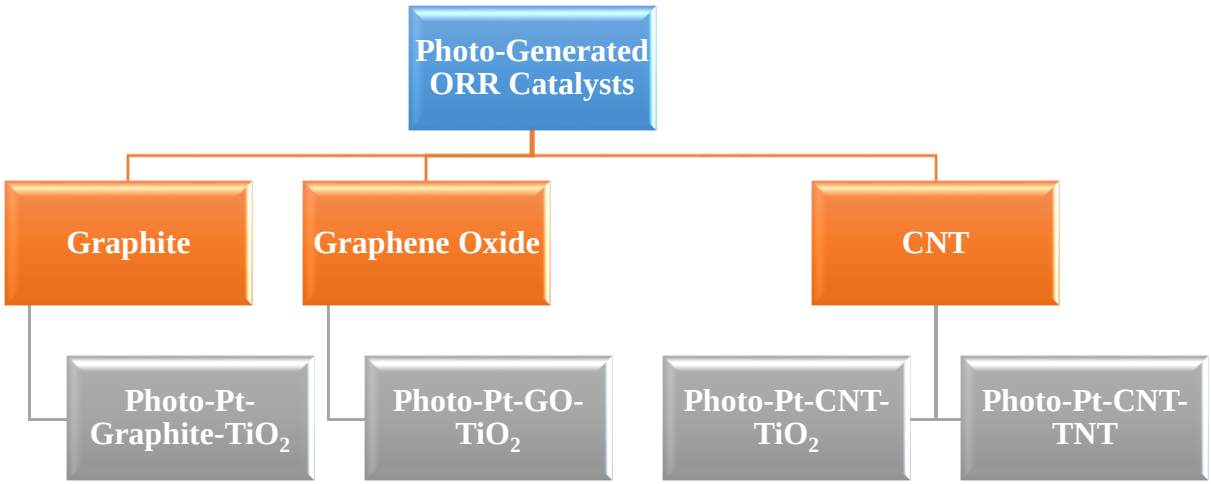

Scheme 3.1 Shows various ORR catalysts made

3.3.2. Physical and Chemical Characterization

Elemental analysis of the materials was studied using X-ray photoelectron spectroscopy (XPS) technique performed on S-probe^{TM} 2803 instrument. The morphological characterization was done using high resolution transmission electron microscopy (HR-TEM) on Hitachi H-7650 model. TEM sample was prepared by dropping a methanolic solution containing well dispersed composite on a carbon coated copper grid.

To determine the exact amount of Pt present on all the four catalysts, inductively coupled plasma mass spectrometry (ICP-MS) measurements were done. In a typical experimental procedure, 20 mg of each catalyst was weighed and heated at 150 ^{o}C for 30 min under N_2(0.2 $Lmin^{-1}$):H_2(1.0 $Lmin^{-1}$). The mixture was then calcinated for 60 mins at 800 ^{o}C in air. The cooled residue was dissolved in 5 mL of aquaregia. The obtained solution was filtered and the filtrate was diluted with water and made up to 100 mL. This solution was used in ICP experiment using Shimadzu ICPE-9000.

3.3.4. Electrochemical Characterization

Further, the materials were studied for its electrocatalytic activity by observing the ORR behaviour using cyclic voltammetry (CV) and rotating disc electrode (RDE) measurements (Automatic polarization system HZ-5000, Dynamic electrode HR-301 and Dynamic electrode controller HR-502). These electrochemical studies were performed using conventional three electrode system, electrocatalyst coated on to glassy carbon electrode as working electrode, platinum wire as counter and reversible hydrogen electrode (RHE) was used as reference electrode at 30 ^{o}C (temperature was controlled by Eyela CTP-1000) in 0.1M $HClO_4$. The Pt loading on the electrode was maintained at 5.07 μg/cm^2. CV was measured by sweeping the voltage between 0.05 V – 1.20 V at the sweep rate of 50 mVs^{-1} in nitrogen saturated 0.1 M $HClO_4$ at 30 ^{o}C. Linear sweep voltammetry was studied using RDE technique across 0.05 – 1.00 V with the voltage sweep rate of 20 mVs^{-1} in oxygen saturated 0.1 M $HClO_4$ solution. The rate of rotation in RDE was varied from 400 – 3600 rpm.

3.4. Results and Discussion

3.4.1. Physical and Chemical Characterization

Exact Pt weight percentage (wt%) decorated on each of different substrate was determined by the ICP-MS technique. The results revealed that Pt wt% on each catalyst was 4.3 wt% in Pt-graphite-TiO_2, 1.6% in Pt-GO-TiO_2, 2.6% in Pt-CNT-TiO_2 and 3.4% in Pt-CNT-TNT.

The elemental composition of the electro catalytic materials prepared was determined by XPS. Figure 3.2 A-D are the typical survey spectrum of the samples exhibiting the peaks at their respective binding energies for C1s, O1s, Pt4f, Ti2p and etc.

Further XPS was employed to analyse the valence states of Pt in the prepared catalysts. High resolution of local scan of Pt 4f peak provides valuable information on various oxidation states of Pt and also elucidates the anchoring strength with which the Pt nps are decorated over various substrates using different catalysts. The high resolution Pt4f peak of the Photo-Pt-graphite-TiO_2 (Figure 3.3 A) consisted of three individual peaks at 71.2, 72.4 and 73.7 eV corresponding to Pt^0, Pt^{II} and Pt^{IV} oxidation states. The Pt^0 was found to be the predominant oxidation state with 66% followed by 27% of Pt^{II} and 7% of Pt^{IV}. Figure 3.3 B shows the deconvolution of Pt 4f peak for Photo-Pt-CNT-TiO_2. This too consists of three peaks at 71.4, 72, and 73.5 corresponding to Pt^0, Pt^{II} and Pt^{IV} respectively. Similar to graphite based material Photo-Pt-CNT-TiO_2 also consists predominantly Pt^0 with around 63 % along with small proportions of Pt^{II} (17%) and Pt^{IV} (20%). Deconvolution of Pt 4f peak of Photo-Pt-CNT-TNT (Figure 3.3 C) revealed that the peak contains only two peaks of Pt^0 and Pt^{II} with 80% and 20% respectively. These two peaks are at 71.78 and 72.70 eVs. The shift in the Pt^0 peak towards high BE was observed. Compared to Pt^0 peak of Photo-Pt-Graphite-TiO_2, Photo-Pt-CNT-TiO_2 and Photo-Pt-CNT-TNT showed 0.2 and 0.58 eVs higher binding energies

respectively. The shift of Pt^0 peak towards high binding energy can be ascribed to SMSI (strong metal and substrate interaction) between Pt and CNT & TiO_2 (particles and nanotubes).

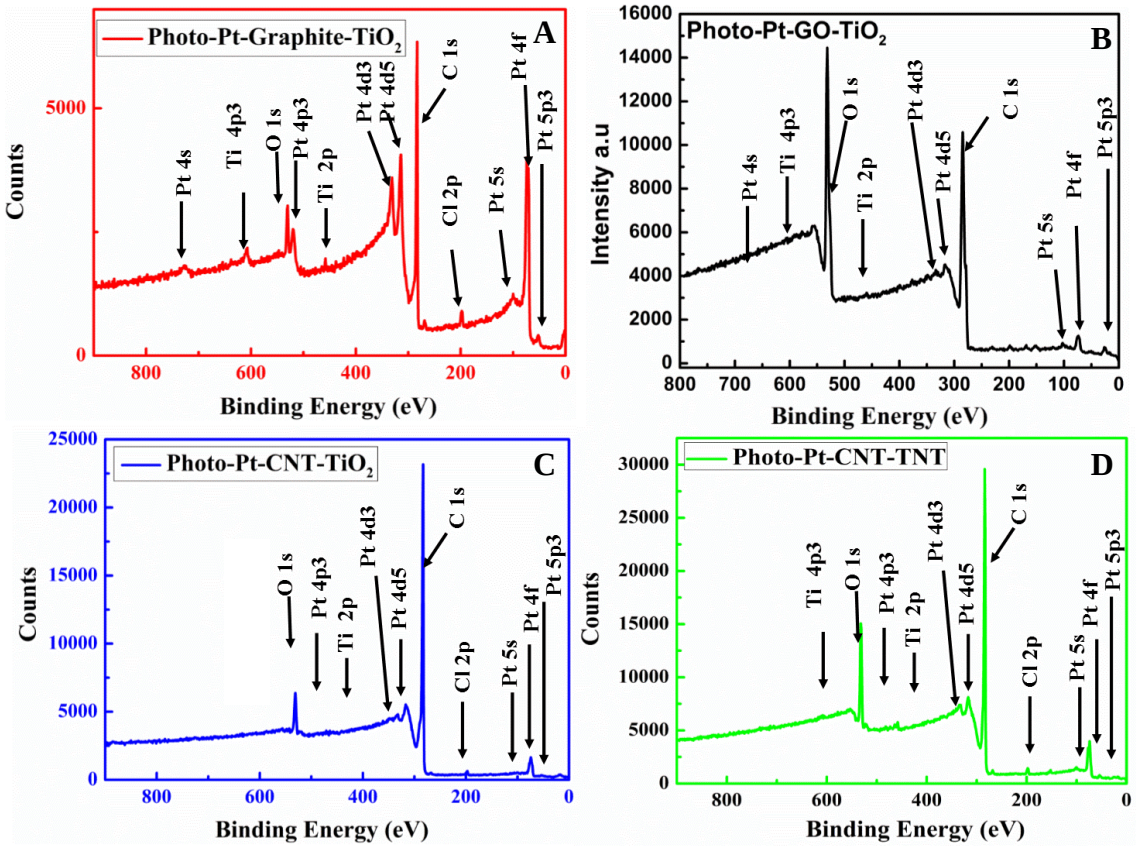

Figure 3.2 XPS survey spectra of Photo-Pt-Graphite-TiO_2 (A) Photo-Pt-GO-TiO_2 (B) Photo-Pt-CNT-TiO_2 (C) Photo-Pt-CNT-TNT (D)

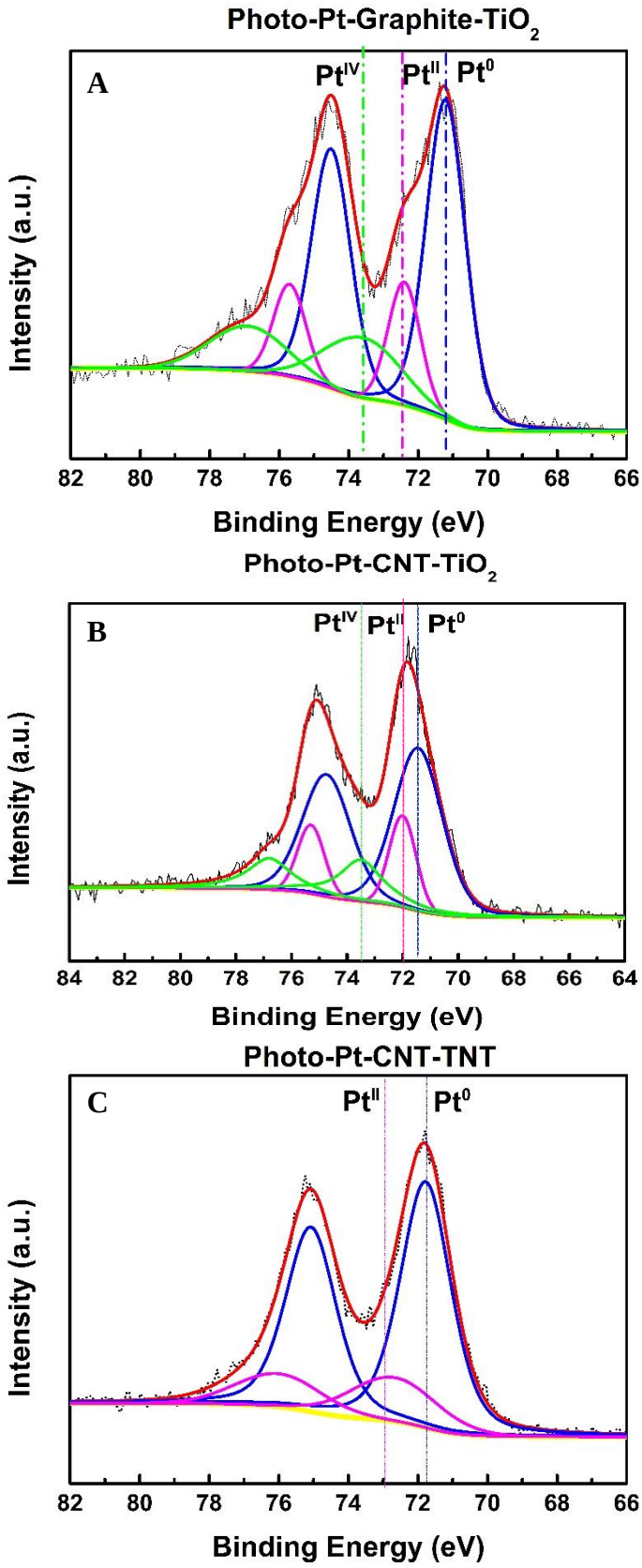

Figure 3.3 Deconvolution of Pt 4f peak of Photo-Pt-Graphite-TiO_2 (A) Photo-Pt-Graphite-TiO_2 (B) and Photo-Pt-CNT-TNT (C) showing Pt^0, Pt^{II} and Pt^{IV} valence states.

Morphology of TiO_2 nano particles, TNT and the Pt nanoparticles (Pt-nps) photo-generated on to various carbon/TiO_2 hybrids was studied using TEM. This analysis shed light on the particle size and distribution of Pt-nps on TiO_2 nanostructures and carbon allotropes. Figure 3.4 A & B shows the TEM images of bare TiO_2 and TNT. It is very clear from the TEM micrographs that the surface of the TiO_2 and TNT does not contain any particles with different contrast before photo-reduction process. Figure 3.4A shows that the TiO_2 particle size is in the range of 50-60 nm. Figure 3.4B shows that TNT consists of ~100 nm tube diameter.

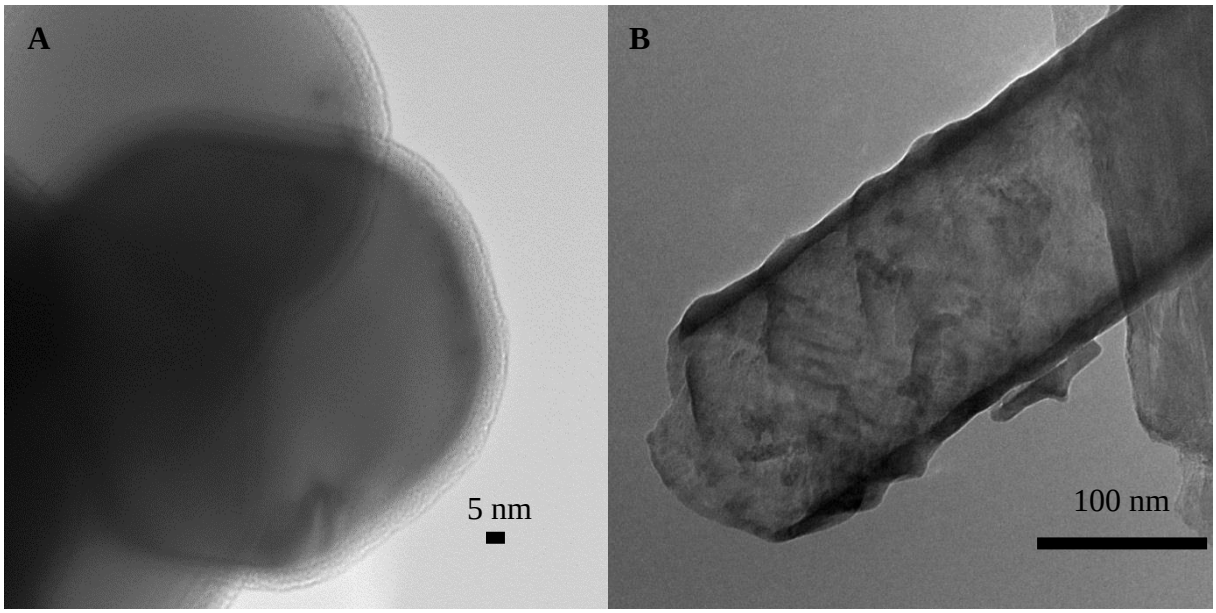

Figure 3.4 TEM micrographs of TiO_2 nano particles (A) and TNT (B)

Figure 3.5 & 3.6 shows the TEM micrographs of all the 4 materials made using photo-reduction method. TEM results can be discussed under two heads based on the type of morphology of the photo-catalyst used. The first one is commercial TiO_2 anatase particles and the second one is, indigenous titania nanotubes (TNT). Both these catalysts have been found to be sufficiently efficient for photo-generation of Pt-nps on conducting carbons.

Photo-Pt-Graphite-TiO_2: Figure 3.5 A & B. shows the TEM micrographs of Photo-Pt-Graphite-TiO_2. Clear indication of uniform photo-deposits related to Pt nps on graphite (Figure 3.5 A) and TiO_2 particles (Figure 3.5 B) was observed. The particles were

uniformly distributed without any agglomerations all through the graphite. Closely looking at Figure 3.5 B, a dark spot of ~50 nm, correlating to the size of TiO_2 (approx. 50 nm) on a 2-dimensional sheet of graphite was seemingly embedded over vast span of dark minute particulate embodies. The photo-deposits with an average particle size of around 2.3 nm have found to be deposited as a layer all around the TiO_2 particle like a shell over the core of TiO_2 nps. The size of the particles predominantly ranged from 3-5 nm on graphite.

Photo-Pt-GO-TiO_2: Similar methodology was adapted with Graphene Oxide (GO), in case of GO, when TiO_2 was used as photo-catalyst the particles decorated only the TiO_2 (Figure 3.5 C & D) with the size ranging around 2-6 nm and no particles were seen on GO.

Photo-Pt-CNT-TiO_2: Figure 3.5 E & F shows the TEM micrographs of Photo-Pt-CNT-TiO_2. The average size of the particle over CNT was observed to be 1.0 nm (Figure 3.5 E) and 2-4 nm (Figure 3.5 D) on TiO_2. In contrast to the results obtained in the case of Photo-Pt-Graphite-TiO_2, the TiO_2 particles in Photo-Pt-CNT-TiO_2 were not covered with the shell of Pt nps. Instead a uniform distribution of Pt nps was seen on TiO_2 particles. With the above results it could be concluded that CNT was very effective in decoration of very small and highly uniform Pt nps in photo-catalytic Pt generation process. Hence, as a spin-off, similar methodology was adapted with TNT as photo-catalyst instead of TiO_2 particles using CNT as conducting substrate.

Photo-Pt-CNT-TNT: Figure 3.6 A & B shows the TEM micrographs showing very uniform and agglomeration free Pt nps over CNT and TNT. The average Pt-nps size on CNT (Figure 3.6 A) as well as TNT (Figure 3.6 B) was approximately 1 nm.

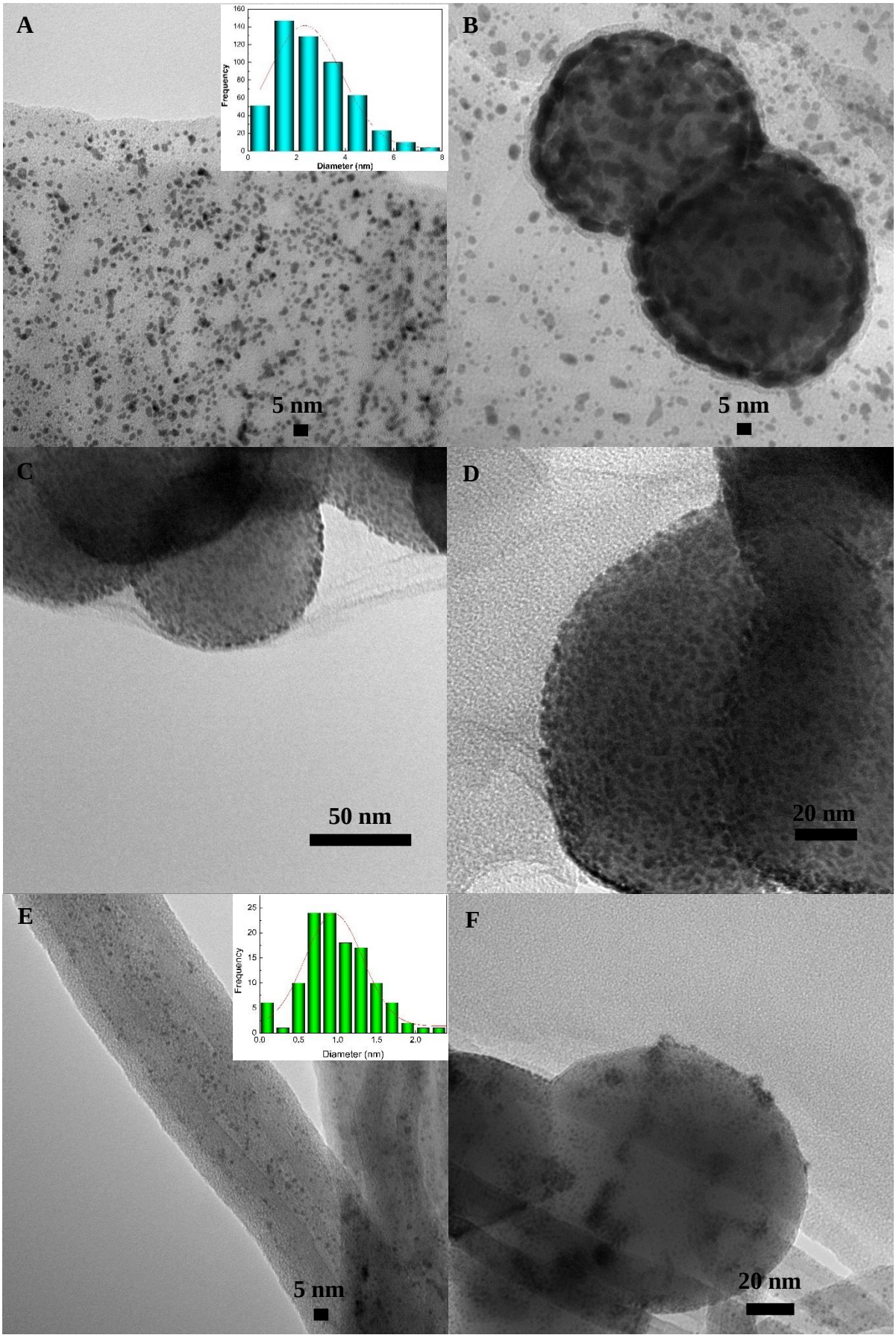

Figure 3.5 TEM micrographs of Photo-Pt-Graphite-TiO_2 (A-B) Photo-Pt-GO-TiO_2 (C-D) Photo-Pt-CNT-TiO_2 (E-F)

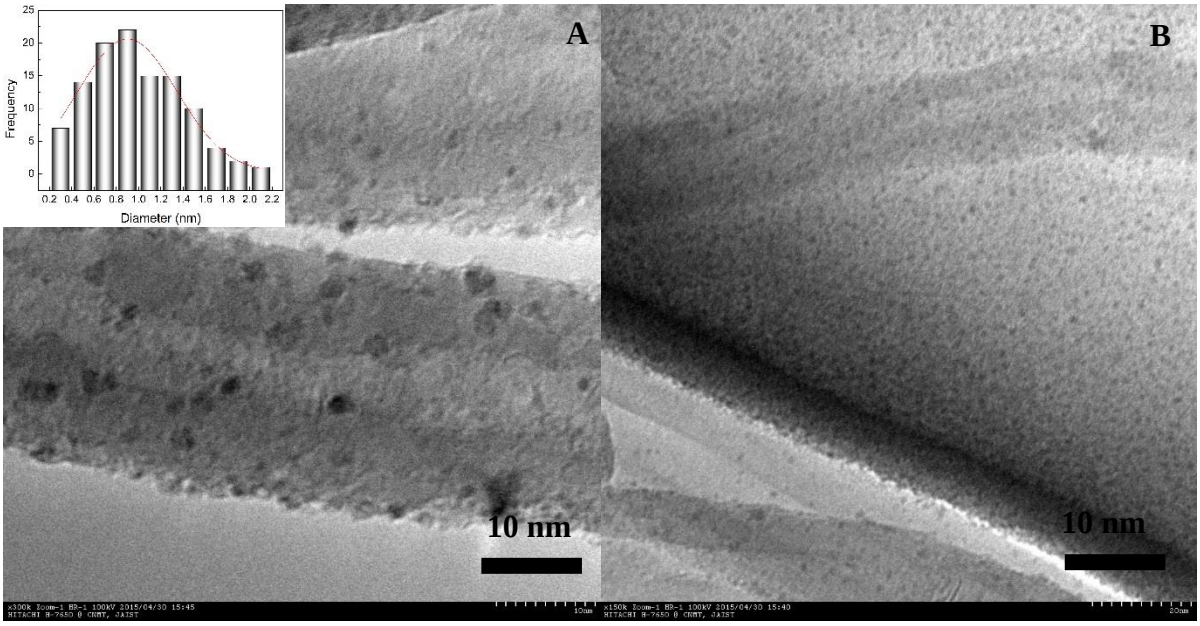

Figure 3.6 TEM images of Photo-Pt-CNT-TNT (A-B)

The three main observations of TEM analysis can be explained as follows (1) formation of a layer of Pt nps on TiO_2 but not on TNT (2) lower size and more uniformity in distribution of Pt-nps with the use of TNT and (3) no/less Pt-nps on GO and particle sizes dependence on substrate. Firstly TNTs are proven in literature to be a better catalyst than that of particles due to its larger surface area and directional charge transfer of the photo-generated electrons to the conducting substrate[25]. Along with the above aspects, the area of catalyst at the point of contact to carbon and the conductivity of the carbon substrate can play an important role as it helps in facile transfer of electrons. When photo-electrons are generated on TiO_2, the rate at which the electrons are dissipated from the surface of TiO_2 to carbon is less due to its lower area at the point of contact. With this, there is a large possibility of Pt (IV) ions being reduced on TiO_2 where probability of finding photo-generated electron is more than that of carbon. Thus a layer of Pt-nps can be expected on to TiO_2 in the presence of graphite. Whereas, a large surface area of TNT and its tubular nature makes the area of contact sufficiently high for efficient charge transfer to carbon. In addition, the directional flow of electron makes the photo-reduction more

controlled which further results in uniform small sized Pt-nps well distributed on both the surfaces of photo-catalyst as well as carbon. Further, the electronic conductivity of the carbon allotropes used, will elucidate the reason behind the variation in the particle size distribution on different carbon substrates. The electronic conductivity of carbon substrates follows the order GO<graphite<CNT. GO is highly functionalized with various oxygen functional groups interrupting the delocalization of electrons. The electrons tends to flow only in the regions where the π electron cloud is uninterrupted, so only in these regions reduction of adsorbed species is more probable. Large particle size on photo-Pt-GO-TNT can be ascribed to this. Moreover, covalently bonded oxygen functionalities are readily reduced than that of adsorbed reducing species in the presence of photo-electron[26] resulting RGO with fewer or no Pt particles. In the same line, CNT being better electronic conductor than that of graphite, smaller and more uniform Pt-np distribution was observed as expected. From the above results, it was very clear that combination of modified TiO_2 and highly conducting carbon composite have efficient charge generation and less recombination with improved electron diffusion length all along (hundreds of nanometers) the surface of the conducting carbon.

3.4.2. Electrochemical Characterization

The cyclic-voltammetry (CV) and linear sweep voltammetry using rotating disc electrode studies were carried out for evaluating the ORR behavior of the prepared samples and the obtained results were compared with commercial TEC10E50E from Tanaka precious metal. Further the charge transfer resistance and the durability of the electrocatalysts were studied using electrochemical impedance spectroscopy and potential cycling using CV, respectively. Cyclic voltammograms given in Figure 3.7 showed a typical Pt-carbon type profile exhibiting Pt fingerprint peaks for hydrogen adsorption (H_{ad}) and desorption, oxygen evolution and reduction peaks. Figure 3.7 A-E shows the cyclic voltammograms of all the materials understudy. It is clear from Figure 3.7 B that the current profile was very less showing ORR

activity of Photo-Pt-GO-TiO_2. Hydrogen desorption peak was used to study the electrochemical active surface area (ECSA) of the all the materials under study. Figure 3.7 E

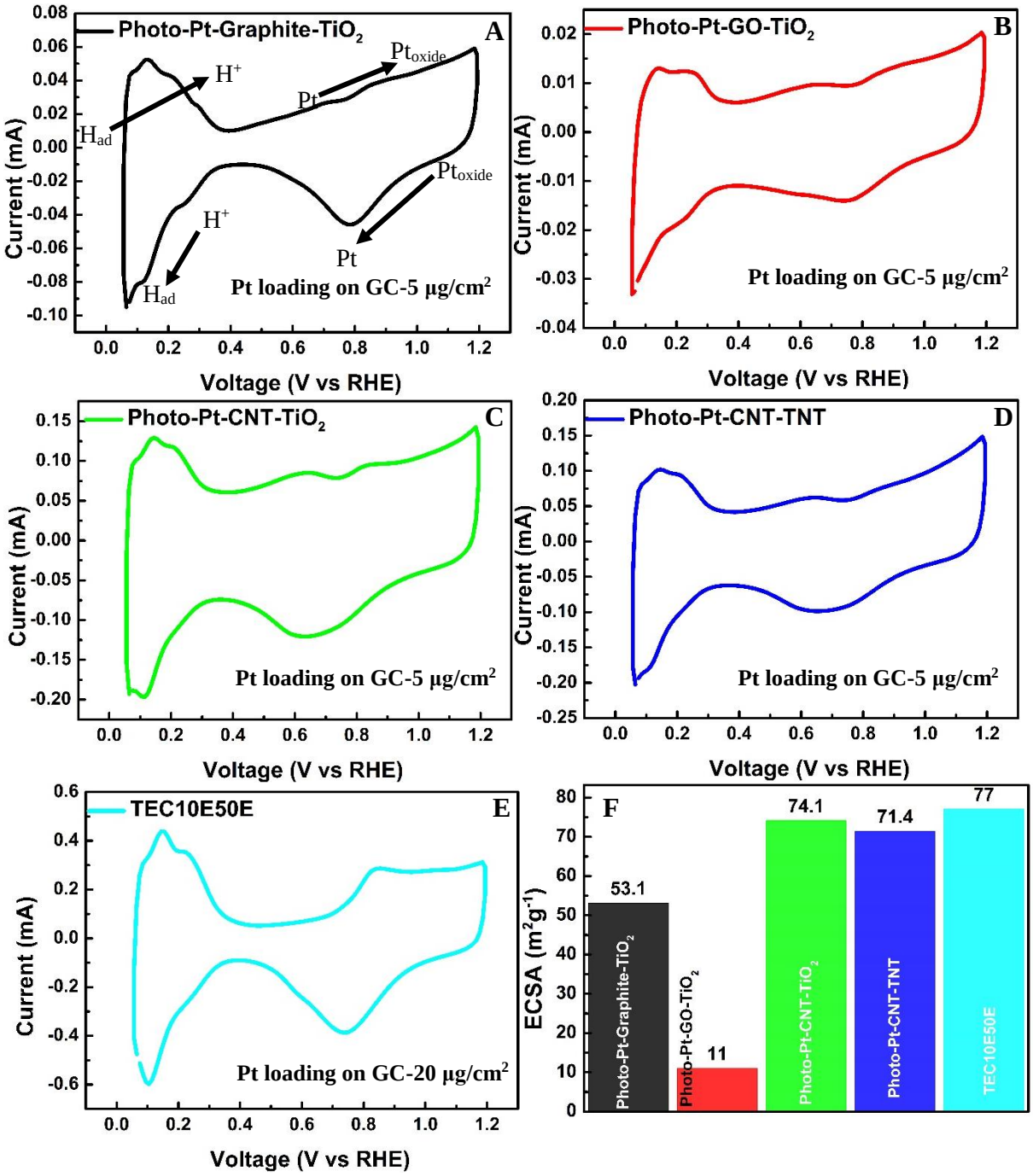

Figure 3.7 Cyclic voltammograms of Pt-Graphite-TiO_2 (A) Pt-GO-TiO_2 (B) Pt-CNT-TiO_2 (C) Pt-CNT-TNT (D) TEC10E50E (E) and ECSA calculated from above voltammograms (F)

shows the ECSA of all the electro-catalysts. ECSA of the materials was found to be in the following range, Pt-Graphite-TiO_2 (53.08 m^2/g), Pt-CNT-TiO_2 (74.13 m^2/g), Pt-GO-TiO2 (11.00 m^2/g), Pt-CNT-TNT (71.4 m^2/g) and TEC10E50E (77.00 m^2/g). Highest ECSA of Pt-

CNT-TiO_2 and Pt-CNT-TNT can be attributed to the smallest particle size in the range of 1-3 nm. Pt-GO-TiO_2 showed very negligible ECSA due very less Pt nps decoration on carbon and Pt nps of high particles size.

Further RDE measurements were carried out to understand the ORR kinetics, reaction rate and the mechanism. This method was found to be a powerful tool to evaluate various kinetic parameters of the electrocatalysts. It is well known that electrocatalytic ORR can takes place in two different routes in acidic medium i.e., less efficient two electron process and an efficient four electron process. To determine the mechanism with which the ORR electrocatalyst operates is very crucial to evaluate the catalyst. The numbers of electrons transferred per O_2 molecule was calculated with well-known Koutecky– Levich equation.

$$\frac{1}{I} = \frac{1}{i_k} + \frac{1}{i_L} \qquad (1)$$

$$i_L = 0.620nFACD^{2/3}\nu^{-1/6}\omega^{1/2} \qquad (2)$$

Where, i_k is the kinetic current for the oxygen reduction at the surface of the electrode, i_L is the Levich current for the electrode reaction of the oxygen by a diffusion controlled process, in other words, it can be called as diffusion-limited current, n is the number of electrons transferred to oxygen, F is the Faraday constant (96,485 C mol^{-1}), A is the area of the RDE used (0.196 cm^2), D is the diffusion coefficient of the dissolved oxygen in electrolyte (1.93×10^{-5} cm^2s^{-1}), C is the dissolved oxygen concentration (1.26×10^{-6} mol cm^{-3}), ν is the kinematic viscosity of the electrolyte (10.09×10^{-3} cm^2 s^{-1}), ω is the rotation rate of electrode.

Figure 3.8 A, C and E shows the liner sweep voltammograms (LSV) of Photo-Pt-Graphite-TiO_2, Photo-Pt-CNT-TiO2 and Photo-Pt-CNT-TNT catalysts. LSV was performed from 1 V to 0.2 V vs RHE at 20 mV/s scan rate in O_2 saturated 0.1 M $HClO_4$ aq. at 30 ^oC. The RDE measurements were done at rotation rate of 400, 900, 1600, 2500 and 3600 rpm. The linear sweep

voltammograms show a typical profiles with the mixed kinetic and diffusion region at around 0.7 to 1 V vs RHE and diffusion limiting current at around 0.2 to 0.7 V vs RHE.

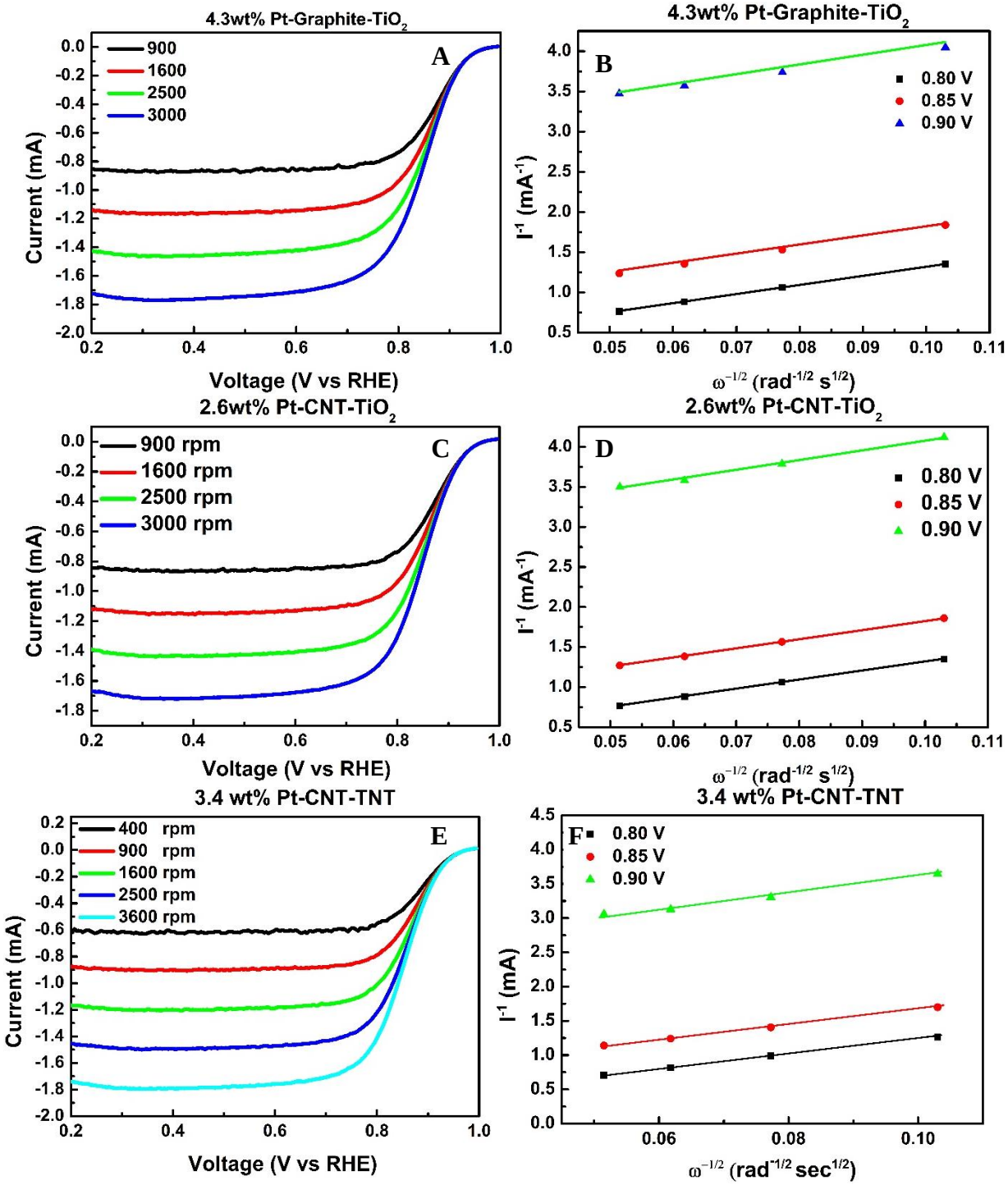

Figure 3.8 RDE curves for Photo-Pt-Graphite-TiO_2 (A), Photo-Pt-CNT-TiO_2 (C) and Photo-Pt-CNT-TNT (E) at 30 °C in oxygen saturated 0.1 M $HClO_4$ aq. at scan rate of 20 mV/s at different rotation speeds (400, 900, 1600, 2500, 3600 rpm) and respective Koutecky-Levich plots (B, D and E) at 0.80, 0.85 and 0.90 V vs RHE (experiments were carried out in dark).

Coresponding Koutecky-Levich plots for all the samples at rotation rates of 900, 1600, 2500 and 3600 rpm are shown in Figure 3.8 B, D & F for diffusion limiting current at 0.80, 0.85 and 0.90 V. It was observed that I^{-1} and $\omega^{-1/2}$ plot have good linear relationship at all the potentials. The linearity and the parallel behaviour of the KL plots corroborates first order kinetics with respect to O_2 in mixed kinetic-diffusion controlled region. The intercept from the KL plot was used to find the kinetic current and subsequently the number of electrons taking part in the

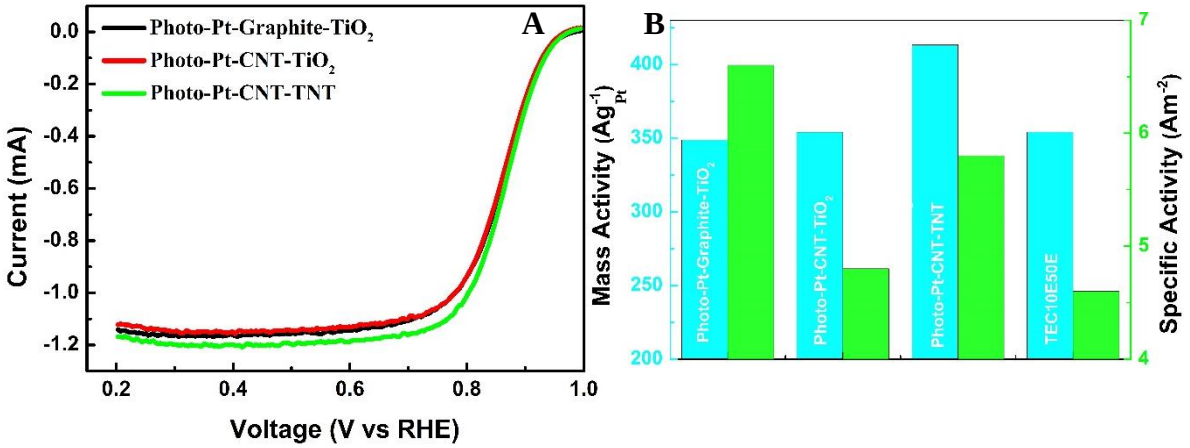

Figure 3.9 Comparison of RDE polarization plots of Photo-Pt-Graphite-TiO_2, Photo-Pt-CNT-TiO_2 and Photo-Pt-CNT-TNT (A) MA and SA comparison of homemade material with commercial counterpart at 0.9 V vs RHE (B)

ORR. The number of electrons transfer during the ORR calculated employing Koutecky–Levich (K–L) plots (ESI) were found to be ~4 at 0.8 – 0.9 V. This corroborates that the ORR is a single step 4 electron process and not sequential 2 electrons process.

Figure 3.9 A compares the polarization curves of materials prepared. Both TiO_2 based material (Photo-Pt-Graphite-TiO_2 and Photo-Pt-CNT-TiO_2) and TNT based material (Photo-Pt-CNT-TNT) exhibited high ORR activity with the onset potential of 0.930 V. The half wave potential ($E_{½}$) of TiO_2 based materials was found to be 0.850 V, in case of TNT based material it was found to be 0.865. This shows that the TNT based material experiences less over potential than that of TiO_2 based materials. A marginally less $E_{½}$ in case of photo generated catalysts compared to commercial catalyst can be due to the decrease in the electronic conductivity of the sample by containing TiO_2 based nano structures. However, this decrease

in the conductivity is compensated with the less amount of Pt loaded on the catalyst. The mass activity (MA) and specific activity (SA) based on the normalization on Pt loading and active surface area respectively have been evaluated (Figure 3.9 B). Interestingly, though the ECSA of the homemade materials were slightly lesser than that of the commercial reference, MA of TiO_2 based samples were found to be same (around 350 Ag^{-1}) and that of Photo-Pt-CNT-TNT was found to be 1.8 times that of the former. SA was found to be in the order of Photo-Pt-Graphite-TiO_2 (6.6 Am^{-2}) > Photo-Pt-CNT-TNT (5.8 Am^{-2}) Photo-Pt-CNT-TiO_2 (4.8 Am^{-2}) > TEC10E50E (4.6 Am^{-2}).

The durability of the materials was studied by potential cycling and EIS experiments. Durability experiments were monitored by observing percentage loss of ECSA and increase in the charge transfer resistance. Potential cycling was performed using CV technique in similar to previously mentioned procedure as in experimental section. Figure 3.10 shows the variation in the ECSA for every 100 cycles. The percentage loss in the ECSA was found to be nominal. %ECSA loss in the case of Photo-Pt-CNT-TiO_2 was 16% and that of Photo-Pt-CNT-TNT was found to be 12%. Along with this the gradual change, charge transfer

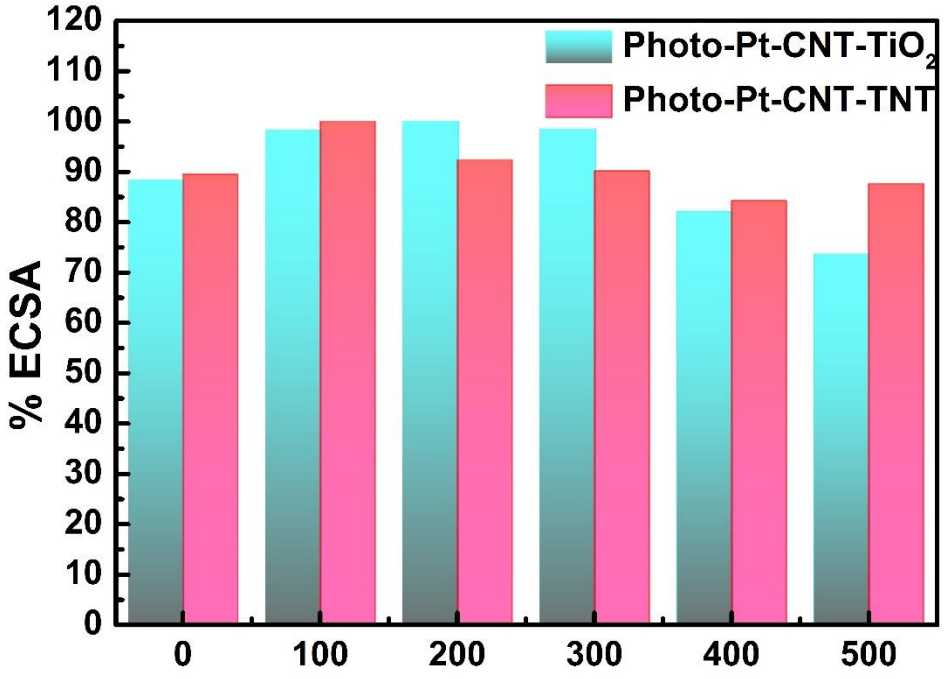

Figure 3.10 %ECSA change measured over 500 potential cycles.

resistance was also monitored through EIS measurements. EIS measurements were performed using conventional three electrochemical set-up in 0.1 M $HClO_4$ aq. at open circuit potential. Figure 3.11 shows the Nyquist plots resulted at various intervals of potential cycling. Figure 3.11 A. shows the Nyquist plot for Photo-Pt-CNT-TiO_2 and Figure 3.11 B. that of Photo-Pt-CNT-TNT. In the inset the equivalent circuit fit for the spectra is shown. It is clear

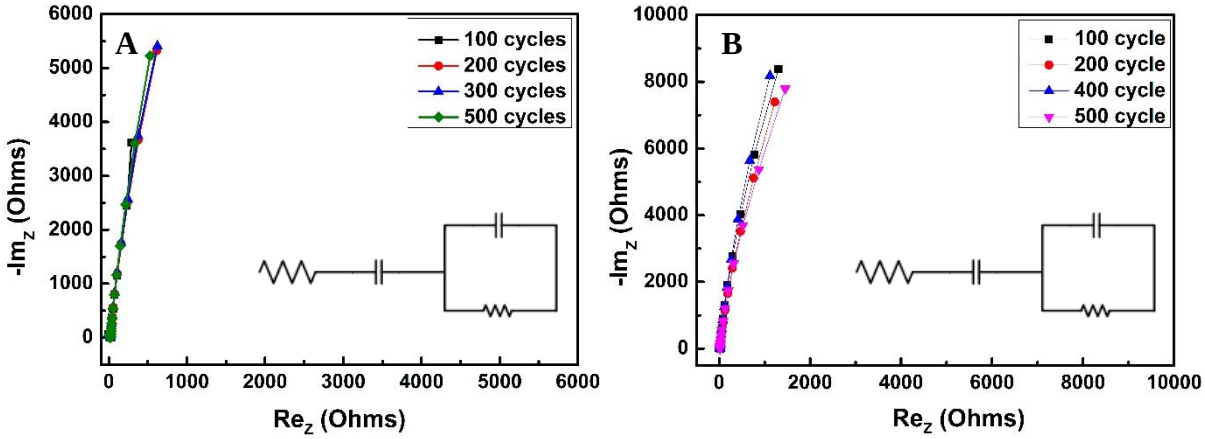

Figure 3.11 EIS measurements at various stages during the potential cycling and equivalent circuit for Photo-Pt--CNT-TiO_2 (A) and Photo-Pt-CNT-TNT (B)

from these plots and Table 3.1 and 3.2 that there is no drastic change in the charge transfer resistance (R_{ct}) of the material with the electrolyte even after many potential cycles. This clearly indicates that there is no evident structural degradation in the substrate and the metal catalyst. Photo-Pt-CNT-TNT with very good SMSI was found to be very stable with very minimal reduction in the ECSA and increase in the charge transfer resistance.

The above results clearly demonstrates that all the photo-generated catalyst are catalytically highly active. The mass activity and specific activity of all the materials with ultra-low Pt amount (2-5 wt%) were found to be higher than the one of the commercially best catalyst with 50 wt% of the Pt made by conventional non-green methods. Basing on the values of ECSA, electrocatalytic activity and durability of TNT based material was found to be superior to that of TiO_2 particle. This can be ascribed to the SMSI characteristics which were revealed by XPS.

Table 3.1Comparison of elements in the equivalent circuit for various potential cycles of Photo-Pt-CNT-TiO_2

Photo-Pt-CNT-TiO_2	R1	C1	R_{ct}	C2	χ^2
100 Cycles	19	0.0002	5.09	2.13E-05	6.60E-03
200 Cycles	18.6	0.0002	5.09	0.00017	6.50E-03
400 Cycles	18.9	0.0002	5.18	1.90E-05	6.40E-03
500 Cycles	19.3	2.73E-05	5.25	1.80E-04	4.40E-03

Table 3.2 Comparison of elements in the equivalent circuit for various potential cycles of Photo-Pt-CNT-TNT

Photo-Pt-CNT-TNT	R1	C1	R_{ct}	C2	χ^2
100 Cycles	21.3	0.0002	384.1	7.70E-05	4.30E-03
200 Cycles	18.9	0.0002	211.7	0.0008	5.50E-03
400 Cycles	19	0.00019	188.0	0.0008	5.60E-03
500 Cycles	18.7	0.0002	858.9	7.00E-04	6.70E-03

3.5. Conclusion

In conclusion, a highly reproducible, environmentally benign, ultrafast and completely green method was developed for the preparation of highly active ORR catalyst with ultra-low Pt content (for use in Fuel cell and Lithium-air battery). The method uses solar light as the only source of energy in the preparation of this catalytically efficient composite utilizing abundant and environmentally benign TiO_2 nano structures as photo-catalyst. Using this green methodology, preparation of novel composites containing TiO_2 particles and nanotubes, CNT/Graphite substrates and platinum nanoparticles was successfully carried out. As prepared material with ultra-low Pt showed excellent ORR catalytic activity comparable to the best of commercial ORR catalysts (containing 50 Wt% of Pt). All the materials showed comparable MA and higher SA than that of commercial one with very high durability. It can also be confirmed that this method is feasible for all the conducting carbon substrates. The above results clearly demonstrates that the novel, green and a very viable method of Pt decoration method is as efficient as rather more efficient as that of well-established methods using SRA.

References

(1) Martins, P. F. B. D.; Ticianelli, E. A. Electrocatalytic activity and stability of platinum nanoparticles supported on carbon–molybdenum oxides for the oxygen reduction reaction. *ChemElectroChem*, **2015**, *2*, 1298–1306.

(2) Esfahani, R. A. M.; Videla, A. H. M.; Vankova, S.; Specchia, S. Stable and methanol tolerant Pt/TiO_x-C electrocatalysts for the oxygen reduction reaction. *Inter. J. Hydr. Ener.*, **2015**, *40*, 14529–14539.

(3) Chauhan, S.; Mori, T.; Masuda, T.; Ueda, S.; Richards, G. J.; Hill, J. P.; Ariga, K.; Isaka, N.; Auchterlonie, G.; Drennan, J. Design of low pt concentration electrocatalyst surfaces with high oxygen reduction reaction activity promoted by formation of a heterogeneous interface between Pt and ceox nanowire. *ACS Appl. Mater. Interfaces.,* **2016**, *8*, 9059–9070.

(4) Luo, Y.; Calvillo, L.; Daiguebonne, C.; Daletou, M. K.; Granozzi, G.; Alonso-Vante, N. A highly efficient and stable oxygen reduction reaction on Pt/CeO_x/C electrocatalyst obtained via a sacrificial precursor based on a metal-organic framework. *Appl. Catal. B: Environ.*, **2016**, *189*, 39–50.

(5) Kamat, P. V.; Bedja, I.; Hotchandani, S. Photoinduced charge transfer between carbon and semiconductor clusters. One-electron reduction of C_{60} in colloidal TiO_2 semiconductor suspensions. *J. Phys. Chem.*, **1994**, *98*, 9137–9142.

(6) Habisreutinger, S. N.; Schmidt-Mende, L.; Stolarczyk, J. K. Photocatalytic reduction of CO_2 on TiO_2 and other semiconductors. *Angew. Chem. Int. Ed.*, **2013**, *52*, 7372–7408.

(7) Ferry, J. L.; Glaze, W. H. Photocatalytic reduction of nitro organics over illuminated titanium dioxide: role of the TiO_2 surface. *Langmuir*, **1998**, *14*, 3551–3555.

(8) De Tacconi, N. R.; Chenthamarakshan, C. R.; Rajeshwar, K.; Lin, W.-Y.; Carlson, T. F.; Nikiel, L.; Wampler, W. A.; Sambandam, S.; Ramani, V. Photocatalytically generated Pt⁄C –TiO_2 electrocatalysts with enhanced catalyst dispersion for improved membrane

durability in polymer electrolyte fuel cells. *J. Electrochem. Soc.*, **2008**, *155*.

(9) Zhou, Y.; Liu, L.; Zhao, Z.; Sun, L. Anatase TiO_2 nanocrystals with exposed {001} facets on graphene sheets via molecular grafting for enhanced photocatalytic activity. *Nanoscale*, **2012**, *4*, 613–620.

(10) Chavez, C. A.; Brumbach, M. T.; Wheeler, D. R.; Washburn, C. M.; Bell, N. S.; Lambert, T. N. Large area mosaic films of graphene–titania: self-assembly at the liquid–air interface and photo-responsive behavior. *Nanoscale*, **2011**, *3*, 188–191.

(11) Li, M.; Tang, P.; Hong, Z.; Wang, M. High efficient surface-complex-assisted photodegradation of phenolic compounds in single anatase titania under visible-light. *Colloids and Surfaces A: Physicochem. Eng. Aspects*, **2008**, *318*, 285–290.

(12) Li, M.; Hong, Z.; Fang, Y.; Huang, F. Synergistic effect of two surface complexes in enhancing visible-light photocatalytic activity of titanium dioxide. *Materials Research Bulletin*, **2008**, *43*, 2179–2186.

(13) Li, M.; Zhou, S.; Zhang, Y.; Chen, G.; Hong, Z. One-step solvothermal preparation of TiO_2/C composites and their visible-light photocatalytic activities. *Appl. Sur. Sci.*, **2008**, *254*, 3762–3766.

(14) Khalid, N. R.; Ahmed, E.; Hong, Z.; Zhang, Y.; Ahmad, M. Nitrogen doped TiO_2 nanoparticles decorated on graphene sheets for photocatalysis applications. *Curr. Appl. Phys.*, **2012**, *12*, 1485–1492.

(15) Khalid, N. R.; Ahmed, E.; Hong, Z.; Ahmad, M. Synthesis and photocatalytic properties of visible light responsive La/TiO_2-graphene composites. *Appl. Surf. Sci.*, **2012**, *263*, 254–259.

(16) Khalid, N. R.; Hong, Z.; Ahmed, E.; Zhang, Y.; Chan, H.; Ahmad, M. Synergistic effects of Fe and graphene on photocatalytic activity enhancement of TiO_2 under visible light. *Appl. Surf. Sci.*, **2012**, *258*, 5827–5834.

(17) Huang, Q.; Tian, S.; Zeng, D.; Wang, X.; Song, W.; Li, Y.; Xiao, W.; Xie, C. Enhanced

photocatalytic activity of chemically bonded TiO_2/Graphene composites based on the effective interfacial charge transfer through the C–Ti bond. *ACS Catalysis*, **2013**, *3*, 1477–1485.

(18) Mahlamvana, F.; Kriek, R. J. Photocatalytic reduction of platinum(II and IV) from their chloro complexes in a titanium dioxide suspension in the absence of an organic sacrificial reducing agent. *Appl. Catal. B: Environ.*, **2014**, *148–149*, 387–393.

(19) Yu, J.; Dai, G.; Huang, B. Fabrication and characterization of visible-light-driven plasmonic photocatalyst Ag/AgCl/TiO_2 nanotube arrays. *J. Phys. Chem. C.*, **2009**, *113*, 16394–16401.

(20) Kriek, R. J.; Mahlamvana, F. Dependency on chloride concentration and "in-sphere" oxidation of H_2O for the effective TiO_2-photocatalysed electron transfer from H_2O to $[PdCl_n(H_2O)^{4-}{}_n]^{2-}{}_n$ (n = 0–4) in the absence of an added sacrificial reducing agent. *Appl. Catal. A: Gen.*, **2012**, *423–424*, 28–33.

(21) Qu, Y.; Gao, Y.; Kong, F.; Zhang, S.; Du, L.; Yin, G. Pt–rGO–TiO_2 nanocomposite by UV-photoreduction method as promising electrocatalyst for methanol oxidation. *Int. J. Hydrog. Energy.*, **2013**, *38*, 12310–12317.

(22) Lightcap, I. V.; Murphy, S.; Schumer, T.; Kamat, P. V. Electron hopping through single-to-few-layer graphene oxide films. Side-selective photocatalytic deposition of metal nanoparticles. *J. Phys. Chem. Lett.*, **2012**, *3*, 1453–1458.

(23) Ando, F.; Gunji, T.; Fujima, H.; Takeda, T.; Tanabe, T.; Kaneko, S.; Matsumoto, F. Preparation of a PtPb/TiO_2/cup-stacked carbon nanotube composite for enhancement of the electrocatalytic reaction of the oxygen reduction reaction. *Chem. Lett.*, **2015**, *44*, 1741–1743.

(24) Roy, N.; Leung, K. T.; Pradhan, D. Nitrogen doped reduced graphene oxide based Pt–TiO_2 nanocomposites for enhanced hydrogen evolution. *J. Phys. Chem. C.*, **2015**, *119*, 19117–19125.

(25) Grimes, C. A. Synthesis and application of highly ordered arrays of TiO_2 nanotubes. *J.*

Mater. Chem., **2007**, *17*, 1451–1457.

(26) Williams, G.; Seger, B.; Kamat, P. V. TiO_2-Graphene nNanocomposites. UV-assisted photocatalytic reduction of graphene oxide. *ACS Nano*, **2008**, *2*, 1487–1491.

Chapter 4

3D-Polythiophene Foam on TiO_2 Nanotube Array as a Substrate for Photo-Generated Pt Nanoparticles as an Advanced ORR Catalyst

4.1 Abstract

The development of novel substrates possessing high durability, strong anchoring to catalytic metal nanoparticle and low charge transfer resistance that can replace conventional carbon is of great importance. In order to improve the durability and reduce the cost of various energy devices, new methodologies are necessary. In this regard, the present chapter highlights the preparation of a macroporous hybrid material containing polythiophene electropolymerized on to TiO2 nanotubes (TNT). The prepared foam like hybrid material showed very low charge transfer resistance and was further modified with novel and green photo-generated Pt nanoparticles. The material exhibited very strong metal substrate interaction which makes it highly durable during the ORR. This chapter proposes a novel macroporous organic/inorganic hybrid material as a candidate material that has a great probability to replace the conventional carbon substrates for ORR catalysts.

4.2. Introduction

The development of very active, stable and economically viable electrocatalysts is the main bottle neck in realizing efficient alternate energy technologies like fuel cells and Li-air batteries. Although Pt nano particles were found to be extremely active, the high cost involved in the preparation and stability of the catalysts are the two principle reasons for the constantly growing interest in this research. Pt nps are well known as a promising material for ORR due to their high efficiencies. However, factors like electrooxidation of carbon substrate, dissolution of their ions, Ostwald ripening and aggregation[1] of nps are the demerits that inhibit their commercialization. Hence, an electrochemically stable catalyst support with tailorable morphology is of great importance. Considering the multifaceted functionalities of conducting polymers, it could best fit as a candidate material for electrocatalysts.[2].

Conducting polymers have gained a great attention and has been subjected to extensive investigation since their discovery in 1970s. The ease in their synthetic procedure gave a huge scope to tailor their electrical conductivity, chemical and mechanical stability. Due to the improvement in the above intrinsic properties of conducting polymers, their application ranges from charge storage devices, electrochromic devices, modified electrodes, anticorrosion coating, molecular transistors etc[3–6].

Amongst many conducting polymers studied so far, polythiophene (PTh) and its derivatives are of great interest. Their high electrochemical stability in stringent oxidizing or reducing electrolytes makes it a good choice for various electrochemical applications. Polythiophene, over the years has evolved as a promising catalyst support material for various electrochemical applications. Schrebler *et al*[7]. modified the PTh by decorating Pt and Pt/Pd metal nanoparticles for electrooxydation of formic acid. In this study, PTh as a support offered a high electrochemical stability and the composite proved PTh to be an effective alternate supporting

material to conventional carbon supports. Yassar *et al*[8]., electrodeposited Pd onto PTh and studied the ORR characteristics by varying the particle size of the Pd nps. Several other researchers also reported PTh as a very stable host polymer matrix[9,10]. PTh, with attractive features like good mechanical, chemical and electrochemical stability particularly in the presence of strong acids or bases, can be highly recommended for application as catalysts supporting material for ORR.

From the synthesis standpoint of polythiophene, electrochemical polymerization of thiophene is one of the most frequently used method for the preparation of porous conducting polymers[11]. Rationally, electrochemical polymerization of thiophene delivers several advantages compared to conventional chemical polymerization techniques. Employing electrochemical polymerization allows facile tailoring of the thickness of the polymer by controlling the number of deposited layers and provides a degree of control over the pore wall dimensions and morphology[12–14]. Secondly, the polymerization rate can be precisely controlled to achieve highly compact polymers[12] and it provides a very good contact with the conducting substrates which is essential in the fabrication of electrical devices[15]. Alongside, electropolymerization provides the selectivity to choose the site of polymerization, Kowalski et al., reported a site-specific deposition of polypyrrole in the gaps of tube walls instead and not inside the tubes of TiO_2 nanotube array[16].

Generally the conducting polymers can be fabricated into shape specific macroporous structures by employing templates with specific dimensions of choice. Ordered macroporous or tubular polymeric nano structures can be fabricated by employing colloidal crystals[12,17,18] or anodic aluminium oxide,[19–22] TiO_2 nanotube (TNT)[23] arrays. In the recent years, TNT has grabbed lot of interest in the research community because of the ability to control the geometry

and functional properties with simple anodization preparation methods. Recent studies showed the preparation and studies of polymer/TNT nano architectures with unique geometries[16,24,25].

It would be worthwhile to recapitulate chapter 3, where, TNT demonstrated promising photo-reduction ability for metal salt to form metal nps onto a conducting substrate and the resulting highly stable triple phase catalyst showed high ORR catalytic efficiency with very low Pt content. With this background and an extension to the previous work, a 3 dimensionally ordered polythiophene foam was electropolymerized using TNT array as the template and imidazolium based ionic liquid as vectors to enable the directional diffusion of monomer to the electrode. Pt nps were decorated onto this conducting polymer/TNT array hybrid material using novel photo-reduction method mentioned in the chapter 3. This chapter highlights the preparation of novel 3D polythiophene foam electropolymerized using ionic liquid as a vector onto TNT template and Pt decoration was done using novel green photo-reduction method.

4.3. Experimental Section

4.3.1. Preparation of TNT array

TiO_2 nano tube array was prepared by anodization method similar to previously reported procedure. Ti chip used for the anodization process was polished 600 grit roughness and the oxide layer was removed by washing the chip in hydrofluoric acid : nitric acid : water (1:3:16 volume ratio) mixture. This chip was degreased by washing the Ti chip in methanol. Cleaned titanium metal strip was anodized at DC voltage of 50 V along with constant ultra-sonication for two and a half hour in an aqueous ethylene glycol solution containing 0.5 wt.% NH_4F using a platinum strip as cathode (Figure 4.1). After the TNT were grown on the Ti strip, it was washed with methanol and sintered at 300 ^oC to make the TiO_2 into a single anatase phase and eliminate all the organic contaminations.

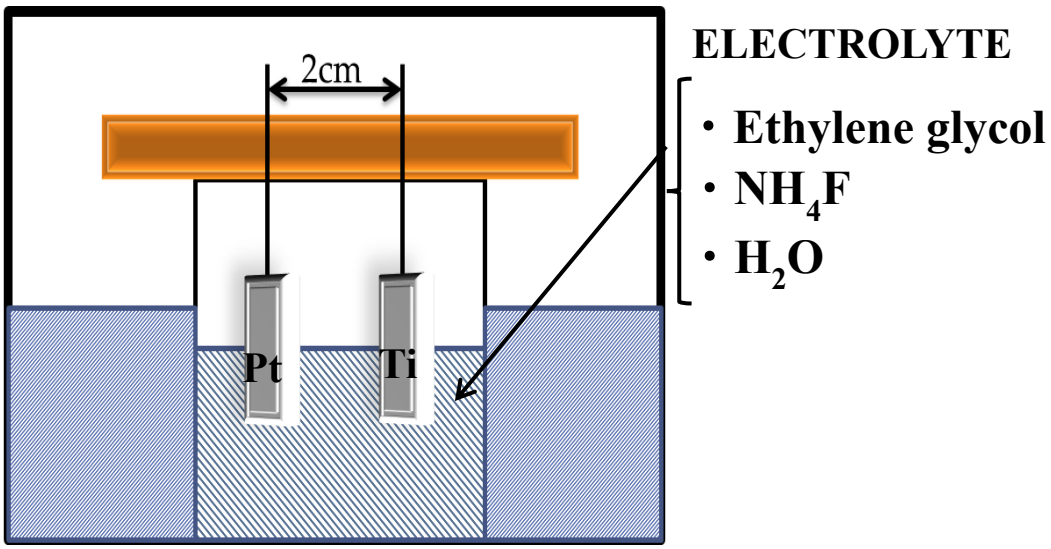

Figure 4.1 Experimental set-up for the anodization method to prepare TNT array

4.3.2. Preparation of 1-methyl- 3-dodecyl bromide (DMImBr)

The preparation of DMImBr was performed using a general procedure of preparing imidazolium ionic liquids[26]. In brief, DMImBr, methylimidazole is treated with dodecyl bromide in acetonytrile at 80 ^{o}C. The solution was refluxed under nitrogen atmosphere for 48 hrs (Scheme 4.1). The volatile material was removed and the resulted material was recrystallized using ethyl acetate and n-hexane mixture to get soft crystalline material.

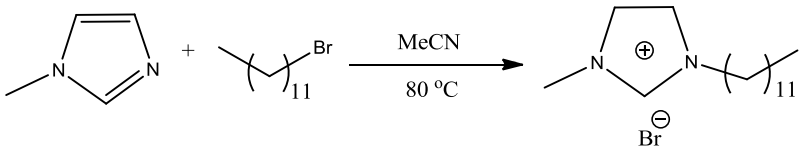

Scheme 4.1 Reaction scheme for the synthesis of DMIMBr

DMImBr was successfully prepared as shown by Scheme 4.1 with 85% yield. The structural determination of DMImBr was performed by ^{1}H-NMR spectroscopy (Figure 4.2) on Bruker BioSpin, Avance III 400MHz instrument .

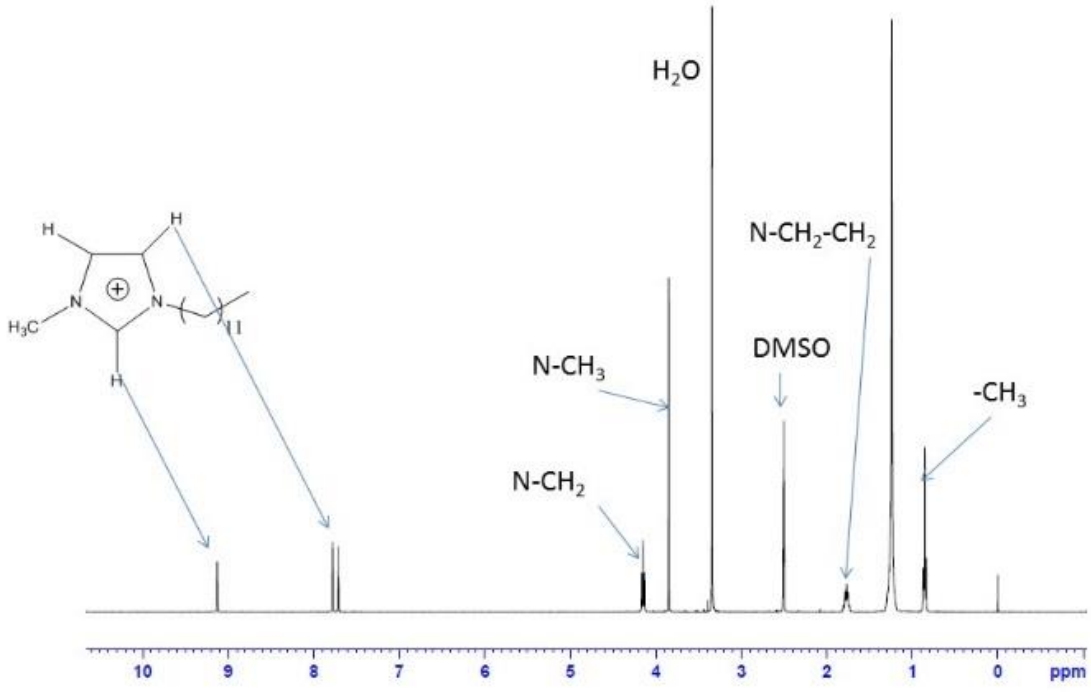

Figure 4.2 Structure of DMImBr and its structural confirmation using ^{1}H-NMR

4.3.3. Electropolymerization of Thiophene using TNT as Template

The electropolymerization was conducted using a conventional three electrode system. TNT was used as working electrode, Ag/Ag^{+} electrode as reference and platinum chip was used as counter electrode. DMImBr was used as vector (Scheme 4.2) instead of using normal surfactant. Thiopene (0.1M) was electropolymerized from the solution of 0.1M 1-methyl-3-dodecylimidazolium bromide in acetonitrile containing 0.1M $HClO_4$ aq. The potential was cycled between -2V to 0 V vs Ag/Ag^{+} at a scan rate of 50 mV/s. This cycling was carried out for 50 times. The TNT chip after the polymerization was washed with acetonitrile to remove any contaminations from the reaction mixtures and was vacuum dried at room temperature to obtain PTh/TNT.

In order to understand the morphological dependence of polymer in the absence of DMImBr and TNT in the reaction method (Scheme 4.3), two control experiments were carried alongside. Firstly, electropolymerization was performed as mentioned above without the addition of

DMImBr in the electrolyte. In the second experiment, electropolymerization was performed on Ti metal without any TiO_2 nanotube (TNT) grown as template. This was to ascertain the difference in the morphology in the absence of a template.

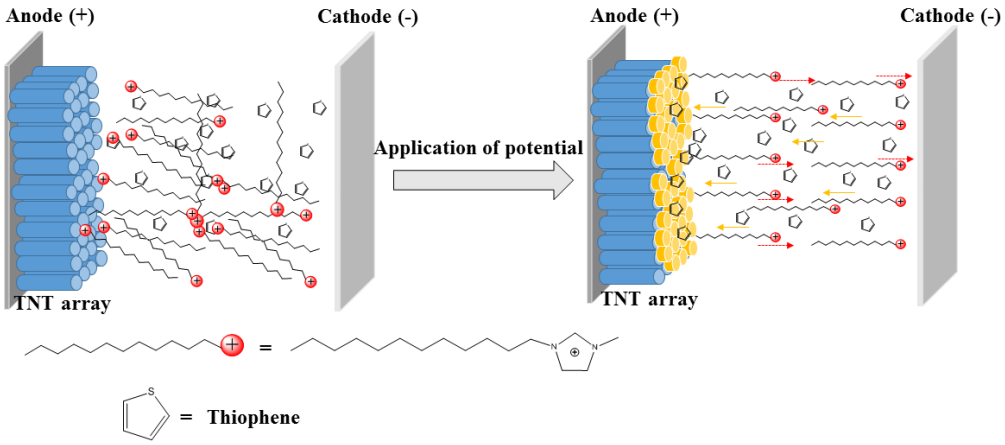

Scheme 4.2 Proposed directional diffusion of monomer in the presence of ionic liquid

4.3.4. Photo-reduction of Pt onto Polythiophene-TNT Hybrid

The reduction of metal salt was done by using the similar procedure to that of chapter 3. Here, the PTh-TNT hybrid on Ti chip was immersed in 100 mL of water containing 800 µL of 0.045M aq. chloroplatinic acid solution and was irradiated by a simulated solar light of ~1 sun intensity (100 $mWcm^{-1}$) for 5 hrs under constant stirring at room temperature. This completely

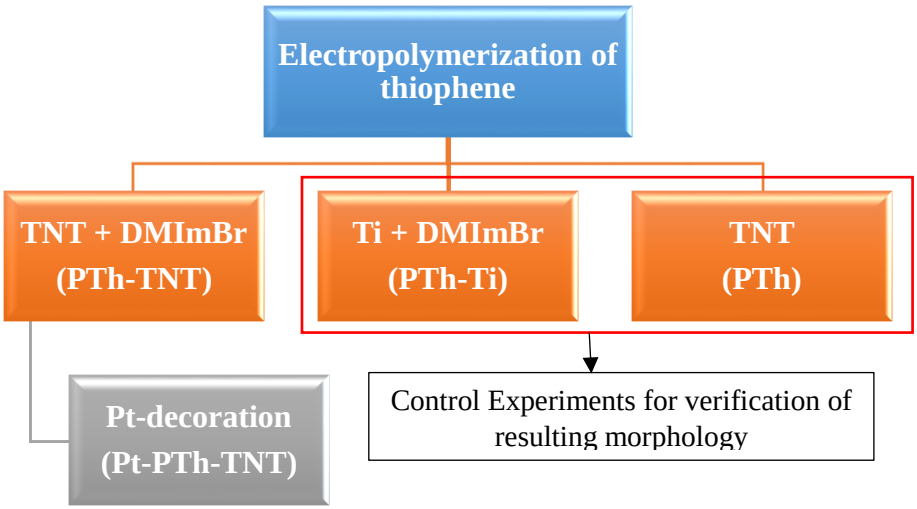

Scheme 4.3 Flow chart showing various hybrid materials prepared

green reduction process doesn't contain even a trace amount of sacrificial reducing agent. The chip with PTh-TNT after the photo-reduction process was cleaned with water and dried at room temperature under vacuum for overnight. The resulting Pt-PTh-TNT was further characterized to study the physical and electrochemical properties.

4.3.5. Chemical, Physical & Electrochemical characterization

Elemental characterization of TNT, Pt-PTh-TNT were performed using X-ray photoelectron spectroscopy (XPS) technique performed on S-probe^{TM} 2803 instrument. The morphology of the 1) as-prepared TNT, PTh-TNT, PTh electropolymerized without TNT (PTh-Ti) and 2) PTh prepared without ionic liquid (PTh) was studied using SEM (Hitachi S-4500). TEM was performed to understand the growth of PTh on Ti as well as TNT, particle size and distribution of Pt nps. The change in the charge transfer resistance before and after polymerization was studied using Electrochemical Impedance Spectroscopy.

4.4. Results and Discussion

The SEM micrographs of the TNT, PTh-TNT are shown in Figure 4.3. Figure 4.3 A details the tubular morphology of TNT with 135 nm diameter. It was evident that the individual tubes were demarcated well. In Fugure 4.3 B-D shows the micrographs of PTh-TNT composites. A clear difference in the contrast between Figure 4.3. A and B was seen corroborating the type of material. The tubular nature is not seen in Figure 4.3. B and C in contrast, a foam-like morphology could be seen in the case of PTh-TNT. The horizontal section can be seen in Figure 4.3. D which shows the demarcation of PTh and the TNT substrate. The tube diameter in case of TNT and PTh foam was found to be in the same range of 130 nm which clearly indicates that the TNT acts as a template. The tube diameter of TNT determines the pore size of the PTh foam.

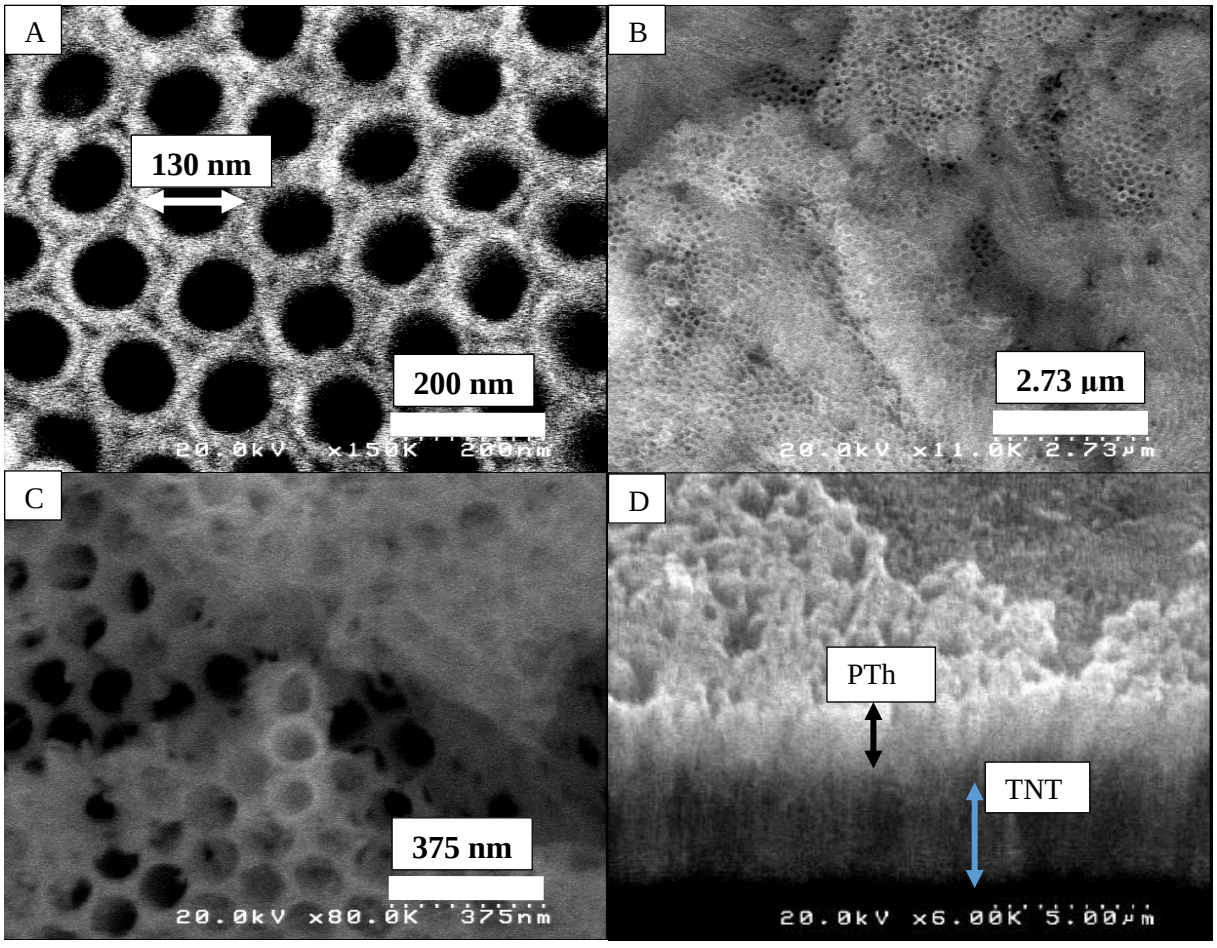

Figure 4.3 SEM micrographs of TNT showing the tube dimensions (A) polythiophene foam grown on TNT (B and C) cross sectional view of PTh-TNT hybrid (D)

SEM micrographs were also studied to determine the morphological changes in the absence of DMImBr in the reaction mixture. It was found from the SEM micrograph (Figure 4.4) that there was no formation of tubes in this case, instead an irregular morphology without any pores was found over the TNT surface.

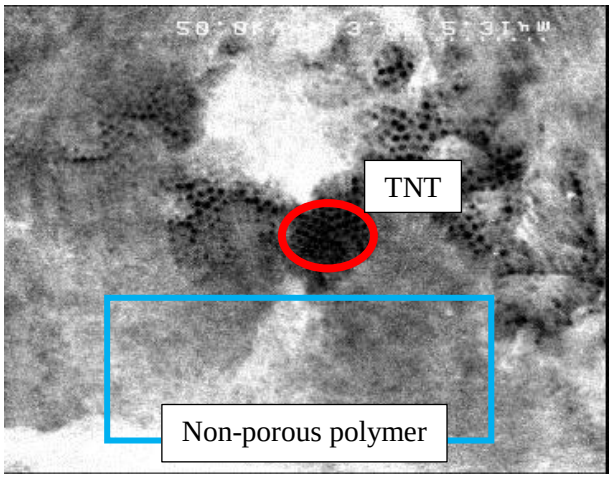

Figure 4.4 SEM micrograph of polymer prepared without ionic liquid (DMImBr)

While in the case of PTh-Ti (polymer formed on Ti) the polymer formed was thin and hence, due to high reflectivity of the metal beneath, it was difficult to record the SEM micrograph of this sample. Hence, only the results from TEM was available to characterize the PTh formed in the PTh-Ti sample (given in TEM section later). With these results, it was confirmed that TNT templating and the presence of ionic liquid in the form of vector was essential for the formation of PTh foam by controlling the directional diffusion of monomer. After these initial conclusions, Pt nps were photo-generated using the green synthetic method mentioned earlier.

Elemental composition of TNT and Pt-PTh-TNT was done using XPS. Figure 4.5 shows the survey spectra of TNT and Pt-PTh-TNT. Survery spectrum of TNT (Figure 4.5 A) showed typical peaks for Ti 3s, Ti2p, C 1s O1s and Ti 2s at their respective binding energies. The survey spectrum of Pt-PTh-TNT showed Pt 4f, 4d5, 4d3 and an increased C 1s peak intensity

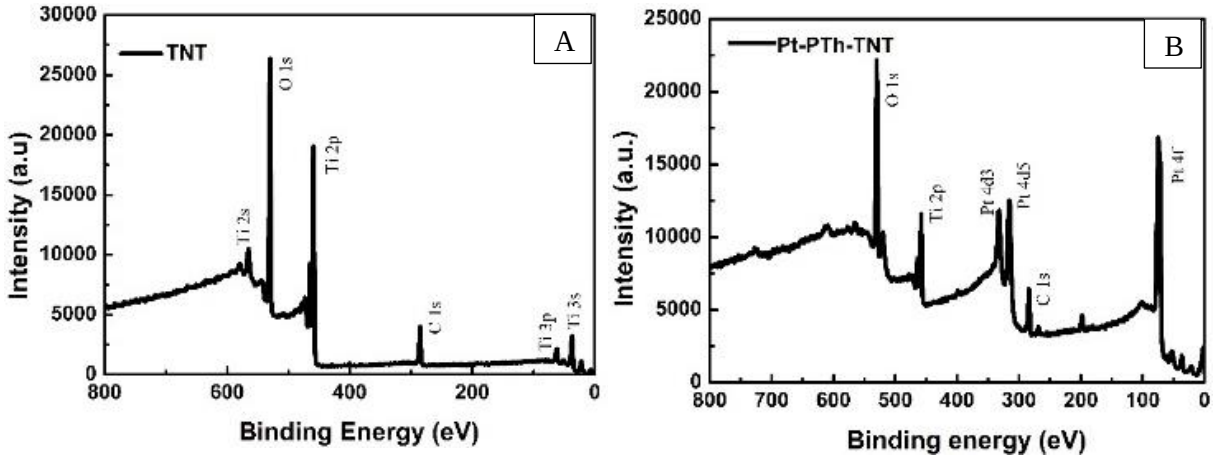

Figure 4.5 XPS survey spectra of TNT (A) and Pt-PTh-TNT (B)

along with the typical peaks of TNT. The calculated amount of photodeposited Pt from XPS was found to be 20 at%. Further XPS was employed to analyse various valence states of Pt in the prepared hybrid material. High resolution of local scan of Pt 4f peak provided valuable information on various oxidation states in which Pt is present. In addition, it also elucidates the strong metal substrate interaction (SMSI) by studying the binding energies of Pt^0. Figure 4.6 shows the high resolution Pt 4f peak of Pt-PTh-TNT consisting of 2 peaks at 71.6 and 73.5 corresponding to Pt^0 and Pt^{IV}. It was found that Pt^0 was in the predominant oxidation state with 61.3 % and 38.7% of Pt^{IV}. The shift in the binding energy of Pt^0 with around 0.4 eV compared to regular Pt/C confirms high SMSI. These results gave a clear indication of the successful photo-generation of Pt nanoparticles from metal salts. Alongside, the decoration of Pt on PTh-TNT hybrid with good adherence to substrate would lead to high durability of the ORR catalyst.

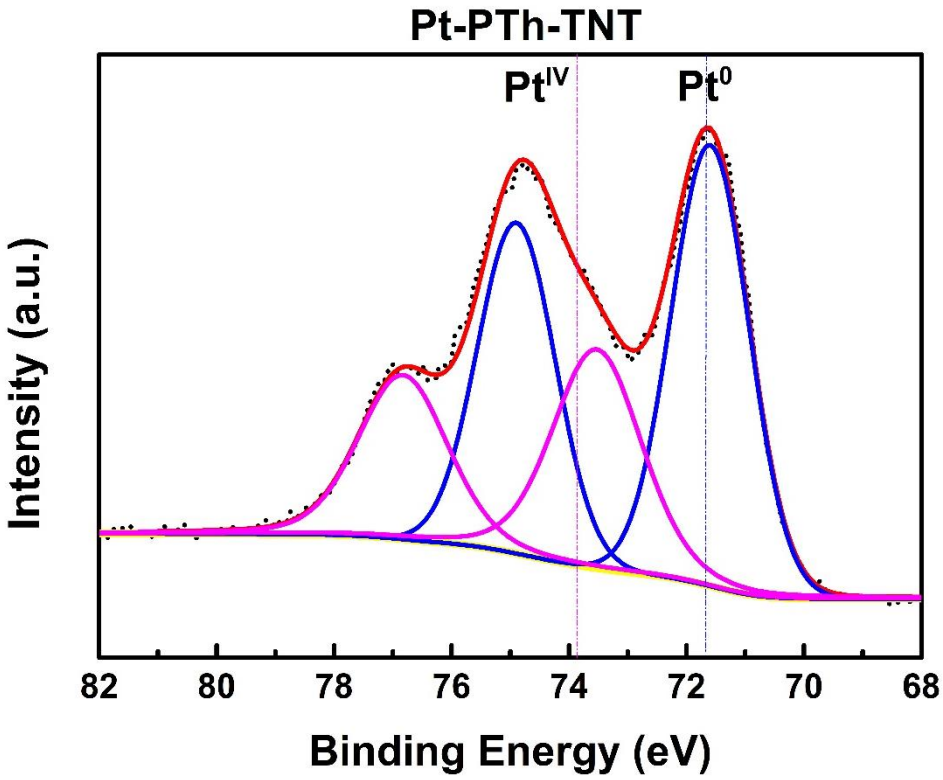

Figure 4.6 Deconvolution of high resolution Pt 4f peak of Pt-PTh-TNT showing Pt^0 and Pt^{IV} valence states

Further, TEM analysis shed light on the detailed morphological aspects of TNT, growth pattern of PTh on TNT and Pt np size and distribution on PTh-TNT. Figure 4.7 A shows the TEM micrograph of bare TNT (before the electropolymerization), in which the tube diameter was found to be ~130 nm. TNT was found to have smooth edges without any particle like material in the as-prepared TNT. While the Pt-PTh-TNT (Figure 4.7 B) showed growth of thin polymer all along the length of TNT and overshooting for some height above the TNT, with an open pore-mouth. These results reiterate the results obtained from SEM micrographs. It was very interesting to find the Pt nps of same size ~10 nm on TNT as well as PTh. This indicates that the novel green photo-generation of metal nps is possible for any conducting substrate coated onto TNT. Hence, it can be confirmed from the results that the interfacial photo-induced charge

transfer to the pre-adsorbed conducting polymer, can efficiently control the rapid recombination of the photo-generated charges of TNT. This spill-over of electrons from the TNT onto highly conducting polymer matrix tend to travel over the conducting matrix until it finds a suitable reducing species, in this case chloroplatinic acid to form Pt nanoparticles.

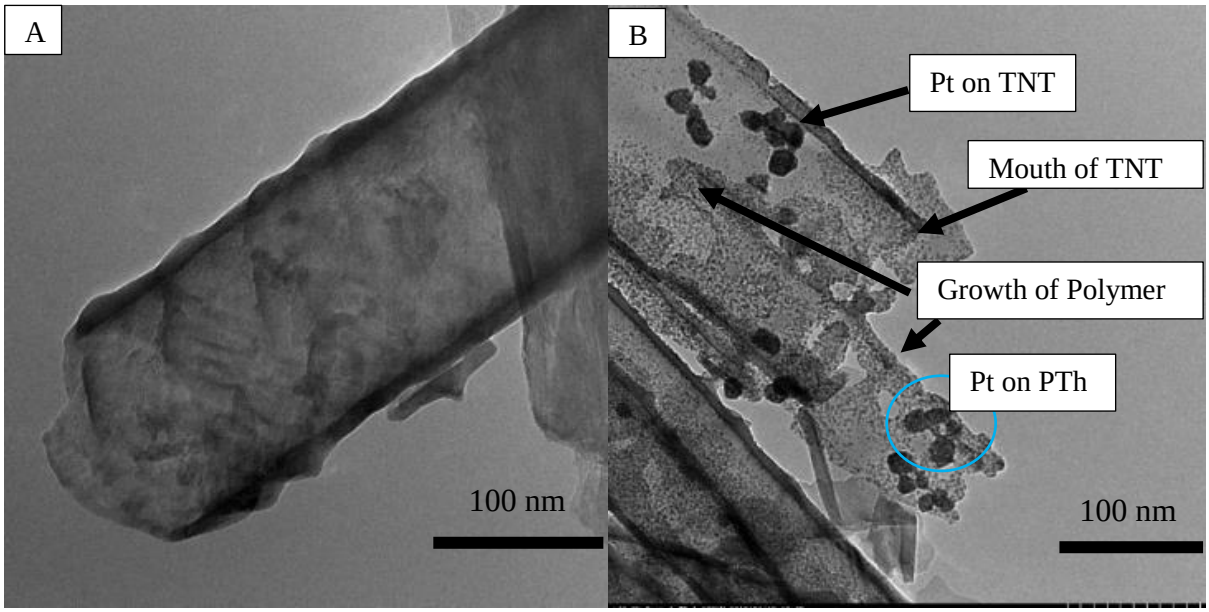

Figure 4.7 TEM micrographs of TNT (A) and Pt-PTh-TNT (B)

The morphology of PTh-Ti was studied using TEM. The polymer was dispersed into methanol using ultra-sonication and the dispersed polymer was transferred onto TEM grid. The TEM images detailed the layer like morphology (Figure 4.8). Due to the lack of any template, electropolymerization led to the formation of transparent and thin polymer layers. Lack of TNT photo-catalysts makes the photo-reduction of Pt impossible onto this phase of polymer.

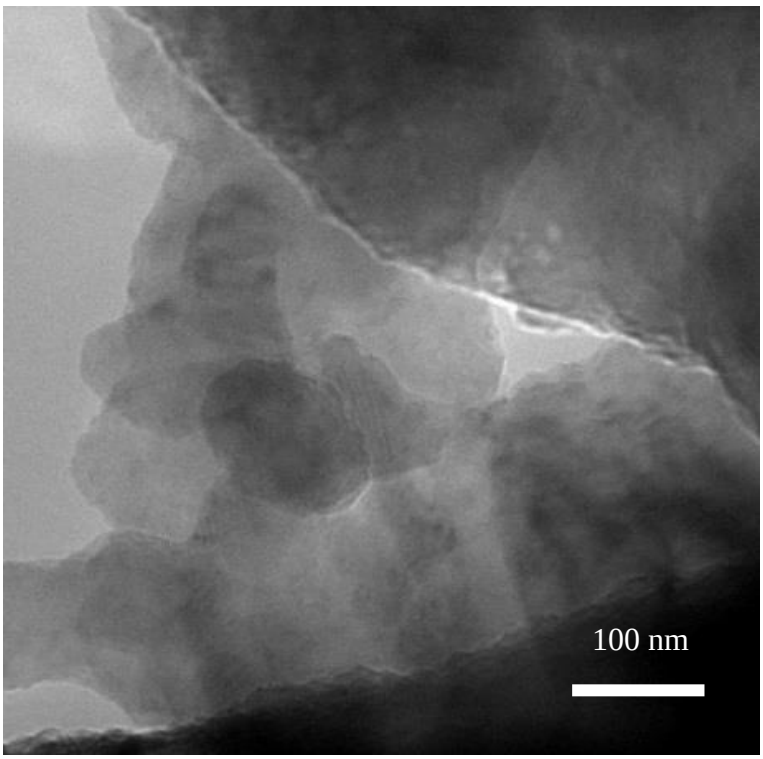

Figure 4.8 TEM micrographs of PTh-Ti highlighting layered structure

The interaction with electrolyte helps to reduce the interface boundaries, which in turn affects the overall catalytic performance of the electrode[27,28]. Hence, interfacial studies are vital to validate the catalytic performance of the electrode, which can be understood by electrochemical impedance studies. Further, chapter 2 and 3 shed light on the correlation between the ORR catalytic activity and the absorptive properties of catalysts. So, to evaluate the charge transfer resistance of the PTh-TNT EIS studies were carried out.

The electrochemical impedance spectroscopy (EIS) studies for the PTh-TNT catalyst substrate was performed using conventional three electrode system using Pt wire as the counter electrode and Ag/AgCl reference electrode in nitrogen saturated 0.1 M $HClO_4$ aq. at open circuit potential. These results were compared with the bare TNT chip before electropolymerization.

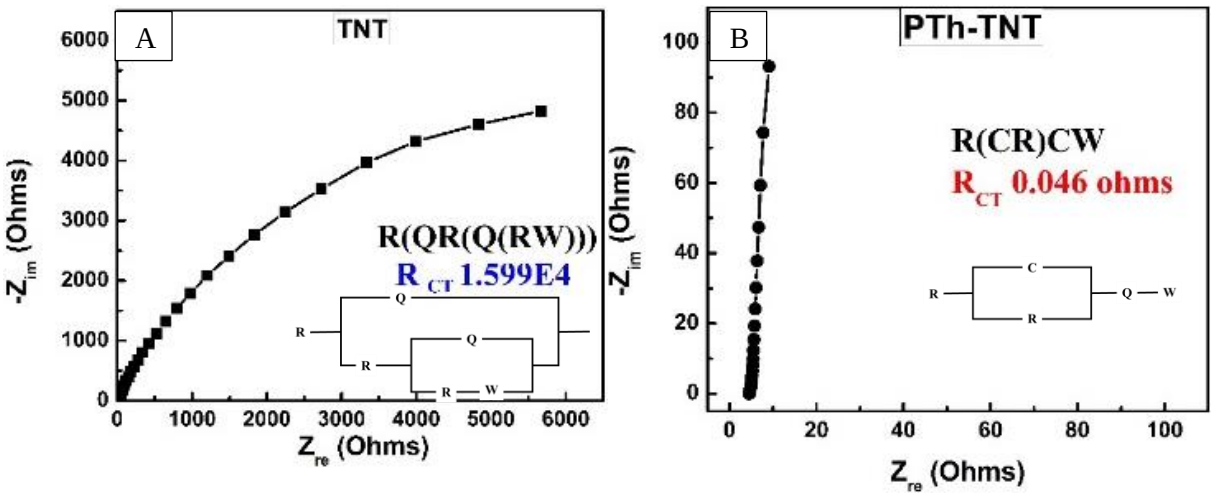

Figure 4.9 Nyquist plots of TNT (A) PTh-TNT (B) and their R_{CT} values given as the inset along with the equivalent circuit accordingly

EIS results presented in Figure 4.9 show the Nyquist plot for TNT and PTh-TNT. Fitting these results with an equivalent circuit (given as the inset in Figure 4.9 A-B) revealed a tremendous change in the R_{CT} value of TNT (1.60E4 ohms) and PTh-TNT (0.046 ohms). Extremely less R_{CT} value suggests that a catalyst made using this conducting substrate would be extremely active. This results apparently indicate the role of ionic liquid (DMImBr) in the reaction mixture during the electropolymerization of thiphene, in modulating the morphology. The presence of ionic liquid was necessary and essential to enable electropolymyerziation over

TNT template. As it is known that for any substrate to act as template suitable wetting agents like surfactants have to be used. In the present strategy environmentally benign ionic liquid acted as the wetting agent as well as vector to form polythiophene foam. Further, this substrate was successfully decorated with the novel green reduction process which leads to the formation of Pt nanoparticles with very good adherence to the substrate. The obtained Pt nanoparticles showed enhanced SMSI, which is one of the crucial factors to determine the stability or durability of the catalyst. Finally, the impedance studies revealed extremely less charge-transfer resistance values which make the PTh-TNT an ideal substrate for ORR catalyst having the ability in substituting carbon substrates.

4.5. Conclusion

A novel 3D polythiophene foam was prepared by electropolymerization employing DMIMBr (ionic liquid) as the wetting agent as well as vector and TNT as the tubular template. The presence of the photoactive TNT in the presence of electronically conductive polymer as hybrid, it was possible to employ green photo-reduction process in the similar lines of chapter 3. XPS analysis of this photo-generated Pt nps showed very high SMSI characteristics that enables high durability during the ORR. Finally EIS studies revealed that this hybrid was found to have extremely less charge transfer resistance with which a high ORR activity can be expected.

References

(1) Colón-Mercado, H. R.; Popov, B. N. Stability of platinum based alloy cathode catalysts in PEM fuel cells. *J. Power Sources*, **2006**, *155*, 253–263.

(2) Reiss, P.; Couderc, E.; De Girolamo, J.; Pron, A. Conjugated polymers/semiconductor nanocrystals hybrid materials preparation, electrical transport properties and applications. *Nanoscale*, **2011**, *3*, 446–489.

(3) Naveen, M. H.; Noh, H.-B.; Al Hossain, M. S.; Kim, J. H.; Shim, Y.B. Facile potentiostatic preparation of functionalized polyterthiophene-anchored graphene oxide as a metal-free electrocatalyst for the oxygen reduction reaction. *J. Mater. Chem. A*, **2015**, *3*, 5426–5433.

(4) Kim, D.M.; Shim, K.B.; Son, J. I.; Reddy, S. S.; Shim, Y.-B. Spectroelectrochemical and electrochromic behaviors of newly synthesized poly [3′-(2-aminopyrimidyl)-2, 2′: 5′, 2 ″-terthiophene]. *Electrochim. Acta*, **2013**, *104*, 322–329.

(5) Rahman, M. A.; Kumar, P.; Park, D.-S.; Shim, Y.B. Electrochemical sensors based on organic conjugated polymers. *Sensors*, **2008**, *8*, 118–141.

(6) Lee, T.Y.; Shim, Y.-B. Direct DNA hybridization detection based on the oligonucleotide-functionalized conductive polymer. *Anal. chem.*, **2001**, *73*, 5629–5632.

(7) Schrebler, R.; Del Valle, M. A.; Go, H.; Veas, C.; Co, R. Preparation of polythiophene-modified electrodes by electrodeposition of Pt and Pt+Pb. Application to formic acid electro-oxidation. *J. Electroanal. Chem*, **1995**, *380*, 219–227.

(8) Yassar, A.; Roncali, J.; Garnier, F. Preparation and electroactivity of poly (thiophene) electrodes modified by electrodeposition of palladium particles. *J. Electroanal. Chem. Interfacial Electrochem.*, **1988**, *255*, 53–69.

(9) Giacomini, M. T.; Ticianelli, E. A.; McBreen, J.; Balasubramanian, M. Oxygen reduction on supported platinum/polythiophene electrocatalysts. *J. Electrochem. Soc.*, **2001**,

148, A323-A329.

(10) Giacomini, M. T.; Balasubramanian, M.; Khalid, S.; McBreen, J.; Ticianellia, E. A. Characterization of the activity of palladium-modified polythiophene electrodes for the hydrogen oxidation and oxygen reduction reactions. *J. Electrochem. Soc.*, **2003**, *150*, A588-A593.

(11) Wu, D.; Xu, F.; Sun, B.; Fu, R.; He, H.; Matyjaszewski, K. Design and preparation of porous polymers. *Chem. Rev.*, **2012**, *112*, 3959–4015.

(12) Tian, S.; Wang, J.; Jonas, U.; Knoll, W. Inverse opals of polyaniline and its copolymers prepared by electrochemical techniques. *Chem. Mater.*, **2005**, *17*, 5726–5730.

(13) Döbbelin, M.; Tena-Zaera, R.; Carrasco, P. M.; Sarasua, J. -. R.; Cabañero, G.; Mecerreyes, D. Electrochemical synthesis of poly (3, 4-ethylenedioxythiophene) nanotube arrays using ZnO templates. *J. Polym. Sci. A Polym. Chem.*, **2010**, *48*, 4648–4653.

(14) Luo, X.; Killard, A. J.; Morrin, A.; Smyth, M. R. Electrochemical preparation of distinct polyaniline nanostructures by surface charge control of polystyrene nanoparticle templates. *Chem. Commun.*, **2007**, 3207–3209.

(15) Cho, S. I.; Lee, S. B. Fast electrochemistry of conductive polymer nanotubes: synthesis, mechanism, and application. *Acc. Chem. Res.*, **2008**, *41*, 699–707.

(16) Kowalski, D.; Schmuki, P. Polypyrrole self-organized nanopore arrays formed by controlled electropolymerization in TiO_2 nanotube template. *Chem. Commun.*, **2010**, *46*, 8585–8587.

(17) Pernites, R. B.; Foster, E. L.; Felipe, M. J. L.; Robinson, M.; Advincula, R. C. Patterned surfaces combining polymer brushes and conducting polymer via colloidal template electropolymerization. *Adv. Mater.*, **2011**, *23*, 1287–1292.

(18) Li, X.; Dai, L.; Liu, Y.; Chen, X.; Yan, W.; Jiang, L.; Zhu, J. Ionic ‐ liquid ‐ doped polyaniline inverse opals: preparation, characterization, and application for the electrochemical

impedance immunoassay of hepatitis b surface antigen. *Adv. Funct. Mater.*, **2009**, *19*, 3120–3128.

(19) Park, S. -. A.; Xiao, R.; Cho, S. I.; Choi, S. J.; Lee, S. B.; Kim, S. H.; Kwon, W. . J.; Son, S. . J.; Kim, J.; Kim, P. Nanotube-based ultrafast electrochromic display. *Adv. Mater.*, **2005**, *17*, 171–175.

(20) Xiao, R.; Cho, S. I.; Liu, R.; Lee, S. B. Controlled Electrochemical synthesis of conductive polymer nanotube structures. *J. Am. Chem. Soc.*, **2007**, *129*, 4483–4489.

(21) Cho, S. I.; Xiao, R.; Lee, S. B. Electrochemical synthesis of poly (3, 4-ethylenedioxythiophene) nanotubes towards fast window-type electrochromic devices. *Nanotechnology*, **2007**, *18*, 405705.

(22) Liu, R.; Cho, S. I.; Lee, S. B. Poly (3, 4-ethylenedioxythiophene) nanotubes as electrode materials for a high-powered supercapacitor. *Nanotechnology*, **2008**, *19*, 215710.

(23) Zhu, J.; Liu, Y.; Dai, L.; Yan, W.; Chen, X.; Jiang, L.; Li, X. Ionic-liquid-doped polyaniline inverse opals: preparation, characterization, and application for the electrochemical impedance immunoassay of hepatitis b surface antigen. *Adv. Funct. Mater.*, **2009**, *19*, 3120–3128.

(24) Kowalski, D.; Albu, S. P.; Schmuki, P. Current dependent formation of PEDOT inverse nanotube arrays. *RSC Advances*, **2013**, *3*, 2154–2157.

(25) Ambade, R. B.; Ambade, S. B.; Shrestha, N. K.; Nah, Y.-C.; Han, S.-H.; Lee, W.; Lee, S.H. Polythiophene infiltrated TiO_2 nanotubes as high-performance supercapacitor electrodes. *Chem. Commun.*, **2013**, *49*, 2308–2310.

(26) Dupont, J.; Consorti, C. S.; Suarez, P. A.; de Souza, R. F. Preparation of 1-butyl-3-methyl imidazolium-based room temperature ionic liquids. *Org. Syn.*, **2003**, 236.

(27) Kim, M.; Park, J.-N.; Kim, H.; Song, S.; Lee, W.-H. The preparation of Pt/C catalysts using various carbon materials for the cathode of PEMFC. *J. Power Sources*, **2006**, *163*, 93-97.

(28) Cai, F.; Liang, J.; Tao, Z.; Chen, J.; Xu, R. Low-Pt-loading acetylene-black cathode for high-efficient dye-sensitized solar cells. *J. Power Sources*, **2008**, *177*, 631–636.

Chapter 5

Conclusions

5.1. General Conclusions

Fuel cells and Li-air battery due to their high energy density, prolonged durability with low emission of global warming gases have gained greater significance among various electrochemical energy devices. The similarity in working of fuel cells and metal air batteries is based on the occurrence of ORR at the cathode end. Electrocatalyst plays an important role in realization of both these devices by enhancing the sluggish kinetics of ORR. So, the design and development of viable electrocatalytic material carries a great degree of importance in this field. Keeping this in view, innovative strategies were adopted to design and develop ultra-high active ORR catalysts comprising novel carbon based nano-architectures.

In brief all the above chapters had a single aim to develop facile and cost effective preparation methodologies for various Pt/C based ORR catalysts which can be readily commercialized. All the materials used during these studies were well known substrates but modified into highly active catalyst by tweaking intrinsic properties employing novel methods. Firstly, Chapter 1 gives an overview of the importance of ORR in various paths of life ranging from being the principle reaction for the sustenance of living being through aerobic respirations to being the most important reaction in the present day flagship devices in the field of energy. It also deals with the brief understanding of the ORR, its catalytic properties and major setbacks. A detailed literature review is presented emphasising on the evolution of strategies for designing and developing ORR active catalysts, present status, problems and targets to achieve. This chapter concludes with by mentioning the probable strategies in designing the electrocatalyst to achieve a) high surface area of carbon based support b) good ability to support the catalyst c) high pore size d) negligible charge transfer resistance and e) high stability in ORR environment. It also

presents simple and commercially viable designing strategies for improving above intrinsic attributes for enhancing the ORR.

In the chapter 2, a well-known and commercially available material, AB was taken and modified using simple method to enhance various intrinsic characteristics. Here a facile and novel single step method was developed for the exfoliation and functionalization of AB to a few layer graphene-like carbon substrate (FAB) incorporating oxygen functional groups. The choice of the starting material was systematically carried out by studying the intrinsic electrolyte absorptive and ORR characteristics of AB without any metal decoration. The strategies adopted were i) exfoliation of the AB to a few layer FAB lead to increased surface area of carbon support ii) deliberate functionalization with controlled acid treatment improves the hydrophilicity, thereby enhancing the substrate metal interaction and iii) incorporation of these functional groups lead to decreased interfacial charge transfer resistance. Highly uniform Pt nano particle nucleation and steady anchoring between Pt nps and the carbon substrate (SMSI) was observed due to the functionalization. The overall durability of the catalyst during ORR and MOR was enhanced. With this strategy in designing and developing a facile methodology lead to an impressive and highly catalytic material crossing the targets set for Pt based catalyst by Department Of Energy, USA (DOE) (Figure 5.1 A). The employed strategy reduced the cost of the material preparation by 38% of its commercial counterpart from Sigma Aldrich. Finally, a real time application in fuel cells (Figure 5.1 B) and Li-air battery showed impressive results (Figure 5.1C).

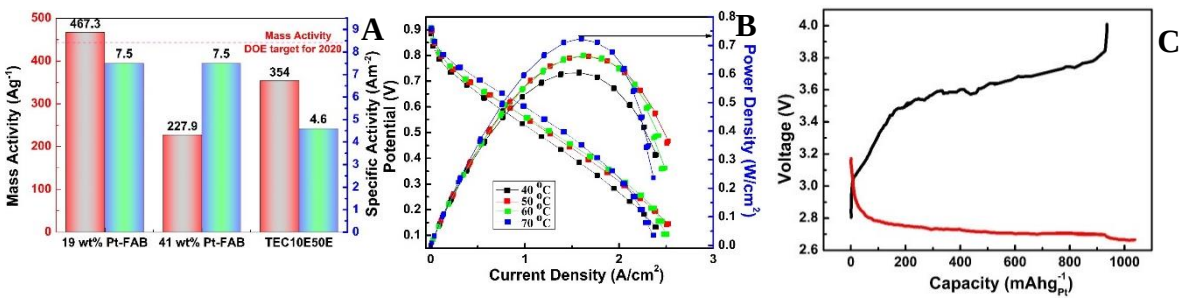

Figure 5.1Comparison of MA and SA 19 wt% Pt-FAB and 41 wt% Pt-FAB with TEC10E50E (A) fuel cell polarization curve of 19 wt% Pt-FAB (B) and charge discharge curves of Li air battery

The successful development of a novel and efficient catalyst using facile method inspired further investigation for refraining the use of non-green reducing agents like ethyleneglycol. The use of sacrificial reducing agent make the preparation method uneconomical. Hence, a green as well as cost effective method was developed using photo-reduction chemistry of TiO_2 in aqueous media at room temperature. The traditionally used graphite and CNT was employed for this study. Chapter 3 corroborates the design and development of a highly reproducible, environmentally benign, ultrafast and completely green method for the preparation of highly active ORR catalyst with low Pt content (for use in Fuel cell and Lithium-air battery). The method used solar light as the only source of energy in the preparation of this catalytically efficient composite utilizing abundant and environmentally benign TiO_2 nano structures as photo-catalyst in water without any further adjustments like pH, temperature etc. Using this green methodology, preparation of novel composites containing TiO_2 particles and nanotubes, CNT/Graphite substrates and platinum nanoparticles was successfully carried out. The method showed exceptionally high diffusion of photo-electrons (> 100 nm) all along the surface of conducting carbon substrate before finding the adsorbed metal ion precursor (Schematic shown in Figure 6.2 A). As prepared material with ultra-low Pt showed excellent ORR activity comparable to the best commercial ORR catalysts (containing 50 Wt% of Pt). All the materials showed exceptional mass and specific activities (Figure 6.2 B). All the materials showed very high durability which can be ascribed to high SMSI of the three phase composite. It can also

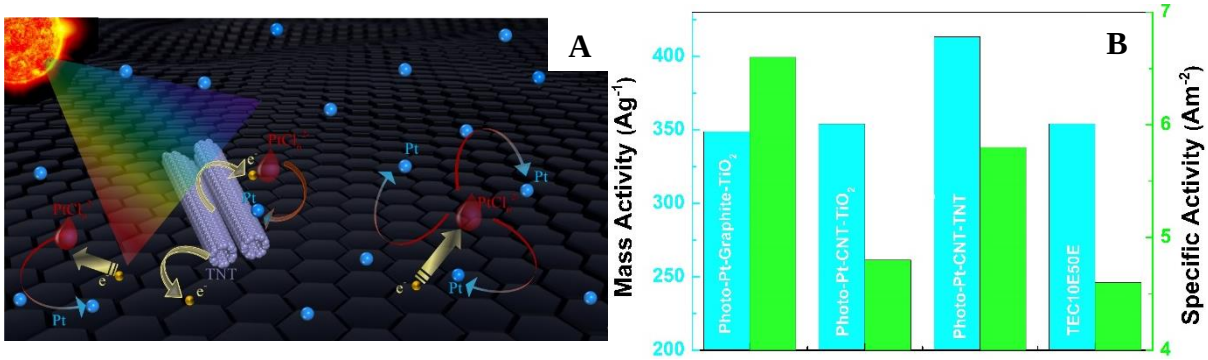

Figure 5.2 Schematic representation of novel photo-reduction method (A) and MA & SA of Photo generated Pt on various TiO_2/Carbon substrates in comparison with commercial counterpart (B)

be confirmed that this method is feasible for all the conducting carbon substrates. The results clearly demonstrated, i) that the novel, green and a very viable method of Pt decoration method is more efficient than that of well-established methods using SRA ii) reiterated that the combination of metal oxide, carbon, and Pt as highly electrocatalytic activity with substantially less amount of Pt and iii) reduction of preparation cost and time of the catalyst with readily scalable simple preparation method.

The importance of preparation method in reaping highly active catalytic material was proven beyond ambiguity from chapter 2 and 3. Finally, the electrooxidation of carbon which plays a major role in durability of catalyst was considered as a subject to be addressed by tweaking methodology. Hence, the necessity for developing an advanced alternative substrate possessing all the intrinsic characteristics of conventional carbon substrate along with improved durability was researched.

In this regard, chapter 4 deals with the design and synthesis of a novel 3D-polythiophene foam using electropolymerization, employing DMIMBr (ionic liquid) as the wetting agent as well as ionic channel and TNT as the tubular template. The preparation of this highly porous nano architecture enabled high absorptivity and interaction with electrolyte, offering extremely low interfacial charge transfer resistance (studied using EIS). The presence of the photoactive TNT, with the introduction of electronically conductive polymer as hybrid was used to tweak the green photo-reduction process in the similar lines of chapter 3 for the generation of Pt nanoparticles. XPS analysis of this photo-generated Pt nps showed very high SMSI characteristics. With this strategy various important factors determining the ORR activity were enhanced like, negligible charge transfer resistance, high pore size and strong anchoring of Pt to the novel substrate.

5.2. Future Scope of the Work

The present work has proved a new path in the fabrication of electrcatalyst, the following are the possible areas of improvement basing on the present studies.

1) Optimization of various parameters like, amount of catalyst loading on MEA and back pressure of air or oxygen in the fuel cell studies. Studying the effect of air pollutants (NO_x, SO_x, CO and CO_2) on the performance of electrocatalyst and durability in the PEMFC.
2) Optimization of catalyst loading amount, charge-discharge current rates, oxygen pressure, type of electrolyte and the lithium salt used and detailed study of interfacial charge transfer resistance will give a complete understanding of the performance of the electrocatalyst in lithium air battery.
3) Further modification of FAB with hetero atom (N or B and both) doping will increase the electrocatalytic activity if the FAB and the optimization of percentage of hetero atom doping will probably lead to the formation of metal less electrocatalysts.
4) Decoration of Pt-transition metal alloy, coreshell nano particles or Pt skin type catalyst onto FAB will further improve the catalytic activity of the materials.
5) The photo-reduction process can be extended to reduce other catalytically active metals individually or in combination to form alloys.

List of Publications and Other Achievements

Name: Badam Rajashekar

Publications

1. Badam Rajashekar, Raman Vedarajan and Noriyoshi Matsumi, Platinum decorated functionalized defective acetylene black; a promising cathode material for oxygen reduction reaction, **Chemical Communications**, 2015, 51, 9841-9844.

Patents:

2. 松見　紀佳、RAMAN, Vedarajan、RAJASHEKAR, Badam, 金属ナノ粒子担持炭素材料およびその製造方法 官能化剥離炭素材料の製造方法, 特願 2013-231393, 2013/11/7.

International Conferences

2015

3. **POSTER:** Badam Rajashekar, Raman Vedarajan, Noriyoshi Matsumi, Sacrificial Reducing Agent Free Photo-induced Green Synthesis of Metal Nano-Particles Over Polythiophene/TiO_2 nano-composite, **Pacifichem 2015**, Hawaii, USA, December 15-20, 2015.
4. **ORAL:** Badam Rajashekar, Raman Vedarajan and Noriyoshi Matsumi, Platinum decorated functionalized acetylene black nano composite for efficient oxygen reduction reaction, **FIMPART'15**, Hyderabad, India, June 13 -15 2015.

2014

5. **POSTER:** Badam Rajashekar, Raman Vedarajan and Noriyoshi Matsumi, Platinum decorated functionalized acetylene black; an efficient cathode material for oxygen reduction reaction, **FiNSTA'14**, Puttaparthi, India, Dec 20 – 21 2014.
6. **POSTER:** Badam Rajashekar, Raman Vedarajan and Noriyoshi Matsumi, Platinum decorated functionalized acetylene black nano composite for enhanced oxygen reduction, **Eurasia-13**, Bangalore, India, Dec 14 – 18 2014.
7. **ORAL:** Badam Rajashekar, Raman Vedarajan and Noriyoshi Matsumi, Platinum decorated functionalized acetylene black nano composite for enhanced oxidation reduction reaction, **Japan-**

India symposium on Automotive Technologies (Energy, Fuel and Plastics), JAIST, Japan, Aug 4 - 5 2014.

8. **ORAL:** Badam Rajashekar, Raman Vedarajan and Noriyoshi Matsumi, Graphene like carbon material decorated with Pt nano particles for enhanced oxygen reduction, **247th ACS National Meeting & Exposition**, Dallas, USA, Mar 19 2014.

2013

9. **ORAL:** Badam Rajashekar, Raman Vedarajan and Noriyoshi Matsumi, Platinum nano particle decorated functionalized acetylene black, a novel 2D composite with enhanced ORR Graphene like 2D carbon material decorated with Pt nano particles for enhanced oxygen reduction reaction, **JAIST International Synposium on Functional Polymer Materials**, JAIST, Japan, Dec 13 2013.

Domestic Conferences

2015

10. **ORAL:** Badam Rajashekar, Raman Vedarajan and Noriyoshi Matsumi, Novel Sacrificial Reducing Agent Free, Photo-Generated Platinum Nano Particle-Carbon composite for Efficient Oxygen Reduction Reaction (ORR), **The 56th Battery symposium in Japan**, Nagoya, Japan, Nov 11-13 2015.
11. **ORAL:** Raman Vedarajan, Badam Rajashekar and Noriyoshi Matsumi, Platinum Nanoparticles Decorated Acetylene Black as an Efficient Electrode Material, Inorganic Polymer Conference, Tokyo, Japan, Nov 5 – 6 2015.
12. **POSTER:** Badam Rajashekar, Raman Vedarajan and Noriyoshi Matsumi, Preparation of Graphite (graphene)/TiO_2 composite and Photo-Catalytic Loading of Metal Nano-Particle, **SPSJ (Society of Polymer Science, Japan) annual meeting**, Sapporo, Japan, May 27 – 29 2015.

2014

13. **POSTER:** Badam Rajashekar, Raman Vedarajan and Noriyoshi Matsumi, Oxygen Reduction Behavior of Exfoliated Acetylene Black with Pt Nanoparticle Decoration, **Regional meeting of Chemical Society of Japan (CSJ)**, Toyama, Japan, Nov 21 2014.

14. **ORAL:** Badam Rajashekar, Raman Vedarajan and Noriyoshi Matsumi, Oxygen Reduction Characteristics of Exfoliated Acetylene Black / Pt Nano Particles Composite, **SPSJ Fall meeting**, Nagasaki, Japan, Sep 24 - 26 2014.
15. **EXHIBITION:** Badam Rajashekar, Raman Vedarajan and Noriyoshi Matsumi, Platinum Nanoparticles Decorated Acetylene Black as an Efficient Electrode, **Innovation Japan**, Tokyo, Japan, Sep 10 – 11 2014.
16. **POSTER:** Badam Rajashekar, Raman Vedarajan and Noriyoshi Matsumi, ORR characteristics of exfoliated acetylene black/platinum nano-particles, **63rd SPSJ Annual Meeting**, Nagoya, Japan, May 28 – 30 2014.
17. **POSTER:** Badam Rajashekar, Raman Vedarajan and Noriyoshi Matsumi, Platinum Nanoparticles Decorated Acetylene Black as an Efficient Electrode Material, **GRIP 2014**, Kanazawa, Japan, Mar 7 - 8 2014.
18. **EXHIBITION:** Badam Rajashekar, Raman Vedarajan and Noriyoshi Matsumi, Platinum Nanoparticles Decorated Acetylene Black as an Efficient Electrode, **Nanotech2014**, Tokyo, Japan, Jan 29 – 31 2014.

2013

19. **ORAL:** Badam Rajashekar, Raman Vedarajan and Noriyoshi Matsumi, Platinum Nanoparticles Decorated Acetylene Black as an Efficient Electrode, **CSJ regional meeting**, JAIST, Japan, Nov 22 2013.
20. **ORAL:** Badam Rajashekar, Raman Vedarajan and Noriyoshi Matsumi, Platinum nanoparticles decorated acetylene black as an efficient electrode material, **Inorganic Polymer Conference**, Tokyo, Japan, Nov 8, 2013.
21. **POSTER:** Badam Rajashekar, Raman Vedarajan and Noriyoshi Matsumi, Platinum nanoparticles decorated acetylene black as an efficient electrode material, **SPSJ fall meeting**, Kanazawa, Japan, Sep 11 - 13 2013.